UNIVERSITÀ DI NAPOLI "FEDERICO II"

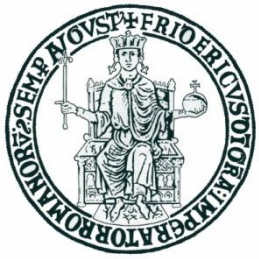

DIPARTIMENTO DI INGEGNERIA CHIMICA

DOTTORATO DI RICERCA IN INGEGNERIA CHIMICA XXII CICLO

Oxidative methanol steam reforming on Cu/ZrO_2 and $Cu/CeO_2/Al_2O_3$ catalysts prepared by sol-gel method

Scientific committee

Prof. Maria Turco

Prof. Antonio Aronne

Prof. Vincenzo Caprio

Prof. Maurizio Lenarda

Candidate

Claudia Cammarano

Anno Accademico 2009

Contents

Abstract

Cu/ZrO_2 and $Cu/CeO_2/Al_2O_3$ systems were investigated as catalysts for oxidative steam reforming of methanol (OSRM). The materials were prepared by modified sol-gel methods and characterized for physical and chemical properties by chemical analysis, XRD, N_2 adsorption, DTA, XPS, TPR and N_2O dispersion measurements. The catalytic activity was investigated in two laboratory plants. The first one allowed a quantitative evaluation of the catalytic activity in oxidative steam reforming of methanol (OSRM) and steam reforming of methanol (SRM). The second apparatus allowed pre-treatments and in situ characterization of the catalysts before and after each SRM catalytic test and on-line semi-quantitative analysis of the products.

Two different procedures, based on different Cu precursors were investigated for the preparation of Cu/ZrO_2 systems: it was found that the preparation method strongly influences all the properties studied. Very high surface areas were observed and a highly dispersed Cu metallic phase was obtained after a reductive treatment with H_2. The presence of ZrO_2 favoured the Cu^+ oxidation state, that has a likely role in the OSRM reaction. The catalysts showed high activity for the oxidative steam reforming of methanol. A noticeable activity was observed also with the not pre-reduced catalysts, indicating that the formation of a metallic phase, although with lower activity, can occur directly under reaction conditions.

$Cu/CeO_2/Al_2O_3$ systems were prepared by a totally new one pot sol-gel method. The catalysts showed a huge surface area and resulted to contain very dispersed CeO_2 and CuO phases on a poorly crystalline alumina matrix. A highly dispersed Cu metallic phase was obtained after a reductive treatment with H_2. The presence of CeO_2 favoured the Cu^+ oxidation state. The activity of the pre-reduced catalysts resulted high, in terms of hydrogen production rate, if compared with data on similar Cu/Ce/Al systems, notwithstanding the absence of the well known promoter ZnO. Also for these systems the unreduced materials showed a noticeable activity for the OSRM process, indicating that the metallic phase, although with lower activity, can be formed directly under reaction conditions. On the other hand, the reduction conditions (under H_2 or methanol with different concentration) strongly influenced the properties of the active phase, since copper obtained under strong reducing conditions (under H_2 or high methanol concentration) was more active than that obtained under milder conditions (low methanol concentration).

The different catalytic performances observed in OSRM and SRM tests indicate a strong influence of the presence of O_2 in the reaction system. The activity for SRM, in the absence of oxygen was, in

fact very low. This behaviour was explained either considering the occurrence of H spillover or the CeO_2 assisted oxidation of Cu to Cu^+.

1 Introduction

1.1 Motivation

The oil crisis and the commitment to reduce the greenhouse gases (GHG) emissions have increased the need of seeking clean and renewable sources of energy.

Energy needs are growing worldwide, strongly pushed by developing countries such as China and India, where nearly 40% of the world population lives. According to BP data [1], in 2008 the OECD (Organization for Economic Cooperation and Development) represented about half of world primary energy consumption, but China alone exceeded the total consumption of the EU, with an increase of 7.2% over 2007 and it will start to overcome the United States in the coming years (Fig.1-1 and Table 1-1). The main sources of energy supply are fossil fuels (Table 1-2), major responsible for the greenhouse effect. The global carbon cycle is in fact in strong disequilibrium because of the input of CO_2 into the atmosphere from fossil fuel combustion and land use change. Fossil fuels presently account for about 85% of total emissions, and land use change for 15% [2].

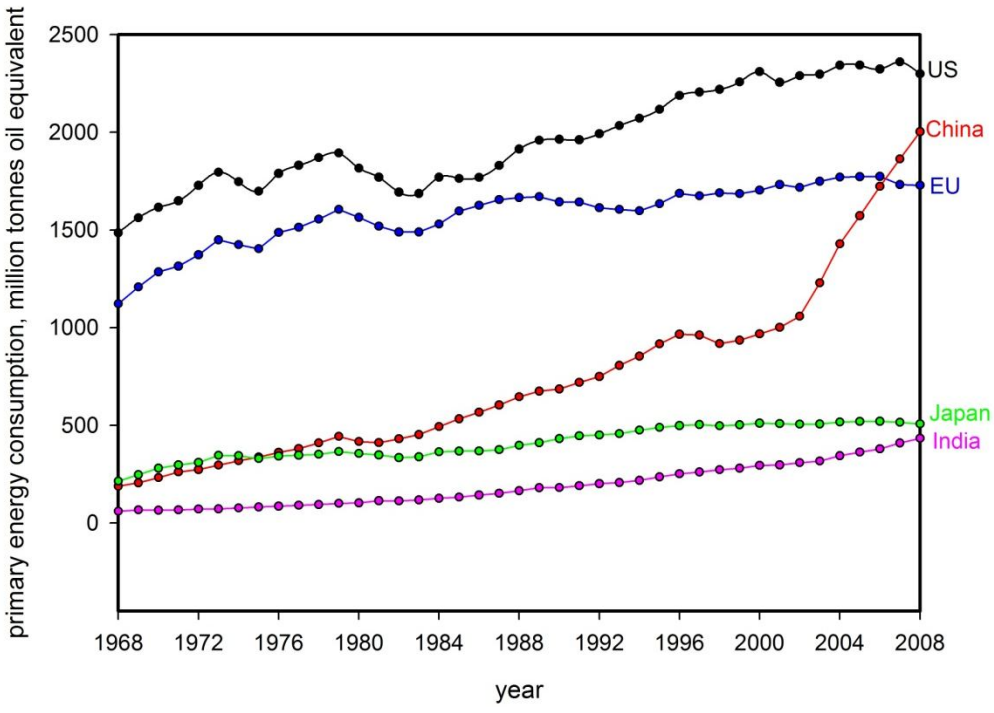

Fig.1-1. BP Statistical review of world energy: Primary energy consumption.

Table 1-1

BP Statistical review of world energy: Primary energy consumption.

Million tonnes oil equivalent	2000	2001	2002	2003	2004	2005	2006	2007	2008	Change 2008 over 2007	2008 share of total
US	2309,5	2254,9	2289,2	2296,7	2341,9	2342,7	2323,1	2359,6	2299,0	-2,8%	20,4%
Total North America	2747,8	2688,4	2728,7	2751,9	2803,6	2819,2	2803,2	2849,4	2799,1	-2,0%	24,8%
Total S.and C. America	459,5	462,3	465,7	470,0	490,9	511,6	538,4	563,5	579,6	2,6%	5,1%
Total Europe & Eurasia	2806,9	2827,9	2835,3	2877,2	2925,9	2937,7	2978,7	2956,9	2964,6	-	26,2%
Total Middle East	399,5	424,4	444,2	463,4	492,6	533,2	555,1	577,6	613,5	5,9%	5,4%
Total Africa	276,1	281,5	289,1	302,3	318,2	323,5	327,5	341,0	356,0	4,1%	3,2%
India	295,1	296,5	307,8	316,2	343,9	362,2	378,8	409,2	433,3	5,6%	3,8%
China	967,3	1000,6	1058,3	1229,3	1429,0	1572,2	1722,6	1862,8	2002,5	7,2%	17,7%
Japan	510,2	508,7	505,7	506,2	517,0	519,7	520,4	515,8	507,5	-1,9%	4,5%
Total Asia Pacific	2572,8	2638,7	2739,8	2945,8	3227,6	3430,0	3617,9	3816,0	3981,9	4,1%	35,3%
Total World	**9262,6**	**9323,1**	**9502,8**	**9810,5**	**10258,8**	**10555,3**	**10820,8**	**11104,4**	**11294,9**	**1,4%**	**100,0%**
EU	1703,9	1731,9	1717,2	1748,6	1770,1	1771,8	1773,4	1732,2	1728,2	-0,5%	15,3%
OECD	5353,9	5318,8	5356,3	5415,7	5513,0	5551,2	5548,0	5568,3	5508,4	-1,3%	48,8%

Table 1-2

BP Statistical review of world energy: World consumption by fuel.

	2007					2008				
Million tonnes oil equivalent	**Oil**	**Natural gas**	**Coal**	**Nuclear energy**	**Hydro electric**	**Oil**	**Natural gas**	**Coal**	**Nuclear energy**	**Hydro electric**
Total world	3939,4	2652,2	3194,5	622,5	695,8	3927,9	2726,1	3303,7	619,7	717,5

At the present time total annual emissions of GHGs are rising. Over the last three decades, GHG emissions have increased by an average of 1.6% per year with carbon dioxide (CO_2) emissions from the use of fossil fuels growing at a rate of 1.9% per year [3]. Atmospheric CO_2 concentration has increased by almost 100 ppm over its preindustrial level, reaching 385 ppm in 2009 (Fig.1-2).

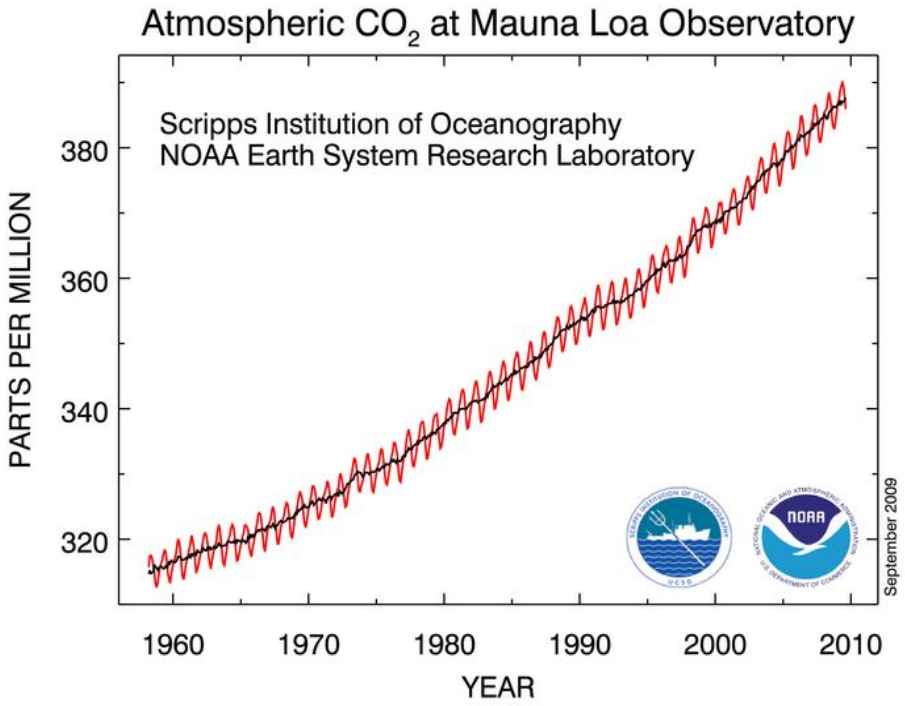

Fig.1-2. The trends in atmospheric concentrations for the greenhouse gas carbon dioxide, CO_2, in ppm (parts per million) from 1958 to present [4].

The largest growth in CO_2 emissions has come from power generation and road transport sectors. Since 1970, GHG emissions from the energy supply sector have grown by over 145%, while those from the transport sector have grown by over 120%; as such, these two sectors show the largest growth in GHG emissions [3].

In absence of modifications of the policy settings currently in force and no special restrictions on the supply of resources, the SRES scenarios (Special Report on Emissions Scenarios) of IPCC (Intergovernmental Panel on Climate Change) projects an increase of baseline global GHG emissions by a range of 9.7 to 36.7 $GtCO_2$-eq (25 to 90%) between 2000 and 2030. In these scenarios, fossil fuels are projected to maintain their dominant position in the global energy mix to 2030 and beyond. Hence CO_2 emissions from energy use between 2000 and 2030 are projected to grow 40 to 110% over that period. For the next two decades a warming of about 0.2°C per decade is projected. Even if the concentrations of all GHGs and aerosols had been kept constant at year 2000 levels, a further warming of about 0.1°C per decade would be expected, with significant changes on all aspects of life and irreversible consequences on the environment [5]. A real revolution in how we produce and consume energy in the world that involves the improvement of energy efficiency,

the development of technologies for renewable energy sources, the nuclear energy and the capture and confinement of CO_2 is necessary.

1.2 Fuel cell technology

An energy system resolutive respect to the potential market instability caused by the exhaustion of fossil fuels, because based on the use of renewable sources, and environmental compatible is the fuel cell. The theoretical principles of a fuel cell date back to early studies in electrochemistry: in the first half of the nineteenth century (1839) Sir William Grove was able to build the first fuel cell. The recognition of the importance of this system, however, is much more recent, dating to the early aerospace missions, while more recent applications concern the study of power and cogeneration. The fuel cell is an electrochemical generator in which a fuel, typically hydrogen, and an oxidant, oxygen or air, enter and that produces continuous electrical power, water and heat.

There are different types of fuel cells, reported in Table 1-3, classified on the basis of the electrolyte used, which greatly affects the operating temperature range, the type of ions and the direction in which they diffuse through the cell, the nature of construction materials, the composition of gaseous reactants, the mechanical resistance and the lifetime of the cell. All these parameters contribute to determine the possible application of the various fuel cells.

A fuel cell typically produces a voltage of about 0.6-0.7 V and currents between 300 and 800 mA/cm^2, then to obtain the desired power and voltage they are usually placed in series to form the so-called multi-cell stack.

Fuel cells, in addition to having a high electrical efficiency, with values ranging between 50 and 60%, may be modular, allowing to increase the installed power demand, with considerable savings in economic terms, have an efficiency independent of plant size and a low environmental impact, which allows to place the facilities in residential areas.

Table 1-3

Fuel cells classification.

Fuel cell	AFC	PEMFC	DMFC	PAFC	MCFC	SOFC
Temperature,°C	60-120	70-100	70-100	160-220	600-650	800-1000
Catalyst	Pt/Pd, Ni	Pt, Pt/Ru	Pt, Pt/Ru	Pt	Ni	-
Fuel	Pure hydrogen (99.99%)	Hydrogen, reformed gas	Methanol	Hydrogen, reformed gas	Hydrogen, reformed gas	Hydrogen, reformed gas
Oxidant	Pure oxygen	O_2 / air	O_2 / air	O_2 / air	O_2 / air	O_2 / air
Electrolyte	Aqueous KOH solution	Solid organic polymer polyperfluoro-sulfonic acid	Solid organic polymer polyperfluoro-sulfonic acid	Phosphoric acid (H_3PO_4)	Liquid solution of lithium, sodium, and/or potassium carbonates	Solid zirconium oxide
Electric efficiency, %	60	40-60	35-40	40-50	45-55	45-60
Power density, mW/cm^2	300-500	300-900	200-400	150-300	150	150-270
Technology state	50-80 kW	1-250 kW	2 kW	Demonstration plant up to 11 MW	Demonstration plant up 2 MW	Stack 25 kW Plant 200 kW
Start-up	minutes	minutes	minutes	1-4 h	5-10 h	5-10 h
Application	Military, space	Electric utility, transportation, portable power	Portable power 1 W- 1kW	Electric utility, transportation	Electric utility	Electric utility

The PEMFCs (Proton Exchange Membrane Fuel Cells) operate by electrochemical oxidation of hydrogen, generating electricity while forming water (Fig.1-3). Compared to other types of fuel cells, PEMFCs generate more power for a given volume or weight of fuel cell. This high-power density makes them compact and lightweight. In addition, the operating temperature is less than 100ºC, which allows rapid start-up, and the use of a solid material as electrolyte allows a simpler construction and reduces problems of corrosion, compared to liquid electrolytes, thus leading to a longer cell and stack life. Fuel cells also permit the realization of vehicles that combine the advantages of low noise and no pollution. These characteristics make the PEMFC the top candidate for automotive power applications, promising alternative to internal combustion engines in a short-medium time perspective, allowing a marked decrease of pollution and CO_2 emissions due to the automotive engines [6].

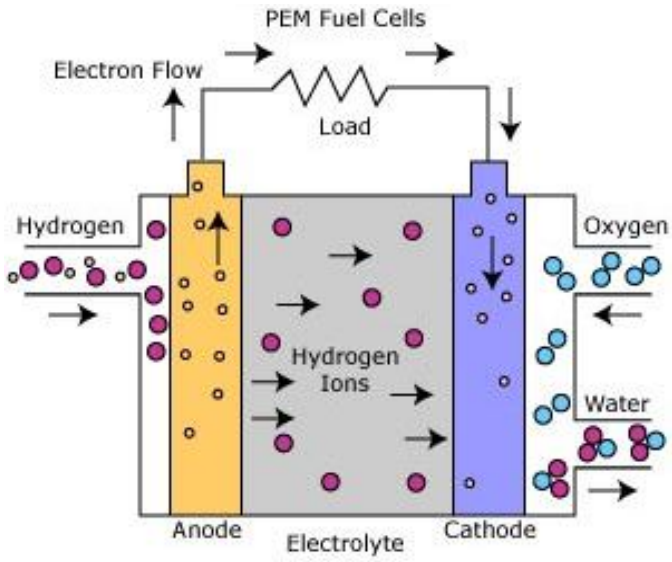

Fig.1-3. PEMFC model

Many fuel cells development projects are currently in action around the world (Fig.1-4) and the major car manufacturers are involved in research programs for the application of fuel cells for automotive power (Daimler, Ford, General Motors, Opel, Hyundai, Mitsubishi, Nissan, Peugeot, Toyota, Volkswagen, Fiat).

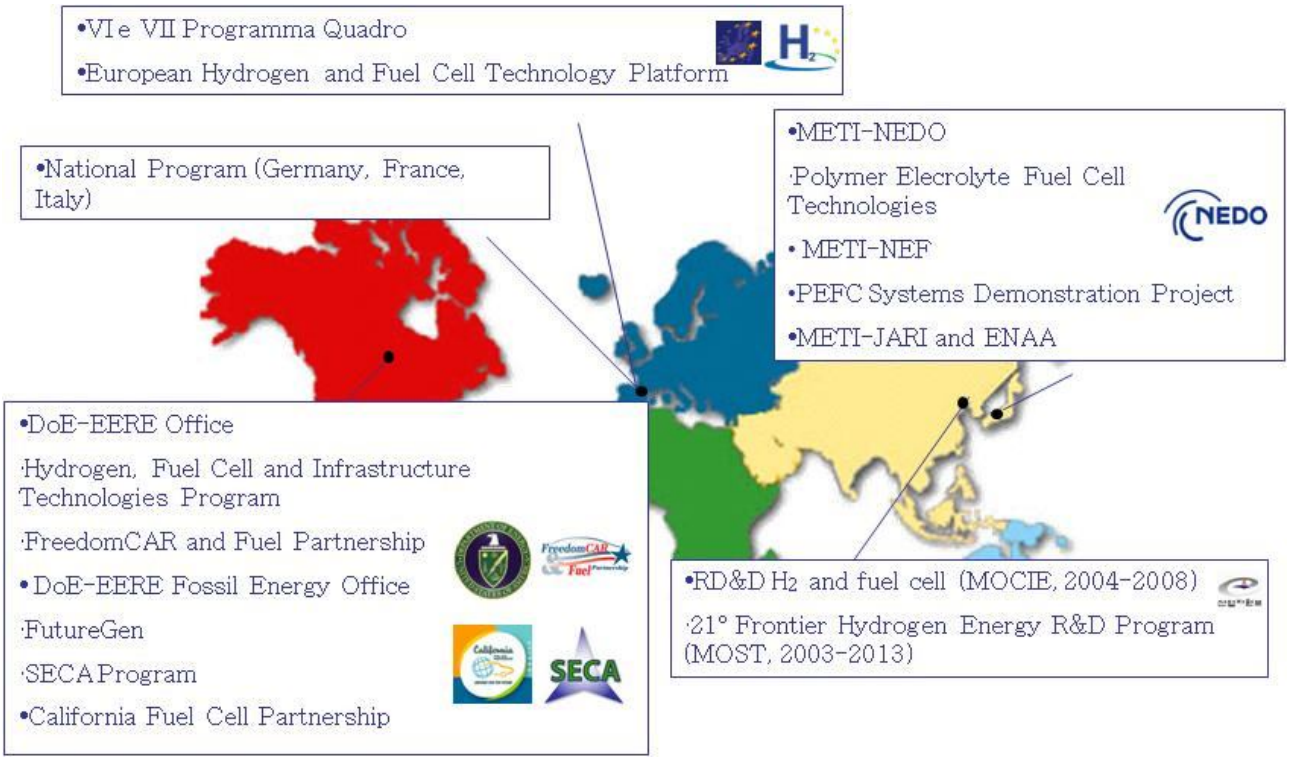

Fig.1-4. Some of principal worldwide fuel cell development projects [7].

The fuel used in a fuel cell vehicle must have technical features and security at least comparable to those of a conventional vehicle: high energy density, ease of production, accumulation and distribution, large availability, toxicity and hazard equivalent to that of other fuels.

Hydrogen is the ideal fuel for cells with polymer electrolyte, because it delivers the best performance. However, the use of hydrogen on a large scale presents problems related to its availability at low cost, the accumulation in vehicles, the creation of adequate distribution facilities. So the application of this technology needs solving the problem of H_2 supply and storage. Various strategies of hydrogen storage, e.g. as liquid (-253°C), as gas compressed (200-700 bar), or in hydrogen storage - materials, such as metal hydrides and carbon nanotubes are possible, but all have disadvantages related to cost of storage and safety.

The choice of the appropriate technology depends on the application and represents a compromise between physical, technological, economic and security features. The requirements for an on board storage system are obviously much more strict than those for a stationary system, since weights and dimensions of the tank are a restriction on the vehicles.

The accumulation in gaseous form is the easiest way to store hydrogen on board, but the most used technology, with steel tanks that operate at pressures below 200 bar, is impractical because of the

low specific energy (0.4-0.5 KWh/Kg) which constitutes a restriction on the vehicle. The development of ultralight tanks with metal or thermoplastic liner, carbon fibre reinforced, capable of operating at higher pressures (350-700 bar) allows considerable progress.

Hydrogen can be stored as a liquid in cryogenic tanks at a temperature of -253 °C. The tanks are designed to minimize transmission of heat from the outside wall to the liquid, and they consist of a double steel jacket in which vacuum is created to prevent the transfer of heat by conduction or convection. The great complexity of the system and the high costs represent a disadvantage of this technology. Liquefying requires approximately 30% of the energy content of fuel, compared to 4-7% of hydrogen compressed.

Hydrogen can also be stored in the form of hydrides, exploiting its ability to create chemically bonds with different metals and metal alloys, penetrating into the metal and occupying the interstitial sites. The most interesting systems are inter-metallic compounds of the type AB5, AB2, AB, materials based on magnesium and alanates. Developments in technology have focused on increasing storage capacity, improving the kinetics of absorption and desorption processes and reducing the costs. A weakness of the technology is represented by the weight of the system, but it is convenient, compact and secure.

In Table 1-4 the current situation of hydrogen storage systems and the stages of development envisaged by NEDO (New Energy and Industrial Technology Development Organisation) are reported [7].

Actually, on-board production of high purity hydrogen from liquid fuels is the most attractive solution to circumvent the problems concerning the storage and handling of H_2 [8]. Several liquid fuel candidates have been discussed for on-board reforming and methanol is considered the most favourable alternative [8,9]. The use of gasoline, that has also been considered, would increase the complexity of the process [10] and cause other disadvantages related to coke formation [11].

A large number of car producers are interested in using methanol as on-board source of hydrogen for its safe handling, low cost and ease of synthesis from a variety of feedstocks [12]. Although mostly produced from natural gas, methanol can also be obtained from renewable sources (“wood alcohol”), thus adding no anthropogenic carbon dioxide to the atmosphere [9,13].

Moreover methanol is recommended as the best source for hydrogen among high energy density liquid fuels, due to the high hydrogen-to-carbon ratio, the lower propensity for soot formation than other hydrocarbons, the relatively low boiling point and the easy storage [14].

Table 1-4

Hydrogen storage roadmap NEDO 2006 [7].

		Hydrogen compressed	Liquid hydrogen	Hydrides at high pressure	Hydrides at low pressure
Today	a	35MPa	3-6 %/day / about 30h	35 MPa	3 MPa
	b	4-5% weight	4 % weight	1 % weight (2.2 %)	0.9 % weight (2 %)
	c	3 Kg	4.3 Kg	7.3 Kg	3 Kg
	d	120 L/ 70Kg	68 L/ 85 Kg	150 L/ 420 Kg	120 L/ 340 Kg
2010	a	70 MPa	1-2 %/day / about 30h	35 MPa	3 MPa
	b	6 % weight	9 % weight	3 % weight (> 4 %)	3.5 % weight (6 %)
	c	5 Kg	5 Kg	5 Kg	5 Kg
	d	120 L/ 75 Kg	80 L/ 50 Kg	100 L/ 165 Kg	110 L/ 145 Kg
2020	a	70 MPa	0.5-1 %/day / about 30h	35 MPa	3 MPa
	b	9 % weight	17 % weight	4 % weight (> 6 %)	4.5 % weight (9 %)
	c	7 Kg	7 Kg	7 Kg	7 Kg
	d	170 L/ 80 Kg	110 L/ 35 Kg	115 L/ 175 Kg	110 L/ 155 Kg

a: tank pressure (Boil-off/Start-up time safety valve)

b: tank gravimetric density (the number in parentheses is relative to the material alone)

c: Hydrogen weight in the tank

d: Hydrogen volume / Tank weight

1.3 Hydrogen from methanol

Hydrogen can be obtained from methanol by different processes: decomposition (Eq.1) [15-17], partial oxidation (Eq.2) [18,19] and steam reforming (Eq.3) [20-24].

Decomposition:

$CH_3OH = CO + 2H_2$ $\Delta H^o = +91$ kJ/mol (1)

Partial Oxidation (POM):

$CH_3OH + ½\ O_2 = 2H_2 + CO_2$ $\Delta H^o = -192.2$ kJ/mol (2)

Steam Reforming (SRM):

$CH_3OH + H_2O = 3H_2 + CO_2$ $\Delta H^o = +49.4$ kJ/mol (3)

The decomposition is a strongly endothermic reaction, producing considerable amount of CO as a by-product, that must be removed since platinum electrodes of PEMFCs are irreversibly damaged even by traces of CO (>20 ppm) [8]. The steam reforming is also endothermic and therefore additional energy supply is necessary, but it can produce H_2/CO_2 in the molar ratio of 3/1 and little amounts of CO below 573 K. The partial oxidation is an exothermic reaction that can produce 2 mol of hydrogen per mole of fuel, but the heat produced could cause sintering of the particles and hence deactivation of the catalyst. Both SRM and POM reactions produce CO as by-product, generally eliminated by preferential oxidation (PrOx), that allows to reduce the CO concentration in the reformed gas from 0.5% - 1% to less than 10 ppm. In alternative to the PrOx reactor, H_2 purification can be obtained in the reforming reactor itself by adding a Pd membrane.
The employment of a further catalytic stage for CO removal [10,25,26], implicates the whole hydrogen production system and reduces its reliability and global efficiency. Therefore it is strongly desired to develop a process for hydrogen production from methanol with high yields and absence of CO.

Recently a new process based on the combination of the POM and SRM reactions, named Oxidative Steam Reforming of Methanol (OSRM) was proposed [21,27-30]. In this process, the ratio of the three reactants can be chosen such that the overall reaction heat is nearly neutral, which means that the heat necessary to maintain SRM is supplied by the POM reaction. This process has the advantage of autothermicity, leading to a more simple system [26], and when performed with proper catalysts and under proper conditions can produce hydrogen containing very low CO concentration [28]. An OSRM system allows to obtain high hydrogen concentration (up to 65% using air as oxidant) and, compared with SRM, has the advantage of a smaller reactor volume and a simpler reactor design [31].

1.4 Catalysts for SRM, POM and OSRM

The formulation of a proper catalyst is the crucial problem of all the researches dealing with hydrogen production from methanol. The research on OSRM catalysts is based on the results obtained for the SRM and POM reactions.

SRM was mainly studied on metallic catalysts: Cu, Ni or noble metals like as Pd, Pt, generally supported on metal oxides. The presence of both Cu and Ni metals seems to increase the catalytic activity [32,33], however Cu promotes the steam reforming reaction whereas Ni prevalently promotes the decomposition of methanol to CO and H_2 [33]. The more recent studies are addressed mainly to catalysts based on metallic copper dispersed on different oxides, like as ZnO, Al_2O_3, ZrO_2 [20,23,24,34], whilst the use of zeolites meets with scarce success [35,36]. ZnO seems to play an important function as promoter by inhibiting copper sintering [20,23,24,34], but also ZrO_2 can improve the catalytic activity [8,20]. More recently some improvement of selectivity was reported for CeO_2 supported catalysts [37,38]. Raney copper [39] and copper based alloys, such as Cu-Zr, Cu-Zr-Pd, Al-Cu-Fe [40,41] were also proposed. Moreover catalysts based on palladium, either alone or alloyed with other metals showed promising results [42,43].

POM was studied on catalysts containing copper supported on ZnO, in which the addition of Al_2O_3 had a beneficial effect on the selectivity and long term stability [44], or palladium supported on ZnO, in which the formation of a Pd/Zn alloy was relevant for catalytic activity [45,46], Pd supported on ZrO_2 [19] or Al_2O_3 or supported rhodium [47,48]. Moreover catalysts derived from hydrotalcite-like layered double hydroxides, obtained by coprecipitation in the presence of Pd(II) [49] and Rh(III) [50], were also reported. New synthesis methodologies aimed at obtaining finely dispersed metal phases have been proposed both for SRM and POM [39,51].

The research on OSRM catalysts is more recent and is limited to the last years of the scientific literature [26,28,52-55]. The catalysts, that are similar to those described for SRM and POM, are generally based on metallic copper dispersed in an oxide matrix such as ZnO [55-58], Al_2O_3 [59], ZnO/Al_2O_3 [26,28,60,61], ZrO_2 [62-65], CeO_2 [66-68], MnO_x [69], Cr_2O_3/Al_2O_3[70], ZrO_2/Al_2O_3 [71], ZnO/ZrO_2 [72,73], $ZnO/CeO_2/Sm_2O_3$ [74], CeO_2/ZrO_2 [75,76]. The active phase is generally obtained through an "in situ" reduction of copper oxide. Similarly to SRM catalysts [20], the role of ZnO as a promoter is well known and is explained by different mechanisms [26,34,77-80]. The catalysts support is generally alumina, that can be partially or completely substituted by zirconia [28]: the support favours the copper dispersion and reducibility [38,81] and can also play a role in the catalysis through adsorption and activation of methanol [82]. It has also been hypothesized that metallic copper and zirconium oxide activate a bifunctional mechanism, similarly to methanol decomposition catalysts [83]. On these catalysts methanol conversions up to 90% can be obtained, however conversions to CO is not negligible.

The use of ZrO_2 as support is of particular interest due to its peculiar characteristics, such as weak acidity and basicity, high thermal and mechanical stability, redox properties, making it more suitable compared to the commonly used Al_2O_3 and SiO_2 supports. Moreover, many authors highlighted a distinctive role of zirconia in determining superior activity in comparison with conventional copper supported catalysts [13,28,72,84].

The synthesis procedures proposed in the literature for Cu/ZrO_2 systems are mainly focused on coprecipitation and impregnation methods [84-90]. Using the impregnation method, a phenomenon of agglomeration of the active phase on the support can occur, especially for high copper concentration, not allowing a high and homogeneous dispersion of active phase. Unlike more conventional methods, the sol-gel synthesis allows mastering the process parameters so to obtain nanocomposites characterised by larger surface areas and higher dispersion degree of the metallic phase (up to the molecular scale) [91-95]. Moreover, some authors [95] reported that the sol-gel synthesis gives more evenly dispersed copper on zirconia support, whereas the formation of copper oxide nanoparticles on zirconia surface is generally observed by using impregnation techniques. Ramaswamy et al. [87], using EPR spectroscopy, managed to identify four types of Cu species into the zirconia matrix: substitutional ions, extra-lattice/interstitial ions, dispersed surface bound ions and CuO cluster. The observation of a specific copper species turned out to be related to both the preparation method and the metal content. The most intimate interaction between copper and the zirconia matrix was observed for the sol-gel prepared materials, namely substitutional and extra-lattice ions were observed only in the copper-containing ZrO_2 samples prepared by sol-gel method,

whereas impregnation and co-precipitation procedure caused the formation of surface bound ions and copper oxide nanoclusters [87]. Copper-containing ZrO_2 catalysts prepared by sol-gel method were characterized by Purnama et al., and they found enhanced catalytic properties in comparison to the commercial catalyst for the steam reforming of methanol [64]. In addition, as reported by Shen et al. [96] Cu based catalysts prepared by conventional methods appear to have relatively low surface area. In spite of the above reported advantages, to our knowledge, no papers in the literature report the use of sol-gel synthesis for the preparation of copper dispersed in zirconia matrix for application in OSRM process.

Recently, new Cu/CeO_2 based catalysts have been considered for SRM and OSRM [38,97-100]. These systems have interesting catalytic properties due to the high oxygen mobility of CeO_2, high dispersion of metallic Cu and strong metal-support interaction (SMSI) [99-103]. The formation of a solid solution $Ce_{1-x}Cu_xO_{2-x}$ can lead to highly dispersed Cu metal particles after reduction [38]. These catalysts were studied for several oxidation processes such as water gas shift (WGS) [104,105], low-temperature carbon monoxide oxidation [106-108], phenol wet oxidation [109]. Moreover they appeared particularly active and selective for the CO-PROX process [110-114]. This suggests that the presence of CeO_2 in Cu based catalysts should lead to a significant suppression of CO formation in OSRM. Moreover other advantages can be expected: the presence of ceria hindering Cu sintering can enhance the thermal stability [115] and can also increase the long term stability because the oxygen storage capacity of CeO_2 favours coke gasification [98]. Cu/CeO_2 catalysts can be prepared by different methods, that is impregnation, co-precipitation, sol–gel synthesis, hydrothermal synthesis, decomposition or combustion of suitable precursor compounds: catalytic properties depend strongly on the preparation procedure of the precursor oxides [38,101,116-118]. The majority of metal based industrial catalysts are usually prepared by impregnation of a porous refractory oxide with solutions of the desired metal salts, followed by thermal treatment. Nevertheless, during the thermal treatment, that must follow the impregnation, a high percentage of pores is usually obstructed by the active phase particles, with a consequent severe decrease of the surface area. In this context, a noticeable improvement can be obtained using supports based on high surface area structurally organized mesoporous oxides. There are, in fact, several studies which report typical phenomena attributable to the regular mesopore system, that appear to influence the catalytic activity [119,120]. A new surfactant-assisted single-step sol–gel method for the preparation of Cu/Ce catalysts supported on alumina [114] allowed to obtain oxide systems characterized by a structurally organized mesoporosity, with high surface area and good thermal stability, exhibiting interesting catalytic activity for the PrOx reaction [114].

Recently several studies on the characterization of redox properties and copper dispersion of supported copper catalysts were reported.

Copper dispersion is usually measured by the N_2O passivation method or CO adsorption and it appears to be influenced by the alumina content [28] and preparation method.

The results of studies on the redox properties are different and sometimes contradictory. There are few information about the oxidation state of copper during and after the reaction and it is not clear what oxidation state of copper is required to activate OSRM. XPS technique is usually used to characterize the oxidation state of copper before and after reduction with H_2 and after the OSRM reaction. Velu et al. [52] reported the presence of Cu(I) and Cu(0) after H_2 reduction and Murcia-Mascaros et al. [26] observed the presence of Cu(I) during the reaction. However there is still a debate on the role of the different oxidation states of Cu in OSRM. A post-reaction XPS and TPD characterization of a $Cu/ZnO/Al_2O_3$ catalyst was performed by Raimondi et al. [59] and they found the presence of Cu(0), Cu(I) e Cu(II) in amount depending on the reaction temperature and the O_2/CH_3OH ratio. These authors correlate the catalytic activity with the presence of Cu(0) and Cu(I). Reitz et al. [55] have a different point of view. Using XANES measurements on $Cu/ZnO/Al_2O_3$ catalysts, they hypothesize that Cu(0) is active for methanol reforming, Cu(II) for methanol combustion, while Cu(I) is inactive. It is clear that metallic copper is necessary for the catalytic activity, but also some oxidized copper species have an important role.

Therefore, one important step, after preparation and calcination of the precursor material and prior to catalysis, is the reduction of copper oxide. The reduction behaviour of copper oxide is thereby dependent on the precursor phases, loading and dispersion, the calcination temperature, the interaction of copper oxide with the support, the copper oxide particle size and morphology [121].

In any case, an examination of literature indicates that some aspects need further investigation: the nature and the oxidation state of copper species having catalytic activity are still uncertain, the role of oxide phases (ZnO, $CuAl_2O_4$, Al_2O_3, ZrO_2, CeO_2) and the influence of heat treatment have been little investigated.

The network of the reactions occurring in OSRM process is very complex and not yet defined. In the reacting system, besides SRM and POM, combustion and decomposition of methanol and water-gas shift reactions can also occur [24,55]. An open question is if the carbon monoxide is formed by decomposition of methanol or by the inverse of the water-gas shift reaction or by decomposition of oxygenate products, like as formaldehyde [20,24,45,46,122]. Kinetic studies are still few and the nature of the active sites and reaction mechanisms are widely debated. It seems that methanol forms a methoxide species adsorbed on OH groups [28] or on oxidized copper species

[123]. Methoxide is subsequently dehydrogenated by metallic copper and then decomposed to CO_2 and H_2 [24,28,123]. A further discussion concerns the rate determining step. For example in [33] it is hypothesized that the rate determining step is the dissociation of methanol OH bond, whilst in [24] the dehydrogenation of methoxide group. Kinetic models that have been proposed are prevalently of semi-empirical type [24,123].

1.5 Sol-gel technology

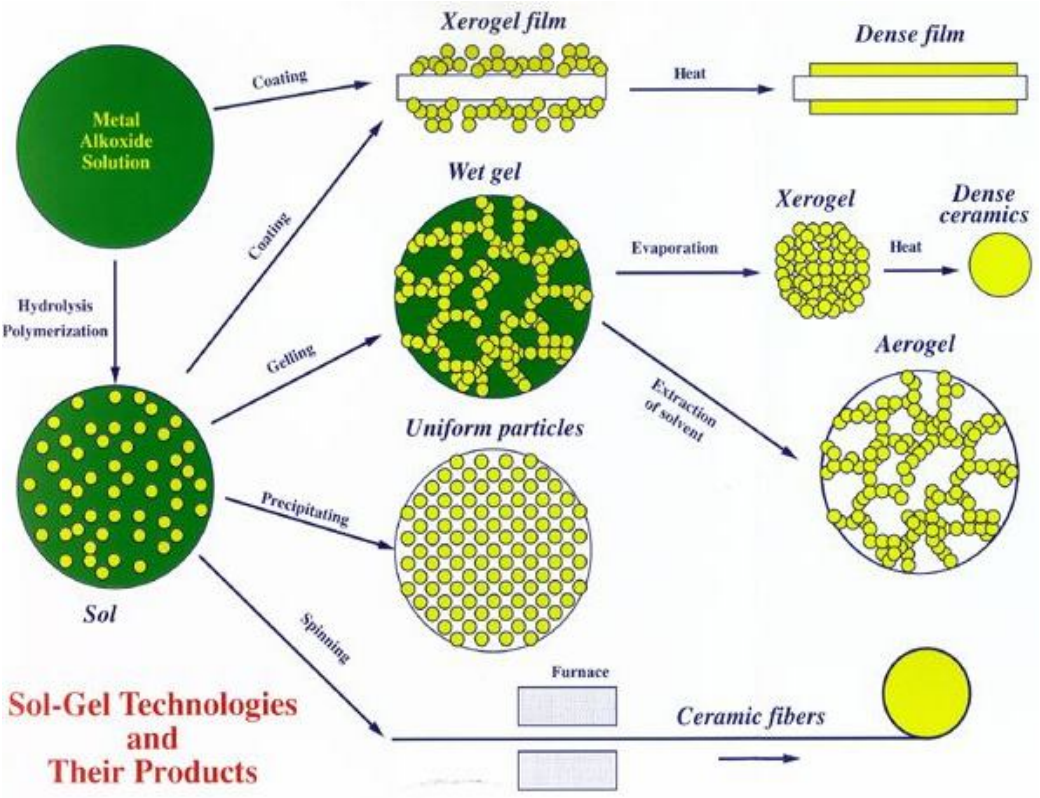

Fig.1-5. Sol-gel process

The sol-gel synthesis technique involves the transition of a system from a colloidal liquid, named sol, into a solid gel phase [124-126].

This process is one of the most studied and used technique for the production of glassy and ceramic materials of high quality. The interest in this technology is stimulated by the extreme versatility of this method that is highly controllable, having many advantages compared to traditional methods.

The sol-gel technique allows to prepare, at relatively low temperatures, materials based on organic and inorganic oxides with the desired hardness, chemical resistance, porosity and thermal resistance. The sol-gel technology allows to prepare materials in a wide variety of forms: ultra-fine or spherical shaped powders, thin film coatings, ceramic fibres, microporous inorganic membranes, monolithics, or extremely porous aerogels, with the desired hardness, chemical resistance, porosity and thermal resistance. An overview of the sol-gel process is illustrated in Fig. 1-5. This technique offers many advantages among them the low process temperature, the ability to control the composition on molecular scale and the porosity to obtain high surface area materials, the homogeneity of the final product up to atomic scale. Moreover, it is possible to synthesize complex composition materials, to form higher purity products through the use of high purity reagents and to provide coatings over complex geometries [124-126]. The starting materials used in the preparation of the sol are usually inorganic metal salts or metal organic compounds, that by hydrolysis and polycondensation reactions form the sol [124-126]. When the sol is cast into a mould, a wet gel will form. By drying and heat-treatment, the gel is converted into dense ceramic or glass materials. If the liquid in a wet gel is removed under a supercritical condition, a highly porous and extremely low density aerogel material is obtained. As the viscosity of a sol is adjusted into a suitable viscosity range, ceramic fibres can be drawn from the sol. Ultra-fine and uniform ceramic powders are formed by precipitation, spray pyrolysis, or emulsion techniques.

1.5.1 Sol-gel chemistry

The sol-gel method can be schematically describes as follows:
1) Preparation of colloidal solutions of alkoxides $M(OR)_n$ (where M indicates the element with valency n and OR is an alkoxide group) as reagents in the reactions of hydrolysis and polycondensation for the formation of the gel.
2) Transformation of the product obtained in step 1 (wet gel) in the dried product (dry gel).
3) Heat treatment of the dry gel in order to obtain the material with the desired features.

Alkoxides, $M(OR)_n$, are usually used as precursors for the preparation of catalysts via sol-gel, because they exhibit useful properties to control the chemical synthesis of oxides:

- easy to purify, a lot of alkoxides can be distilled in order to obtain highly pure products;

- wide variety, it is possible to choice R among a large number of alkylic groups in order to obtain the required reactivity;
- possible control, of the alkoxides hydrolysis and the polycondensation of hydrolysed species;
- mixed alkoxides, as a further control means of the stoichiometry and homogeneity of the final products.

The transition from sol to gel involves two key steps, such as hydrolysis and polycondensation reactions. The hydrolysis takes place also by small amounts of water. Because water and alkoxides are immiscible, a mutual solvent such as alcohol is normally used as a homogenizing agent.
Hydrolysis can be described by Eq.4

$$M(OR)_n + H_2O \rightarrow M(OR)_{n-1}(OH) + ROH \qquad (4)$$

For this reaction, in which an alkoxide group is replaced by a hydroxyl group, a mechanism of nucleophilic substitution is considered. It consists, in the absence of a catalyst, in an addition of the nucleophile followed by a proton transfer to the outgoing group and a subsequent removal of the protonated species. The hydrolysis rate depends on many factors. Indeed, the reaction can favourably be promoted by an increase in the charge density on the metal, the number of metal ions bridged by a hydroxo- or oxo-ligand, and the size of the alkyl groups [127,128]. Conversely, inhibition occurs as the number of hydroxo-ligand coordinating M increases or when pH, temperature, or water and solvent amount tend to favour the reverse reaction (esterification).
As concerns the metal oxides, due to high oxygen electronegativity compared to the metal, the M-O-M bonds are generally highly polarized and the hydrolysis rates are high. On the contrary, the hydrolysis rates of non-metal alkoxides (M = Si, P, Ge..) are slower.
This aspect is very important for multi-component systems (mixed oxides) where the different hydrolysis rates of the precursors give to different gelation times, by means of homo-condensation instead of hetero-condensation, with formation of M-O-M and M'-O-M' instead of M-O-M' linkages. In this case a non-homogeneous gel is formed.
Many solutions can be adopted to solve the above problem:

- modification of the hydrolysis rate of the more reactive precursor using reaction inhibitors (for example chelants);

- use of double alkoxides, with precise stoichiometry;
- modification of the hydrolysis rate of the slower precursor by a catalyzed pre-hydrolysis (acid or basic).

At the same time, the polycondensation occurs. Alkoxide molecules, partially hydrolysed, can react with each other or with alcohol molecules to form oligomers with different molecular weight and of course water (Eq.5) or alcohol ROH (Eq.6) as reaction products:

$$M(OR)_{n-1}(OH) + M(OR)_{n-1}(OH) \rightarrow (RO)_{n-1}M\text{-}O\text{-}M(OR)_{n-1} + H_2O \quad (5)$$

$$M(OR)_n + M(OR)_{n-1}(OH) \rightarrow (RO)_{n-1}M\text{-}O\text{-}M(OR)_{n-1} + ROH \quad (6)$$

If the polymers contain only alkoxyl as terminal groups, the polycondensation reaction will stop. The presence of terminal hydroxyl groups allows, instead, a continuation of the polycondensation reaction, allowing the growth of the oxide lattice.
An equation that allows to describe the reactions of alkoxide hydrolysis and polycondensation, for a tetravalent metal M, taking into account the nature of the polymer gel can be written as:

$$nM(OR)_4 + (2n+(x-y)/2)H_2O = M_nO_{2n-(x+y)/2}(OH)_x(OR)_y + (4n-y)ROH \quad (7)$$

where n is the number of monomer units that react, while x and y represent respectively the number of terminal hydroxyl and alkoxyl groups interrupting the polymer chain [129].

The gel state is best described as a viscoelastic material composed of interpenetrating solid and liquid phases [129]. Its structure is strongly dependent on the water content in the system and on the catalysis nature. In acidic solution or for low water concentration, weakly crosslinked linear chains are produced (Fig.1-6a), resulting in a soft gel which can be readily redispersed in solution. On the other hand, in based-catalyzed solutions, branched clusters are preferentially formed (Fig.1-6b) and their tendency to coalesce is responsible of the solution gelation [130,131].

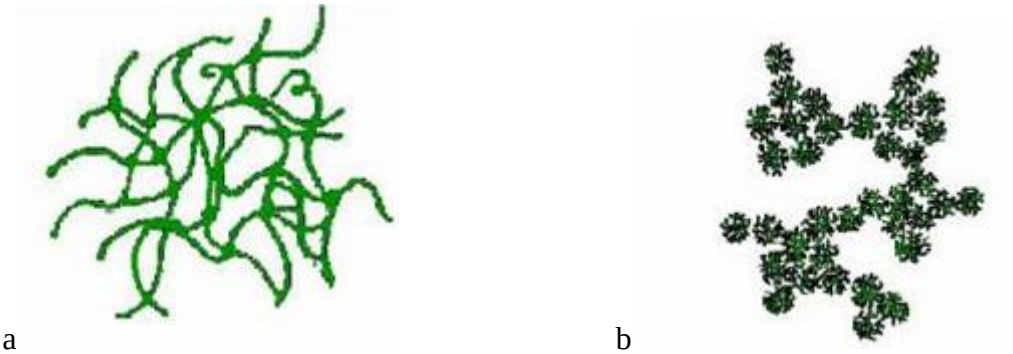

Fig.1-6. Gel structure: a crosslinked linear chains; b branched clusters.

The wet gel obtained from the reactions of alkoxide hydrolysis and polycondensation is then subjected to a drying process and an appropriate heat treatment to obtain the material with the required features. The transformation of the polymeric gel (wet-gel) into the dried product (dry-gel) is obtained by removal of the residual liquid phase, consisting essentially of water and alcohols, using a mild heating at temperatures below 100 °C. This transformation involves a strong decrease in linear dimensions of the gel producing a porous solid (xerogel), which may consist of small pieces or powder, depending on the heating conditions used. Many difficulties arise during the drying stage, mainly caused by the removal of large amounts of solvent trapped in the polymeric network. The transformation of the wet gel in dried gel leads to a volume decrease, and it is often associated with the formation of cracks. To minimize these effects, gels are dried by slow heating rate. The subsequent heat treatment depends on the desired product. During this treatment the condensation of residual alkoxyl groups inside and on surface of the gel can occur. Generally, the differential thermal analysis (DTA) is used to determine the nature and the temperatures of reactions that may occur during the heating of the gel. In this way, information on the heat treatment that must be applied to the wet gel to obtain the product with the desired features can be collected. An appropriate variation of the experimental conditions of synthesis in each of these stages allows the control of chemical and physical properties of the finished product. This high flexibility makes sol-gel an attractive technique also in the synthesis of catalysts.

1.6 Outline of the work

Literature data allow to conclude that catalysts with activity and selectivity adequate to a technological development of the OSRM process have not yet been obtained. It is needed therefore to go deep into the research by studying systems that have been partially investigated, with the aim of improve their performances, and at the same time to widen the research field to new systems. At the same time considerable uncertainty about the reactions network and the kinetics of the reaction of interest appears in the literature. Therefore the development of a new technology for the production of hydrogen for fuel cells by the OSRM process requires a research on new catalysts and on the kinetics of the reacting system.

In this work Cu/ZrO_2 and $Cu/CeO_2/Al_2O_3$ catalysts prepared by modified sol-gel methods are studied with the aim of investigating the possibility of employing these systems as selective catalysts for the OSRM process. Both preparation methods involve the direct incorporation of the metal salt into the synthesis gel used to prepare the support, allowing to obtain more homogeneously dispersed mixed oxides samples. Moreover the preparation method of $Cu/CeO_2/Al_2O_3$ catalysts is a totally new sol-gel approach, in which metal salts (stearates) are used both as Cu and Ce sources and as structural directing agents, thus allowing to obtain catalysts with an organized mesoporosity and a very narrow pore size distribution.

The research activity concerns the study of catalytic activity for SRM and OSRM and the characterization of physical and chemical properties of the catalysts.

The characterization measurements concern structural, morphological and surface chemical properties that can play an important role in catalytic activity, i.e. surface specific areas, pore volume, pore size distribution, thermal stability, dispersion and reducibility of the metallic phase.

The materials prepared were characterized for physical and surface chemical properties by chemical analysis, X-ray diffraction, nitrogen adsorption, differential thermal analysis, XPS, TPR and N_2O dispersion as described in Chapter 2.

X-ray diffractometry (XRD) was useful for identification of the phases present in as prepared or thermally treated materials. Nitrogen adsorption at 77K allowed to determine isotherms, surface areas and pore size distribution. Simultaneous differential thermal analysis (TG-DTA) was employed in order to evidence eventual phase transitions and obtain information on the stability of materials, in connection with the temperatures at which the studied reactions will be carried out. XPS was used to identify the oxidation state of copper before and after the reaction. The characterization of redox properties was carried out by Temperature Programmed Reduction (TPR) technique and the copper

dispersion was evaluated by N_2O passivation. The results of all these measurements are presented in Chapter 3.

In Chapter 4 the catalytic activity study is presented with the following main goals:

-to identify the best catalyst formulation and the best preparation method;

-to identify the catalysts with high activity and selectivity to be considered of potential interest for OSRM process;

-to identify the optimal operating conditions, i.e. temperature, catalysts heat pre-treatment.

In Chapter 5 a new experimental plant, that allows pre-treatments and in situ characterization of the catalysts before and after each catalytic test and on-line analysis of the products by mass spectrometry, was used in order to investigate the effect of the reaction conditions on the Cu oxidation state and the oxidation state of copper species having catalytic activity.

2 Experimental

2.1 Materials Cu/ZrO_2

2.1.1 Reagents

Zirconium(IV) propoxide, $Zr(OCH_2CH_2CH_3)_4$ ($Zr(OPr)_4$), 70 wt % solution in 1-propanol from Aldrich, 1-propanol ≥ 99.80 % from Aldrich (Pr(OH)), anhydrous ethanol (Et(OH)), copper (II) nitrate hydrate, $Cu(NO_3)_2 \cdot 2.5H_2O$, 99.999 % from Aldrich, copper (II) acetate monohydrate, $Cu(CH_3COO)_2 \cdot H_2O$, 98+ % from Aldrich, acetylacetone 99 + % from Aldrich (Acac), acetic acid glacial from Carlo Erba (Hac), doubly distilled water were used for all preparations.

2.1.2 Preparation of catalysts $NZrCu_6$, $AZrCu_7$, $AZrCu_{14}$

Copper–zirconium mixed oxides nanocomposite containing 4.5 % wt - 8.3 % mol (*$NZrCu_6$*), 5.5 % wt - 7.8 % mol (*$AZrCu_7$*), 11 % wt - 14.7 % mol (*$AZrCu_{14}$*) of Cu were prepared by sol-gel method according to the procedures described in the flow-charts (Figs. 2-1 and 2-2). Zirconium propoxide was used as Zr source, whilst two different salts, $Cu(NO_3)_2 \cdot 2.5H_2O$ and $Cu(CH_3COO)_2 \cdot H_2O$ were used as copper source in order to identify the best precursor. Zirconium alkoxides show a very high reactivity towards the hydrolysis-condensation reactions due to the great polarity of Zr-O bond that in turn generate a positive partial charge on the zirconium atom, making it very susceptible to nucleophilic attack [132]. Therefore acetylacetone (acac) or acetic acid glacial were used to control the hydrolysis reaction rate of zirconium propoxide [133,134].

Method I: Preparation of catalyst $NZrCu_6$

Operating in a dry box, a solution of $Zr(OC_3H_7)_4$ (40 mL) in 52 mL of anhydrous 1-propanol was prepared and 4.6 mL of acetylacetone was added to control the hydrolysis reaction. 8.08 mmol of $Cu(NO_3)_2 \cdot 2.5H_2O$ dissolved in 60 mL of 1-propanol was added to the solution of $Zr(OC_3H_7)_4$ under continuous stirring for 60 min at room temperature. Finally a mixture of water and 1-propanol with a volume ratio water/alcohol =1/8 was added. Complete gelation occurred at room temperature in 30 minutes.

Method II: Preparation of catalysts $AZrCu_7$, $AZrCu_{14}$

Operating in a dry box, a solution of $Zr(OC_3H_7)_4$ (20 mL) in 42 mL of anhydrous ethanol was prepared and 4 mL of acetic acid glacial was added as alkoxide modifier. 4.5 mmol (*$AZrCu_7$*) or 10.12 mmol (*$AZrCu_{14}$*) of $Cu(CH_3COO)_2 \cdot H_2O$ was added to the solution of $Zr(OC_3H_7)_4$ under continuous stirring for 60 min at room temperature. Finally a mixture of water and ethanol with a volume ratio water/alcohol =1/4 was added. Complete gelation occurred at room temperature in 2 days.

The gels obtained by *Method I* and *Method II* were kept two days at room temperature and then dried in an electric oven at 150°C for 1 day. The catalysts were obtained after thermal decomposition of the precursors in air at 340°C for 2 h (heating rate of 10 °C min^{-1}) and subsequent reduction in situ with 2% H_2/Ar mixtures at 300°C or 450°C for 2 h. The calcination temperature of 340°C was selected to completely remove the organic material as indicated by TG/DTA analysis (see *Section 3.1.1*), instead the reduction temperature of 300°C was chosen to completely reduce the copper oxide to metallic copper according to TPR data (see *Section 3.1.3*), avoiding the sinterization of metallic Cu. However also the reduction temperature of 450°C was employed because this temperature, being higher than the operating range of the OSRM tests, ensured a higher stability of the catalysts under reaction conditions.
Hereafter, the notation used for the samples is referred to the copper precursor used for the preparation and the relative weight percentage of copper oxide in the catalyst: $NZrCu_6$ is a CuO-ZrO_2 sample containing 5.6 wt.% of CuO, prepared by *Method I* using copper nitrate as precursor, while the $AZrCu_7$ and the $AZrCu_{14}$ samples, prepared by *Method II* using copper acetate as precursor, contain respectively 6.8 wt% and 13.8 wt.% of CuO.

.

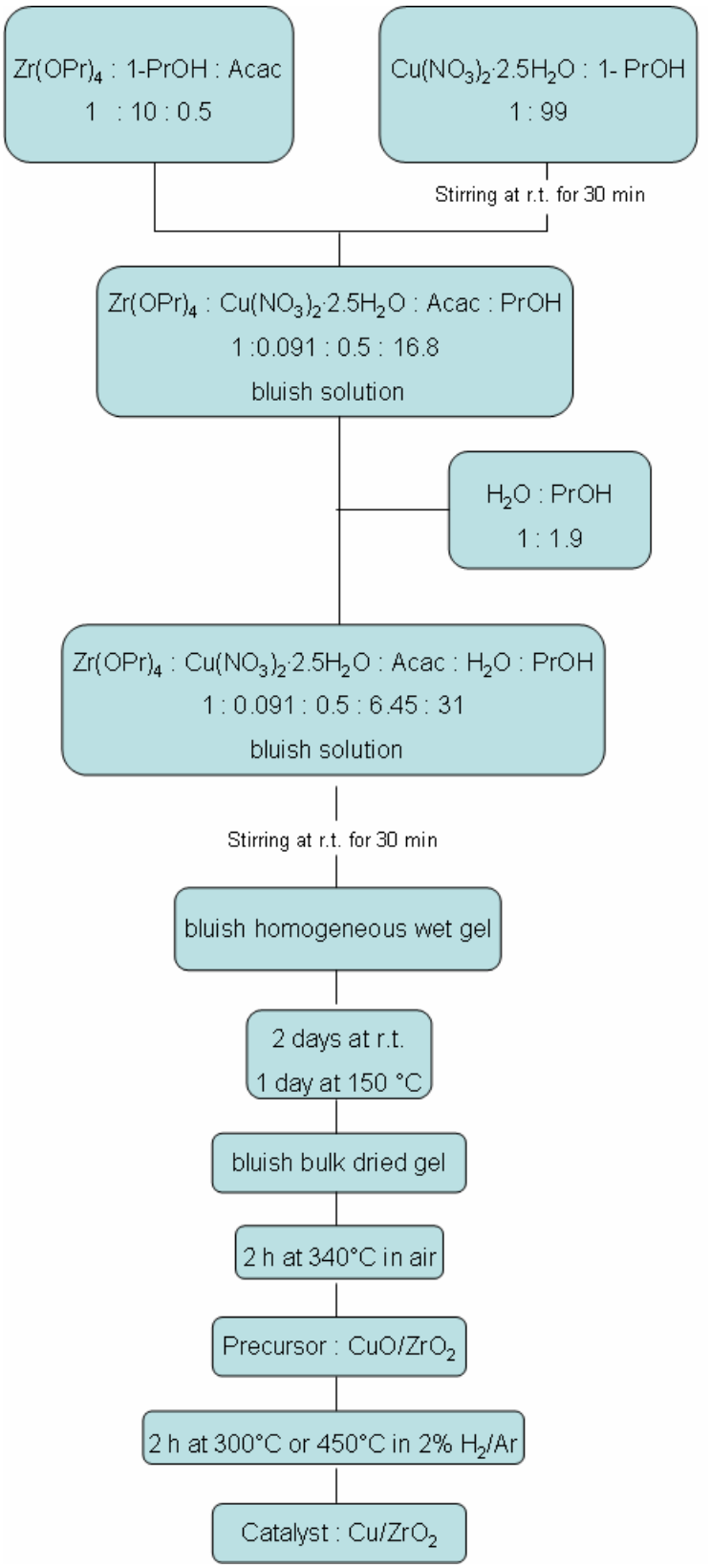

Fig.2-1. Flow-chart of the synthesis procedure showing the molar ratios employed for $NZrCu_6$.

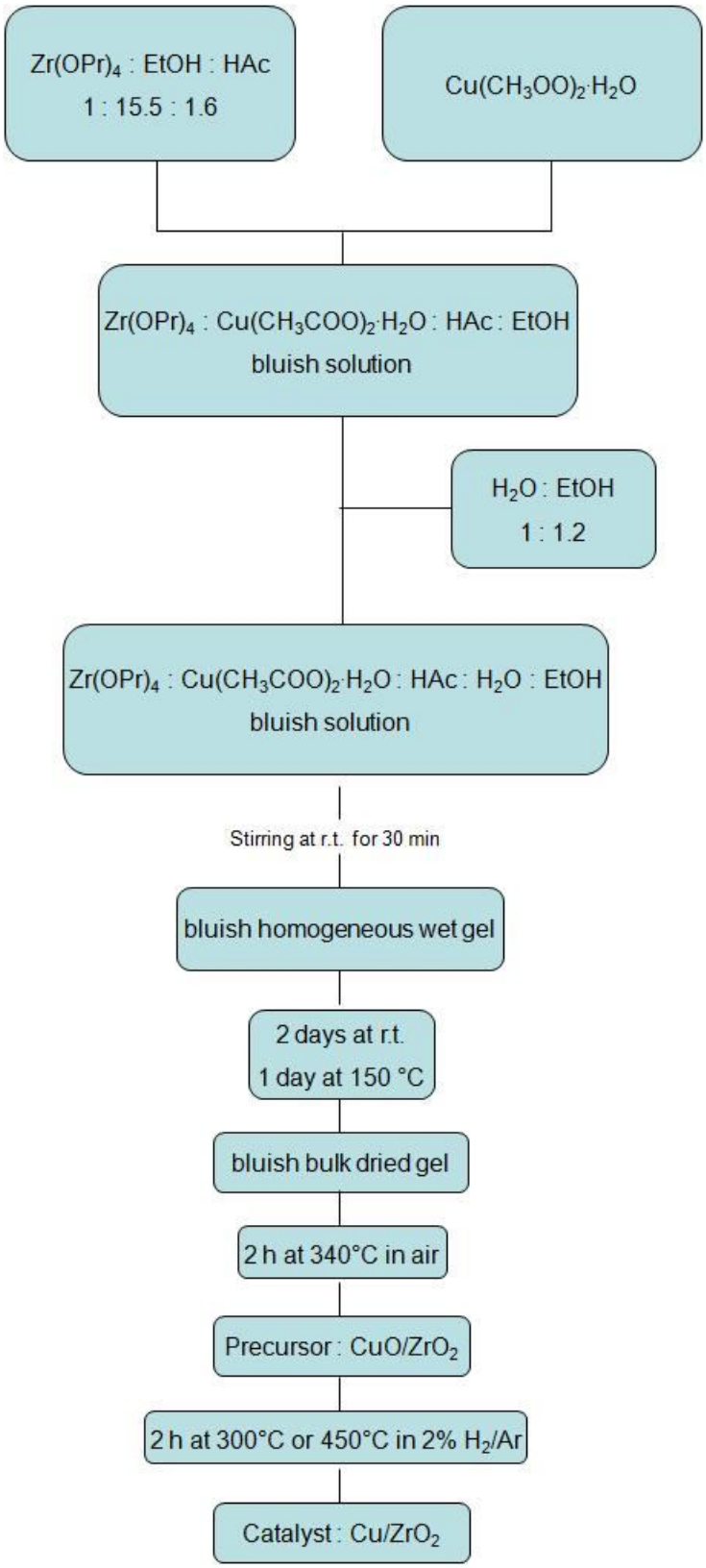

Fig.2-2. Flow-chart of the synthesis procedure showing the molar ratios employed for $AZrCu_7$ and $AZrCu_{14}$.

2.1.3 Preparation of ZrO_2 reference samples

Since the activity of these catalysts seems to be critically determined by the phase structure of ZrO_2 as well as by the nature of interaction between copper and zirconia, pure zirconia gel-derived samples were synthesised by hydrolysis of $Zr(OPr)_4$ in the same conditions described above in *Method I* and *Method II*, in order to study the extent of copper-zirconia interaction obtained by the sol-gel procedure used and to establish how the metallic phase influences the crystallisation behaviour of the matrix and, at the same time, how the dispersion degree and the reducibility of copper species are influenced by the crystallisation extent of the selected matrix and its surface area. The notation used for these samples is $NZrO_2$ for zirconia prepared by *Method I* and $AZrO_2$ for that obtained by *Method II*.

In Table 2-1 the composition of catalysts and reference samples is reported.

Table 2-1
Elemental composition of the catalysts and reference samples.

	Composition, %wt		
Sample	Cu	CuO	Zr
$NZrO_2$-$AZrO_2$	-	-	73.0
$NZrCu_6$	4.5	5.6	69.9
$AZrCu_7$	5.5	6.8	69.0
$AZrCu_{14}$	11.0	13.8	63.8

2.1.4 Characterization of precursors and catalysts

Thermogravimetric/differential thermal analyses (TG/DTA) were carried out by using a Netzsch simultaneous thermoanalyser STA 409C with Al_2O_3 as reference material. The STA curves, recorded in air from room temperature up to 1200 °C at a heating rate of 2 °C min^{-1}, were carried out on 50 mg of the dried gel. The studied samples were prepared by heating at 10 °C min^{-1} to the required temperature and then held at this temperature for the time selected.

The amorphous nature of the dried gels as well as the nature of the crystallising phases was ascertained by X-ray diffraction with a Philips X'PERT diffractometer by using monochromatised

CuKα radiation (40 mA, 40 kV) with a step width of 0.02° 2θ, and 1 s data collection per step. The mean ZrO_2 particle sizes were determined from the line broadening of the diffraction lines at 2θ = 50.4° and 30.2° (for tetragonal phase), using the Scherrer equation. The lattice parameters of the ZrO_2 tetragonal phase (space group P 42/n m c) were evaluated by X'PERT Plus software.

N_2 adsorption-desorption isotherms at -196 °C were obtained with a Micromeritics Gemini II 2370 apparatus. The sample was previously treated at 250°C for 2h under N_2 flow. Surface areas were calculated by the BET and α-plot methods. The accuracy of surface areas values was ±5%. Pore volumes were determined from the amounts of adsorbed N_2 at P/P° = 0.98 (desorption curve), assuming the density of liquid N_2 (0.807 g cm^{-3}) under these conditions. Micropore volumes were calculated from α-plots. For the application of this method, the N_2 adsorption isotherm of a non-porous ZrO_2 sample was used as reference. Since no isotherm of this kind was available from literature, it was obtained from experimental measurements on a non-porous ZrO_2 sample prepared *ad hoc* in the laboratory by the same procedure as described above, followed by treatment at 800°C for 2 h. The reference isotherm of ZrO_2 is reported in Fig. 2-3 in terms of α vs P/P^0 , where α is:

$$\alpha = \frac{V_{N_2}\,adsorbed}{V_{N_2}\,adsorbed}\;\overline{at}\;\frac{}{P/P^o = 0.4} \qquad (8)$$

For comparison, the corresponding normalized isotherm of SiO_2 derived from standard data is also reported [135]. It can be observed that the zirconia isotherm is slightly different from that of standard SiO_2 and corresponds to a constant c = 60 in the range of validity of the BET model, against the value c = 172 for SiO_2. This would indicate a weaker adsorption of N_2 on ZrO_2 compared to that on SiO_2.

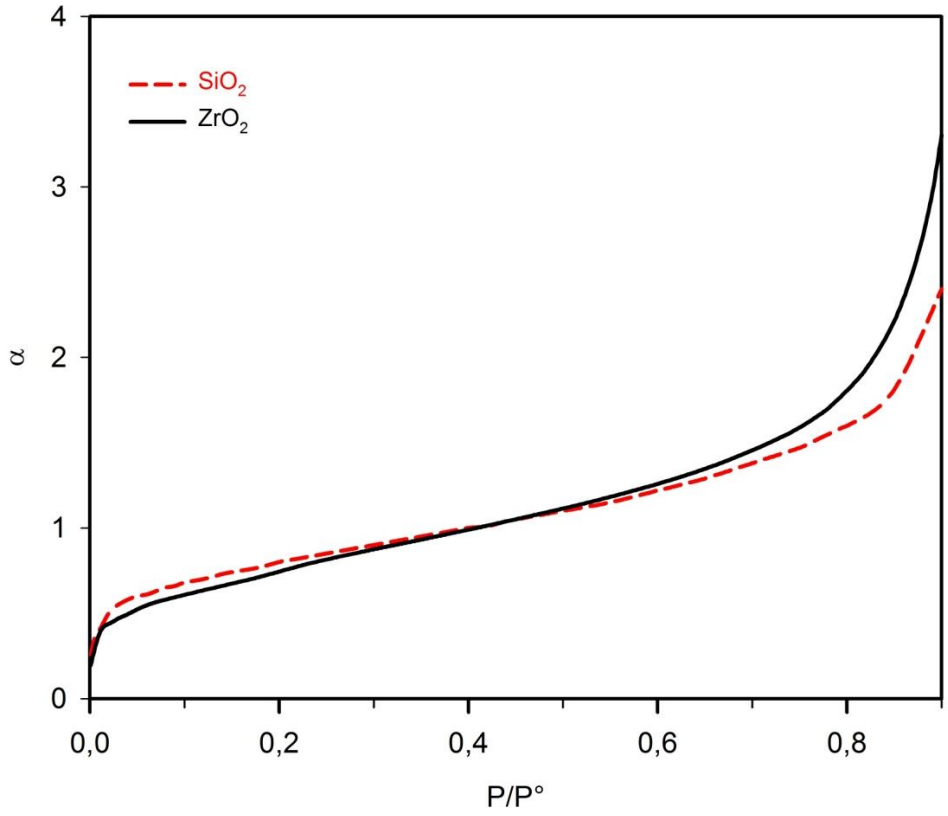

Fig.2-3. N_2 adsorption isotherm of a non-porous ZrO_2 sample at 77 K compared to the corresponding isotherm of non-porous SiO_2. Data of SiO_2 are derived from ref. [135].

TPR measurements were carried out on samples treated in air flow at 340 °C using a 2% H_2/Ar mixture and a heating rate of 10 °C min^{-1} with a Micromeritics 2900 apparatus.

Copper dispersion was measured by the N_2O passivation method [136] using a Micromeritics 2900 apparatus. The method has the advantage of simplicity and gives satisfactory results when special attention is paid to avoid the presence of oxygen in the gaseous streams [136].

The method involves the following steps:

1) treatment in air flow at 340°C;

2) reduction with hydrogen: first TPR (2 % H_2/Ar mixture, 10°Cmin^{-1} from 20 to 300°C or 450°C);

3) treatment in N_2O flow at 60°C;

4) reduction with hydrogen: second TPR (2 % H_2/Ar mixture, 10°Cmin^{-1} from 20 to 600°C).

The first TPR (step (2)) gives the total amount of reduced Cu, through integration of the TPR peaks. The treatment (3) causes the oxidation of metallic Cu to Cu_2O that, under the mild conditions employed, is limited to surface Cu atoms:

$2Cu_{(surf)} + N_2O \rightarrow Cu_2O_{(surf)} + N_2$

In the following step (4) $Cu_2O_{(surf)}$ is reduced:

$Cu_2O_{(surf)} + H_2 \rightarrow 2Cu_{(surf)} + H_2O$

From the amount of H_2 consumed in step (4), the amount of $Cu_{(surf)}$, and then the Cu dispersion=100x$Cu_{(surf)}$/Cu total, are calculated. Both Cu surface areas and Cu particle sizes can be calculated assuming a surface Cu concentration of $1.47 \cdot 10^{19}$ atoms m^{-2} [137].

2.2 Materials $Cu/CeO_2/Al_2O_3$

2.2.1 Reagents

All the materials used in this work are Aldrich products and no further purification was carried out. Cu(II) and Ce(IV) octadecanoates (Cu(II) and Ce(IV) stearates) were prepared analogously to what described in literature for nickel octadecanoate (Ni(II) stearate) [138] as described in [139].

2.2.2 Preparation of catalysts $EMCeCu_4$, $EMCeCu_8$, $EMCeCu_{16}$

Copper–cerium-aluminium mixed oxides nanocomposites containing 3.4% wt ($EMCeCu_4$), 6.6% wt ($EMCeCu_8$), 12.9 % wt ($EMCeCu_{16}$) of Cu were prepared by sol-gel method according to the procedure described in the flow-chart (Fig. 2-4).
The new surfactant-assisted single-step sol–gel method for the preparation of Cu/Ce catalysts supported on alumina [139] allows to obtain systems characterized by a structurally organized mesoporosity, a high surface area and a narrow pores distribution using aluminium tri-sec-butoxide as alumina source, octadecanoic acid as chemical template and Cu(II) and Ce(IV) stearates both as Cu-Ce sources and as structural directing agents.
The following molar ratios were used: 1 $Al(sec\text{-}BuO)_3$: 0.053 $(C_{17}H_{35}COO)_3Ce$: 0.036 or 0.072 or 0.144 $(C_{17}H_{35}COO)_2Cu$: 24 $n\text{-}C_3H_7OH$: 3 H_2O.
In a typical synthesis, the required amount of octadecanoic acid (stearic acid) (10.2 g) was dissolved in 1-propanol (193 ml) by sonication. After the addition of deionized water (6 ml) and of Cu(II) and Ce(IV) stearates, prepared in advance, the solution was stirred for 30 min. Successively, aluminium tri-sec-butoxide (26.5 g) was added and the reaction mixture was stirred for further 30 min. The resulting suspension was aged for 50 h in a Teflon-lined autoclave at 100°C and autogenous pressure. After cooling to room temperature, the product was recovered by centrifugation, washed with ethanol and then dried overnight at 50°C.
The resulting materials were thermally treated up to 410°C in nitrogen flow (heating rate 3°Cmin^{-1}), kept at this temperature for 6 h and then heated to 550°C in a stream of air (heating rate 3°Cmin^{-1}) and kept at this temperature for 5 h. The calcination temperature of 550°C was selected to completely remove the organic material as indicated by TG analysis (see *Section 3.2.1*). After calcination, the materials were reduced in situ by heating the samples at rate of 10 °C min^{-1} up to 450°C and then keeping them at 450°C for 2h in a flow of 2% H_2/Ar mixture. The reduction

temperature of 450°C was chosen to completely reduce the copper oxide to metallic copper according to TPR data (see *Section 3.2.4*).

Hereafter, the notation used for the samples is referred to the relative weight percentage of copper oxide in the catalyst: $EMCeCu_4$ is a $CuO\text{-}CeO_2\text{-}Al_2O_3$ sample containing 4.2 wt.% of CuO, while the $EMCeCu_8$ sample contains 8.3 wt% of CuO and the catalyst identified as $EMCeCu_{16}$ contains 16.2 wt.% of CuO.

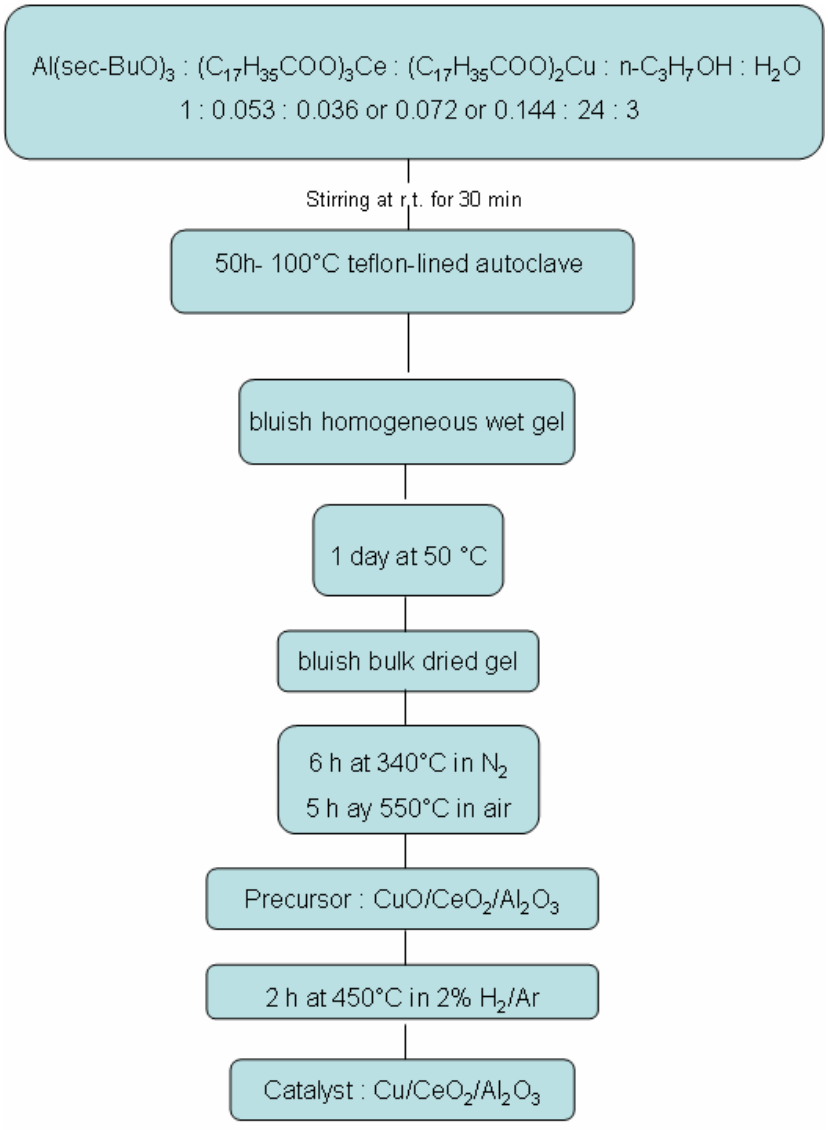

Fig.2-4. Flow-chart of the synthesis procedure showing the molar ratios employed for $EMCeCu_4$, $EMCeCu_8$ and $EMCeCu_{16}$.

2.2.3 Preparation of CeO_2/Al_2O_3 and CuO/Al_2O_3 reference samples

The mesoporous alumina support was prepared following the synthetic procedure reported by Čejka [140], based on the use of aluminium tri-sec-butoxide and stearic acid dissolved in 1-propanol (specific surface area BET = 338 m^2g^{-1} after calcination).

CeO_2/Al_2O_3 and CuO/Al_2O_3 were prepared by impregnation of 5 g of this alumina respectively with 10 ml of an aqueous solution of $Ce(NO_3)_3 \cdot 6H_2O$ or $Cu(NO_3) \cdot 3H_2O$, in order to obtain a Ce loading of 15.0 wt.% and a Cu loading of 5.0 wt.%. The impregnated alumina samples were dried overnight and calcined up to 500°C for 3h in air flow (heating rate 3°$Cmin^{-1}$). After thermal treatment, the sample CeO_2/Al_2O_3 showed a BET specific surface area of 208 m^2g^{-1}, while the sample CuO/Al_2O_3 showed a surface area of 278 m^2g^{-1}. The reference materials CuO (specific surface area BET = 30 $m^2\ g^{-1}$) and CeO_2 (specific surface area BET = 80-100 $m^2\ g^{-1}$) were supplied by Aldrich.

In Table 2-2 the composition of catalysts and reference samples is reported.

Table 2-2
Elemental composition of the catalysts and reference samples.

	Composition, %wt			
Sample	Cu	CuO	Ce	Al
CuO/Al_2O_3	5.0	6.3	-	49.6
CeO_2/Al_2O_3	-	-	15.0	43.2
$EMCeCu_4$	3.4	4.2	11.6	43.1
$EMCeCu_8$	6.6	8.3	11.2	41.1
$EMCeCu_{16}$	12.9	16.2	10.3	37.7

2.2.4 Characterization of precursors and catalysts

Thermogravimetric analysis was carried out with a Netzsch STA 409 instrument. 50 mg of the dried gel was heated in air from room temperature up to 900°C at a heating rate of 10°C min^{-1}.

X-ray diffraction patterns were obtained with a Bragg-Brentano powder diffractometer using CuKα radiation (λ = 1.54184 Å) and a graphite monochromator in the diffracted beam. The samples were disc shaped pressed powders. The average dimension of the crystallites was determined by Scherrer's equation.

N_2 adsorption-desorption measurements (BET method) were performed at liquid nitrogen temperature (-196°C) with an ASAP 2010 apparatus from Micromeritics. The analysis procedure is fully automated and operates with the static volumetric technique. Before each measurement, the samples (0.100 g) were outgassed first at 130°C for 12 h at 5 10^{-3} torr and then at room temperature for 2 h at 0.75 10^{-6} torr. The N_2 isotherms were used to determine the specific surface areas (S.A.), using the BET equation, and the specific pore volume (Vs), calculated at P/P^0=0.98. The pore size distribution was calculated following the BJH method, assuming a cylindrical pore model.

TPR measurements were carried out on samples treated in air flow at 550 °C using a 2% H_2/Ar mixture and an heating rate of 10 °C min^{-1} with a Micromeritics 2900 apparatus.

Copper dispersion was measured by N_2O passivation method [136] using a Micromeritics 2900 apparatus. The method has the advantage of simplicity and gives satisfactory results when special attention is paid to avoid the presence of oxygen in the gaseous streams [136].

The method involves the following steps:

1) treatment in air flow at 550°C;

2) reduction with hydrogen: first TPR (2 % H_2/Ar mixture, 10°Cmin^{-1} from 20 to 450°C);

3) treatment in N_2O flow at 60°C;

4) reduction with hydrogen: second TPR (2 % H_2/Ar mixture, 10°Cmin^{-1} from 20 to 600°C).

The first TPR (step (2)) gives the total amount of reduced Cu, through integration of the TPR peaks. The treatment (3) causes the oxidation of metallic Cu to Cu_2O that, under the mild conditions employed, is limited to surface Cu atoms:

$2Cu_{(surf)} + N_2O \rightarrow Cu_2O_{(surf)} + N_2$

In the following step (4) $Cu_2O_{(surf)}$ is reduced:

$Cu_2O_{(surf)} + H_2 \rightarrow 2Cu_{(surf)} + H_2O$

From the amount of H_2 consumed in step (4), the amount of $Cu_{(surf)}$, and then the Cu dispersion=100x$Cu_{(surf)}$/Cu total, are calculated. Both Cu surface areas and Cu particle sizes can be calculated assuming a surface Cu concentration of $1.47 \cdot 10^{19}$ atoms m^{-2} [137].

X-Ray photoelectron spectra were collected using a Physical Electronics PHI 5700 spectrometer with non monochromatic Mg Kα radiation (300W, 15 kV, 1253.6 eV) for the analysis of photoelectronic signals of O 1s, Al 2p, Ce 3d and Cu 2p and with a multi-channel detector. Spectra of powdered samples were recorded with the constant pass energy values at 29.35 eV, using a 720 μm diameter analysis area. During data processing of the XPS spectra, binding energy values were referenced to the C 1s peak (284.8 eV) from the adventitious contamination layer. The PHI ACCESS ESCA-V6.0 F software package was used for acquisition and data analysis. A Shirley-type background was subtracted from the signals. Recorded spectra were always fitted using Gauss-Lorentz curves, in order to determine the binding energy of the different element core levels more accurately. The error in BE was estimated to be ca. 0.1 eV. Short acquisition time of 10 min was used to examine C 1s, Cu 2p and Cu LMM XPS regions in order to avoid, as much as possible, photoreduction of Cu^{2+} species. Nevertheless, a Cu^{2+} reduction in high vacuum during the analysis cannot be excluded [141].

2.3 Catalytic activity measurements

Catalytic activity measurements were carried out in two laboratory flow apparatus. The first one, equipped with a gas-chromatograph, allows a quantitative evaluation of the catalytic activity in OSRM and SRM reactions in terms of methanol conversion and yield to products at the desired temperature. The second apparatus allows pre-treatments and in situ characterization of the catalysts before and after each SRM catalytic test and on-line semi-quantitative analysis of the products by mass spectrometry. Tests can be performed under isothermal conditions or increasing the temperature linearly. The results of the two apparatus are complementary. The former allowed operation with higher reagent concentration and a more precise evaluation of the activity, while the latter allowed characterization in situ of the catalysts and rapid evaluation of the catalytic activity as a function of temperature.

2.3.1 Apparatus 1

Catalytic activity measurements were carried out in a laboratory flow apparatus schematically represented in Fig.2-5. The plant was equipped with a fixed bed reactor operating at atmospheric pressure. The catalyst (mass = 0.09 g, size = 90– 110 μm) was diluted with fused quartz powder in 1:10 ratio to guarantee isothermal conditions (see *Section 2.3.1.1*). Before starting the test, the catalyst was pre-reduced in situ as described in *Section 2.1.4* and *Section 2.2.4* . The liquid feed (H_2O/CH_3OH) was regulated by a Varian HPLC metering pump and the gaseous feed (O_2, He) by Brooks electronic mass flow controllers. The liquid feed vaporized inside the reactor in a pre-heating zone, appropriately designed (see *Section 2.3.1.1*). The desired temperature was achieved introducing the reactor in a vertical electric furnace with an electronic temperature controller-programmer. The reaction products were sent through a line heated at 110°C to a gas-chromatograph HP 5890 equipped with a double-packed Porapak-molecular sieve column and a TCD detector. Products analyzed were H_2, CO (detection limit = 0.01%), CO_2, O_2, CH_4, CH_3OH, H_2O. Methanol total conversion and partial conversions to different products were evaluated from concentrations in the effluent stream, taking into account the volume variation due to the reaction, according to the following definitions:

$$CH_3OH\ conversion\ = \frac{mol\ CH_3OH\ reacted}{mol\ CH_3OH\ fed}\ x\ 100 \quad (9)$$

$$yield\ to\ i-product\ = \frac{mol\ CH_3OH\ converted\ to\ i-product}{mol\ CH_3OH\ fed}\ x\ 100 \quad (10)$$

$$H_2\ yield\ = \frac{mol\ H_2\ produced}{mol\ CH_3OH\ fed} \quad (11)$$

Mass balances of C, H and O were fulfilled within ±5%. A Hiden mass spectrometer was employed for identification of products not detected by GC. The OSRM tests were carried out at T = 200–400 °C, $H_2O/CH_3OH/O_2$ molar ratios = 1.1/1/0.12, (CH_3OH concentration = 17.8%), GHSV = 6 x $10^4 h^{-1}$ (helium as balance).

Note that the maximum H_2 yield, corresponding to 100% methanol and oxygen conversion and 100% selectivity to H_2 (according to the stoichiometry of reactions (2) and (3), and feed composition) is 2.76 mol H_2 per mol methanol.

SRM tests were carried out in the same conditions, but excluding O_2. Each test lasted 1.5–2 h and in this time the products were sampled and analyzed two or three times to verify that constant conversion values were attained. Preliminary tests were carried out to ascertain that diffusive resistances were negligible.

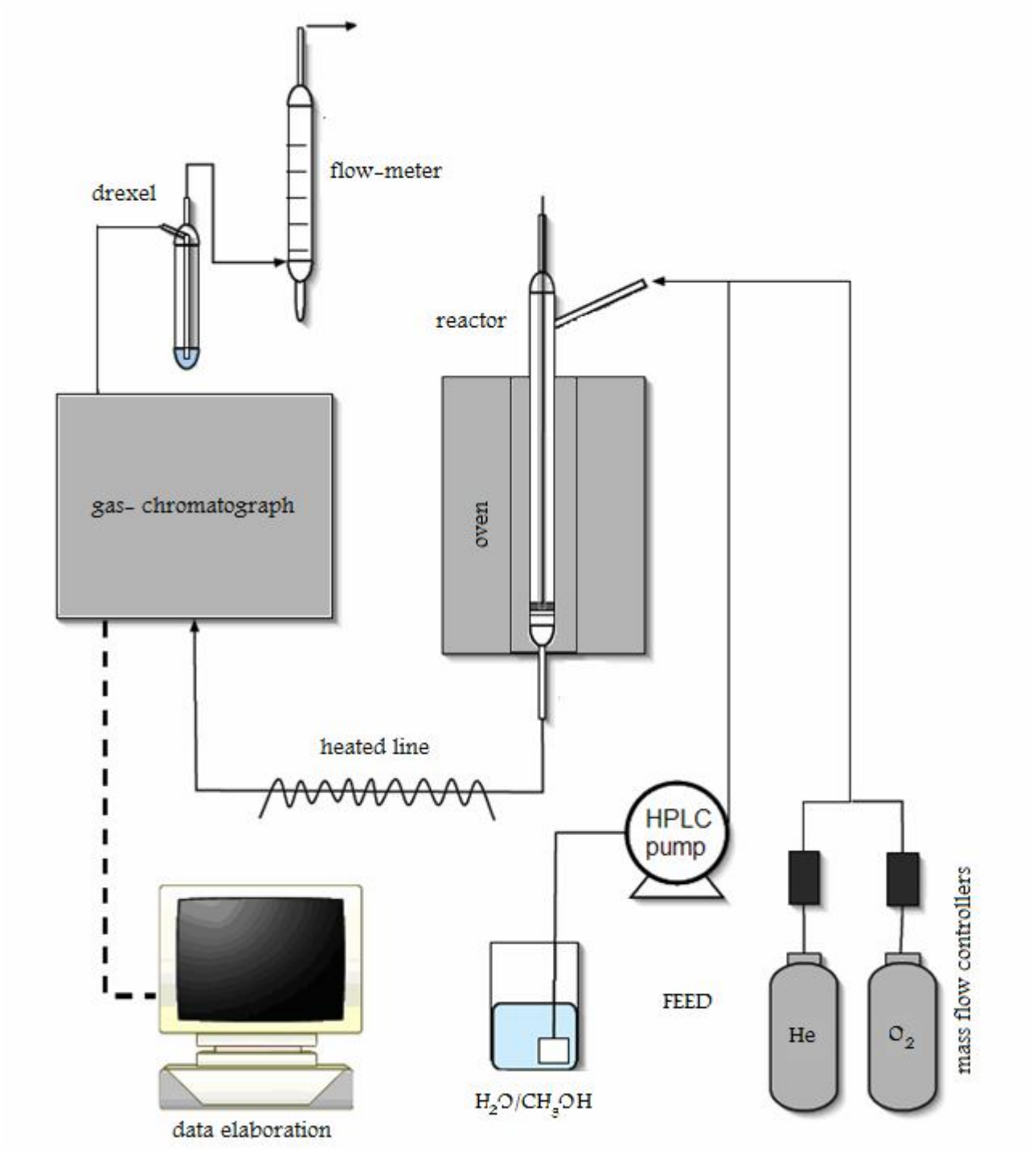

Fig. 2-5. Apparatus 1 for OSRM and SRM tests.

2.3.1.1 Reactor for OSRM

The design and construction of the Apparatus 1 for OSRM tests were carried out with considerable care. Particular emphasis was given to the design of the reactor in order to control the temperature inside the catalytic bed.
It was needed to ensure in fact, through design of the heat exchange surface, that the reagents fed to the reactor, reached the catalytic bed with the temperature required for the reaction and that the reaction run at constant temperature.
The feed was in part liquid (CH_3OH and H_2O) and was fed, as the gaseous feed (O_2 and He) at room temperature: so a pre-heating zone, extending from the point where the feed was introduced up to the catalytic bed, was required to vaporize the liquid reagents and bring the full feed, thus obtained, to the desired temperature.
The furnace was 45 cm high, the isothermal zone was 5 cm high and 20 cm from both upper and lower ends. The catalytic bed was few centimetres high and it was collocated in the isothermal area: so the pre-heating area was 20-24 cm high.
The pre-heating zone was filled with spherical particles of inert quartz, with a diameter of 500 μm and a vacuum degree of 0.5. It can be considered, at the steady state, that these particles had the same temperature of the oven, so their presence was very useful to increase the heat exchange surface. Another positive effect of the inert particles was related to the ability of reducing the radial gradient of velocity, concentration and temperature of the feed flowing through it, so that this feed could arrive to the catalytic bed with uniform properties along the section.
The quantity of heat per unit time, Q, which must be provided in the pre-heating zone is given by the following balance (Eq.12):

$$Q = n_l \cdot C_P \cdot (T_{vap} - T_{r.t}) + n_l \cdot \lambda_{vap} + n_l \cdot C_{Pvap} \cdot (T_{react} - T_{vap}) + n_g \cdot C_{Pg} \cdot (T_{react} - T_{r.t}) \quad (12)$$

in which each term is indicated in Table 2-3.

Table 2-3
Terms compared in Eq.12.

nl	Liquid feed	0.0824 mol h^{-1}
ng	Gaseous feed	0.1384 mol h^{-1}
C_P	Liquid feed specific heat capacity	19.92 cal mol^{-1} K^{-1}
C_{Pvap}	Vapour feed specific heat capacity	10.48 cal mol^{-1} K^{-1}
C_{Pg}	Gaseous feed specific heat capacity	5.04 cal mol^{-1} K^{-1}
T_{vap}	Average temperature of vaporization	87°C
T_{react}	Reaction temperature	200°C
λ_{vap}	Liquid feed latent heat of vaporization at T_{vap}	6546 cal mol^{-1}

The reaction temperature was assumed 200 °C, the lowest value tested, since the pre-heating should be effective even in the less advantageous test conditions.
At 200°C, Q = 931 cal h^{-1}.
This value must correspond to the heat exchanged in the pre-heating area.
Considering, as previously anticipated, that the inert particles were at the same temperature of the furnace, the exchange surface was due mainly to the particles surface: the coefficient of heat transfer between fluid and particles can be evaluated through the following empirical relationship (Eq.13) [142]:

$$jH = 0.91 \cdot \mathrm{Re}^{-0.51} \cdot \psi \quad \text{with Re} < 50 \qquad (13)$$

$$\text{where} \quad jH = h \cdot (C_P\, \mu\, k^{-1})_f^{0.667} \cdot (C_{P\,b}\, G_o)^{-1} \qquad (14)$$

$$\mathrm{Re} = G_o \cdot (a_v\, \mu\, \psi)^{-1} \qquad (15)$$

The subscript b indicates that the properties were evaluated at the bulk temperature, while the subscript f indicates that the properties were evaluated at the film temperature.
Considering the temperature profile of the furnace, the input was at a temperature of 118 °C and, approximately 20 cm from the upper end, the feed reached the isothermal area, which was at 200 °C. The feed, however, entered at 25 °C and reached the catalytic bed located in the isothermal area, at a temperature of 200 °C.
Using these temperatures, the terms presented in Table 2-4 and 2-5 can be calculated:

Table 2-4

T_f^{in}	Film temperature at the oven input	71°C
T_f^{out}	Film temperature at the pre-heating zone output	200°C
T_f	Film average temperature between the input and the output of the pre-heating zone	136°C
T_{oven}	Oven average temperature	159°C
T_{fluid}	Feed average temperature	112°C
H_{fill}	Filling height	0.2 m
S_{react}	Reactor section	$1.57 \cdot 10^{-4}$ m^2
V	Reactor volume	$3.14 \cdot 10^{-5}$ m^3
V_p	Single particle volume	$6.5 \cdot 10^{-11}$ m^3
S_p	Single particle surface	$7.85 \cdot 10^{-7}$ m^2
n_p	Number of particles evaluated from $V_{filled} = n_p \cdot V_P = V \cdot (1 - \varepsilon)$	$2.41 \cdot 10^5$

Table 2-5

G_o	Fluid mass velocity	18.47 Kg $h^{-1} m^{-2}$
a_v	Particle surface per volume calculated from $a_v = n_p \cdot S_P \cdot V^{-1}$	$6.019 \cdot 10^3$ m^{-1}
μ	Fluid viscosity	0.09 Kg m^{-1} h^{-1}
ψ	Particle size coefficient	Sphere = 1
k	Fluid thermal conductivity $K_{He} = 2.5 \cdot Cv_{He} \cdot \mu_{He}$ [143] Where $C_{vHe} = C_{pHe}/1.66$ =2.99 cal mol^{-1} K^{-1} [144]	168.2 cal h^{-1} m^{-1} K^{-1}
Re	Reynolds number	$3.36 \cdot 10^{-2}$
jH	Colburn factor	5.13

And using Eq.13, 14, 15 the coefficient of heat transfer can be evaluated: h = 151934 cal h^{-1} m^{-2} K^{-1}. Q_{preh} exchanged in the pre-heating zone was obtained by Eq. 16:

$$Q_{preh} = h \cdot A \cdot (T_{oven} - T_{fluid}) \quad (16)$$

where A was the exchange thermic surface, ie the area of all the inert particles, that was $1.88 \cdot 10^{-1} m^2$. Finally, a value of Q_{preh} = 1342 Kcal h^{-1}, which was much higher than the needed Q = 931 cal h^{-1}, was obtained: therefore the liquid vaporized and the gas mixture, thus obtained, reached the catalytic bed at the reaction temperature.

The presence of filling obviously influenced the pressure drop related to the passage of the gas stream: Δp should be limited for security reasons in order to ensure an operating pressure close to the atmospheric one. A Δp not exceeding 50 mmHg can be tolerated in the pre-heating and the reaction zone.

Δp in the pre-heating zone can be estimated using Ergun equation (Eq.17):

$$\frac{\Delta P}{G^2} \cdot \rho \cdot \left(\frac{D}{L} \right) \cdot \frac{\varepsilon^3}{1 - \varepsilon} = 150 \cdot \left(\frac{1 - \varepsilon}{D \cdot G} \right) \cdot \mu + 1.75 \qquad (17)$$

The fluid properties, considering only helium, were evaluated at the average temperature of 112 ° C. At this temperature, the density is equal to 0126 kg m^{-3} and the viscosity is 0.0864 kg $h^{-1}m^{-1}$.

G is the velocity of mass, D is the diameter of the inert particles and L is the height of the filling. In these conditions a Δp of only $1.18 \cdot 10^{-1}$ mmHg was obtained, which means that there were no problem in the pre-heating zone.

The reaction must occur under isothermal conditions. This means that only a little change of temperature can be allowed to the gas feed passing through the catalytic bed: the maximum variation allowed was only 5 °C.

Assuming a one-dimensional reactor model, considering that the reaction temperature was 200 °C and assuming that the oxygen was consumed completely by the partial oxidation of methanol (Eq.2) and that the rest of the methanol reacted, up to the full conversion, by steam reforming reaction (Eq.3), the heat produced by the reaction was Q_{react} = - 67.9 cal h^{-1}.

A_{react}, the surface inside the reactor which was in contact with the catalytic bed had to be calculated in order to avoid a too large increase of temperature. A_{react} represented the fluid heat transfer surface and its temperature can be considered equal to the temperature of the oven, T_{oven}, which was 200 °C. A_{react} was evaluated using Eq.18:

$$Q_{react} = A_{react} \cdot h \cdot (T_{fluid} - T_{oven}) \qquad (18)$$

where h can be evaluated using the following relationships [145] and Table 2-6:

$$Nu = 3.66 + (0.19 \cdot Gz^{0.8}) \cdot (1 - 0.117 \cdot Gz^{0.467})^{-1} \qquad (19)$$

$$Nu = (h \cdot L) \cdot k_f^{-1} \qquad (20)$$

$$Gz = Re \cdot Pr \cdot (D_h \cdot L^{-1}) \quad (21)$$

$$Re = (G_o \cdot D_h) \cdot \mu_f^{-1} \quad (22)$$

$$Pr = (C_{Pf} \cdot \mu_f) \cdot k_f^{-1} \quad (23)$$

Table 2-6

L	$\mathbf{k_f}$	***G_o***	$\mathbf{D_h}$	$\mathbf{C_{Pf}}$	$\boldsymbol{\mu}$
Catalytic bed length	Fluid thermal conductivity	Fluid mass velocity	Hydraulic diameter	Fluid specific capacity at 200°C	He viscosity at 200°C
1 cm	168.2 cal h^{-1} m^{-1} K^{-1}	18.47 Kg h^{-1} m^{-2}	10^{-2} m	653 cal Kg^{-1} K^{-1}	0.08 Kg m^{-1} h^{-1}

so

Re = 2, Pr = 0311; Gz = 0.64, Nu = 3.78, H = 63.6 kcal h^{-1} m^{-2} K^{-1}.

And $A_{react} = 4.3\ cm^2$.

This value was realized with a height of the catalytic bed slightly less than 1 cm, obtained diluting the catalyst with inert quartz powder.

Using the Ergun equation and considering a bed height of 1 cm and a temperature of 200 °C, the calculated Δp was only 1.65 mmHg, that is well below the maximum tolerable limit.

The reactor is represented in Fig.2-6.

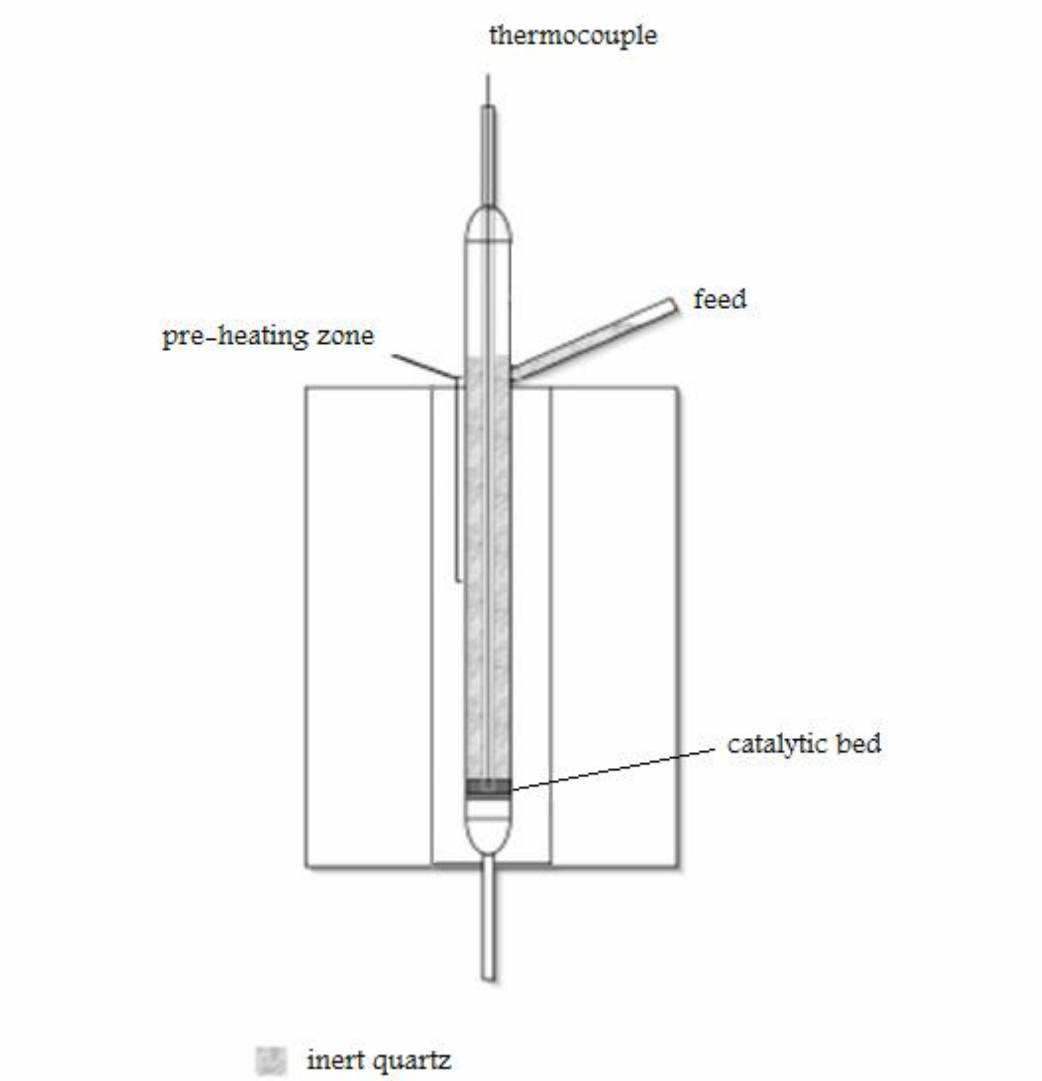

Fig.2-6. Reactor for OSRM

2.3.2 Apparatus 2

Temperature programmed reduction (TPR), Cu dispersion measurements and catalytic tests were carried out in a laboratory made apparatus, schematically represented in Fig.2-7. The apparatus allowed pre-treatments and in situ characterization of the catalysts before and after each catalytic test and on-line analysis of the products by mass spectrometry.

The apparatus was made up of three main sections: a feed section, a fixed bed micro-reactor and an analysis section.

The vapour feed (H_2O and CH_3OH) was controlled by a thermostated saturator at 0°C, by flowing Ar streams, regulated as the other gases (air, H_2/Ar, O_2, N_2O) by Brooks electronic mass flow controllers. Temperature was controlled by a chromel-alumel thermocouple inserted in the reactor in close contact with the catalytic bed. The effluent stream from the reactor was sent to a Hiden quadrupole mass spectrometer, a TCD detector for the analysis of H_2 and an IR spectrophotometer for the analysis of CO and CO_2. A H_2O trap (anhydrous KOH) could be introduced after the reactor when required.

The catalyst (mass = 0.20-0.30 g, size = 75 – 90 μm) was contained in a fused silica microreactor operating at atmospheric pressure and heated by a thermally programmed oven. The operating conditions were established to guarantee a perfect mixing.

TPR measurements were carried out in situ with a 2% H_2/Ar mixture, heating at rate of 10°Cmin^{-1} up to 450 or 600°C as required and keeping the sample at the final temperature for 2 h.

Cu dispersion was measured in situ by the N_2O oxidation/TPR method [114]. The sample, reduced with a standard TPR run up to 450°C (rate = 10°Cmin^{-1}), was superficially oxidized treating in N_2O flow at 60°C, then a further TPR run allowed to determine the amount of Cu_2O(surf) and so the amount of Cu(surf). The Cu surface area and Cu particle size were calculated assuming a Cu surface concentration of $1.47 \cdot 10^{19}$ atoms m^{-2} [137].

SRM tests were carried out under the following conditions: total flow rate = 100 cm^3min^{-1}, CH_3OH concentration = 0.54%, H_2O concentration = 0.54%, Ar balance; GHSV = $1.8 \cdot 10^4$ h^{-1}. The tests were carried out increasing the temperature linearly from room temperature to 400°C with rate of 5°C min^{-1}. Using Ar as carrier allowed to analyze H_2 by TCD with 5% precision. The mass spectrometer effected semi-quantitative analysis of H_2, CH_3OH, CO_2, CO, CH_2O, CH_4, $(CH_3)_2O$. The IR spectrophotometer allowed to analyze CO and CO_2 with 5% precision and 200 ppm sensitivity.

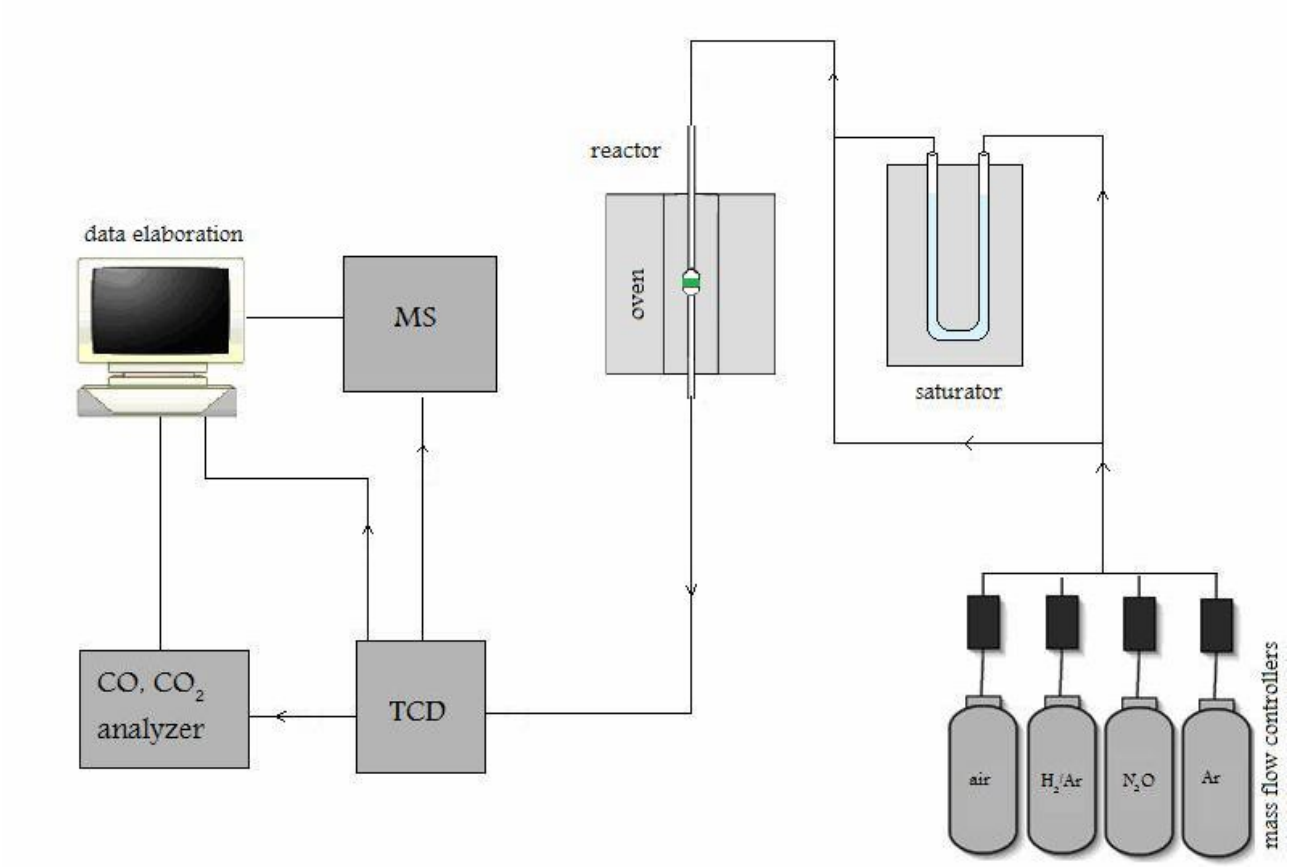

Fig.2-7. Experimental plant for catalytic activity tests and in situ characterization

Before the test, the sample was pretreated in air flow at T =550°C for 1 h (rate = 10°Cmin^{-1}). Tests were carried out according to the following sequence:

- TPR up to 450°C
- SRM reaction
- TPR up to 450°C
- Cu dispersion measurement.

The first TPR was omitted when the SRM reaction had to be tested on the oxidized catalyst.
The apparatus used previously for testing catalytic activity (see *Section 2.3.1*) and the present one gave complementary information. The former allowed operation with higher reagent concentration and a more precise evaluation of the activity, while the latter allowed characterization in situ of the catalysts and rapid evaluation of the catalytic activity as a function of temperature.

2.3.3 Kinetic study

The purpose of this research is to obtain:

-a parameter to compare catalysts which are different for the preparation method, the composition and the physical and chemical properties;

-a quantitative information about reactions whose mechanisms are not yet well known.

The reaction taken into consideration is the consumption of methanol, but under OSRM conditions several reactions can occur, so the calculated kinetic parameters are only apparent values, which refer to the pseudo- reaction of CH_3OH consumption.

The mechanism and the network of reactions are not well know, so a pseudo first order reaction rate is assumed for OSRM.

The reaction rate is expressed as:

$$r = kc_{CH_3OH} \qquad [mol \cdot s^{-1} \cdot g_{cat}^{-1}] \qquad (24)$$

Where k is the kinetic constant [$cm^3 \cdot s^{-1} \cdot g_{cat}^{-1}$] and c_{CH3OH} is the methanol concentration [mol cm^{-3}].

Assuming that the reactor described in *Section 2.3.1.1* is a constant pressure plug flow type, the relationship between the contact time (τ, [$s \cdot cm^{-3} \cdot g$]) and the conversion is expressed by Equation 25:

$$\tau = \frac{m_{cat}}{Q_{in}} = C^{in}_{CH_3OH} \int_0^{x_f} \frac{dx}{r(x)} \qquad (25)$$

Since the reaction occurs in gas phase and leads to a change in the number of moles, there will be a variation of the volumetric flow with the reagent conversion. The relationship between conversion, concentration and flow is expressed by Equation 26:

$$x_f = \frac{Q^{in}c^{in} - Q^{out}c^{out}}{Q^{in}c^{in}} = 1 - \frac{Q^{out}c^{out}}{Q^{in}c^{in}} \qquad (26)$$

Assuming an ideal behaviour of reagents, the relationship Q_{out}/Q_{in} can be expressed as a linear function of the conversion degree by Equation 27:

$$\frac{Q^{out}}{Q^{in}} = 1 + \varepsilon x \qquad (27)$$

where ε, fractional expansion of the system, can be calculated using the ratio Q_{out}/Q_{in} in the case of complete conversion.

For OSRM $Q_{in} = 5.4\ l\ h^{-1}$ and the feed composition is the following:

% CH_3OH = 17.778%

% O_2 = 2.1%

% H_2O = 19.540%

% He = 60.582%

Assuming that only partial oxidation (Eq.2) and steam reforming (Eq.3) are responsible for methanol consumption and that all the oxygen reacts in the partial oxidation and only the remainder methanol reacts in steam reforming, the output flows for a complete conversion are expressed as:

$$Q^{out}_{CH_3OH} = 0$$
$$Q^{out}_{O_2} = 0$$
$$Q^{out}_{H_2} = 4Q^{in}_{O_2} + 3(Q^{in}_{CH_3OH} - 2Q^{in}_{O_2}) = 2.65 l/h$$
$$Q^{out}_{CO_2} = 2Q^{in}_{O_2} + (Q^{in}_{CH_3OH} - 2Q^{in}_{O_2}) = 0.96 l/h$$
$$Q^{out}_{H_2O} = Q^{in}_{H_2O} - (Q^{in}_{CH_3OH} - 2Q^{in}_{O_2}) = 0.32 l/h$$
$$Q^{out}_{He} = Q^{in}_{He} = 3.27 l/h$$

The total out flow is $Q^{out}_{tot} = 7.14 l/h$

So for OSRM $\varepsilon = \frac{Q^{out}}{Q^{in}} - 1 = 0.3232$

For SRM, instead Q_{in} = 5.4 l h^{-1} and the feed composition is the following:

% CH_3OH = 17.778%

% H_2O = 19.540%

% He = 62.682%

Assuming only steam reforming (Eq.3) responsible for methanol consumption, the output flows for a complete conversion are expressed as:

$$Q^{out}_{CH_3OH} = 0$$
$$Q^{out}_{H_2} = 3Q^{in}_{CH_3OH} = 2.88\,\text{l/h}$$
$$Q^{out}_{CO_2} = Q^{in}_{CH_3OH} = 0.96\,\text{l/h}$$
$$Q^{out}_{H_2O} = Q^{in}_{H_2O} - (Q^{in}_{CH_3OH}) = 0.095\,\text{l/h}$$
$$Q^{out}_{He} = Q^{in}_{He} = 3.38\,\text{l/h}$$

The total out flow is $Q^{out}_{tot} = 7.32\,\text{l/h}$

So for SRM $\varepsilon = \frac{Q^{out}}{Q^{in}} - 1 = 0.36$

The mass of catalyst used is 90 mg, so at room temperature τ is:

$$\tau = \frac{m_{cat}}{Q^{in}} = 0.06\ \text{s}\ \text{g}_{cat} \cdot \text{cm}^{-3}$$

τ is a decreasing function of temperature as the rise of the latter increases the value of volumetric flow. The relationship between temperature and τ is expressed by Equation 28:

$$\tau(T) = \tau(T_{amb})\frac{T_{amb}}{T} \qquad (28)$$

where T is the temperature expressed in K.

Expressing the concentration of reagent as a function of the conversion degree by Eq.29 :

$$C_{CH_3OH} = C^{in}_{CH_3OH} \frac{1-x}{1+\varepsilon x} \qquad (29)$$

Equation 30 can be found for a PFR:

$$k\tau = \int_0^{x_f} \frac{1+\varepsilon x}{1-x} dx \qquad (30)$$

And finally the kinetic constant at a given temperature can be calculated from the Equation 31:

$$\ln k = \ln\left[-\frac{1}{\tau}\left[\varepsilon x + (1+\varepsilon)\ln(1-x)\right]\right] = \ln ko - \frac{E}{RT} \qquad (31)$$

Obviously, the calculation excludes data obtained under conditions of not negligible contribution of parasitic reactions as well as conversion values close to 0 or 1.

3 Results and discussion
Characterization of catalysts

3.1 Materials Cu/ZrO_2

3.1.1 Thermogravimetric analysis

TG/DTA curves of zirconia and copper doped zirconia dried gels are shown in Fig.3-1. The total weight losses given by the TG curves are: 22.5wt% ($NZrO_2$), 22.5wt% ($AZrO_2$), 30 wt% ($NZrCu_6$), 32.7 wt% ($AZrCu_7$), 32.2 wt% ($AZrCu_{14}$). In each case, the majority of the weight loss takes place from room temperature to about 400 °C. In this range, for a typical gel-derived sample, the evaporation of the solvents and the subsequent pyrolysis and/or burning of residual organic molecules generally occur [124]. TG/DTA curve of the pure zirconia $NZrO_2$, obtained by *Method I* (see *Section 2.1.2*) is perfectly identical to that of the pure zirconia $AZrO_2$ obtained by *Method II* (see *Section 2.1.2*), therefore only one curve is described.

Two separate thermal effects are seen in the DTA curve of ZrO_2: the endothermic hump from room temperature to about 150 °C and the broad exothermic peak with a maximum at 345 °C. The former is related to the evaporation, from open pores, of water and alcohol physically trapped in the gels, the latter to the burning of residual organic groups. These two effects can be observed also for the $AZrCu_7$ and the $AZrCu_{14}$: the DTA endothermic hump from room temperature to 150°C is related to the evaporation of water and alcohol molecules and the exothermic peaks at 320°C for $AZrCu_7$ and at 291°C and 317°C for $AZrCu_{14}$ are related to the elimination of residual organic groups. For $NZrCu_6$, besides the DTA endothermic hump related to the evaporation of water and alcohol molecules, a large and sharp DTA exothermic peak takes place at 277 °C and in the corresponding TG curve a distinct slope change is seen. The phenomenon that causes the appearing of this sharp peak is explained by the assumption that the burning of organics is driven by the un-decomposed nitrate groups that act as comburent for the organics oxidation. This hypothesis is backed by literature data: the decomposition of copper nitrate is reported to happen at ~ 225 °C but results to be complete at about 300 °C [146].

The crystallisation of zirconia, both in pure ZrO_2 and in the $AZrCu_7$ and $AZrCu_{14}$ samples, takes place at about 429°C and is related to the DTA exothermic peaks observed at this temperature.

A further difference in the thermal behaviour in the temperature range where the crystallisation of zirconia takes place can be observed for the $NZrCu_6$ sample: the DTA exothermic peak observed at

429 °C for pure ZrO_2 is in fact shifted to 493 °C for the $NZrCu_6$ sample. In both cases the peak is very sharp, indicating a fast phenomenon, and is related to the formation of ZrO_2 nanocrystals of the tetragonal polymorph, as indicated by XRD data reported below (see *Section 3.1.2*). This crystallisation delay was also detected by Labaki et al. [147] and related to the introduction of Cu^{2+} ions into the zirconia matrix.

Finally, the endothermic DTA peak at 1048 °C seen for $NZrCu_6$, $AZrCu_7$ and $AZrCu_{14}$, with a corresponding slight weight loss in the TG curve, is the result of the decomposition of cupric oxide to form cuprous oxide through the reaction $2\ CuO \rightarrow Cu_2O + 1/2\ O_2$ (32).

Based on these data, the calcination temperature of 340°C was selected, because at this temperature organic materials have been completely eliminated, but the crystallisation of zirconia, leading to a reduction of surface area, has not yet occurred.

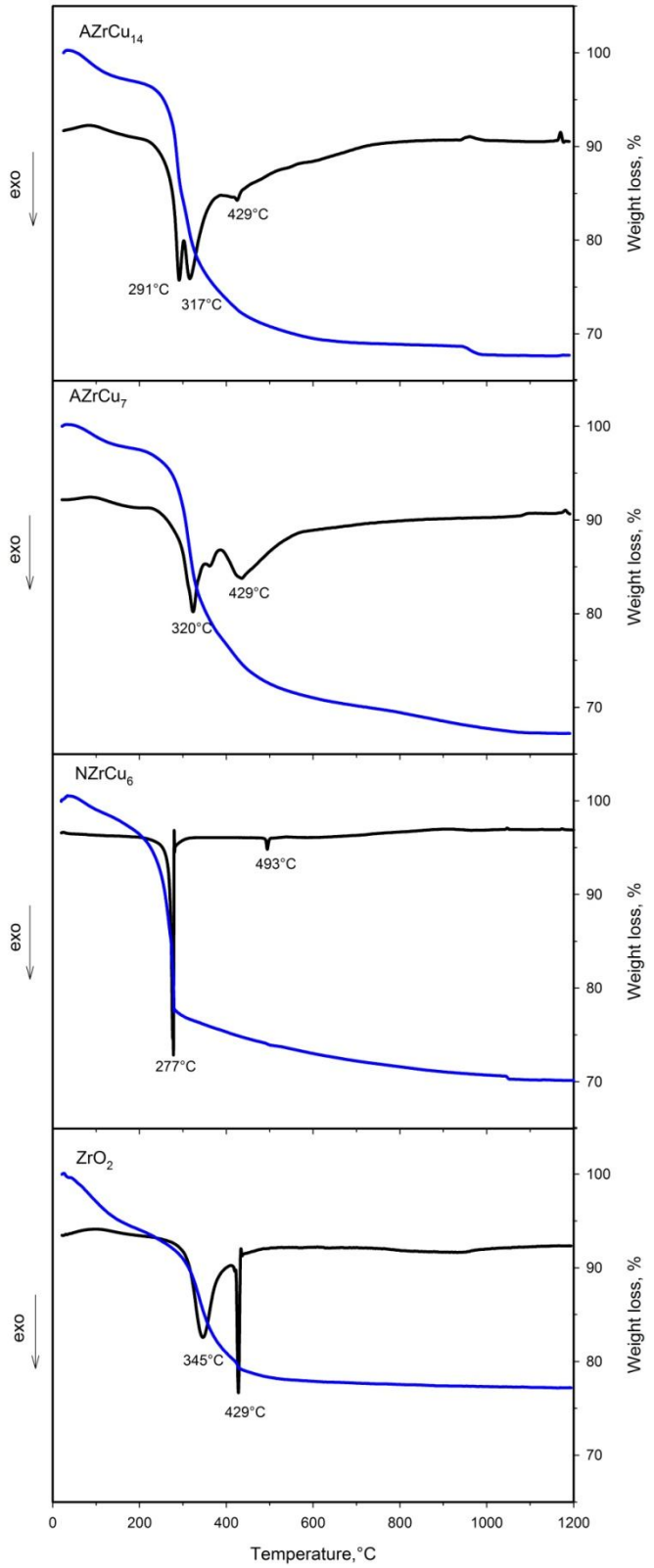

Fig.3-1. DTA (black line) – TG (blue line) curves of the dried gels recorded in air at 2°C min^{-1}.

3.1.2 XRD analysis

To evaluate the effect of the presence of Cu on the crystallisation behaviour of ZrO_2, XRD spectra were performed on samples annealed in air at different temperatures (Fig. 3-2). These heat treatments were chosen on the basis of thermal analysis data: (i) 3h at 340 °C (trace (a) of Fig. 3-2) to obtain stable gel-derived samples; (ii) 30 min at 600 °C (trace (b) of Fig. 3-2) to force the crystallisation of the prepared gel derived samples. Note that the samples are identified with a number indicating the temperature of the heat treatment. Broad peaks are seen in the $ZrO_2$340 XRD profile (trace (a) of Fig. 3-2), indicating the formation of nanocrystals with average size of about 7 nm related to its tetragonal polymorph (JCPDS card N. 50-1089). The distinction between tetragonal and cubic phase is not an easy task on account of the overlapping reflections; nevertheless, we are confident of the above reported assignment given the lack of (040) reflection at $2\theta = 73.9°$ characteristic of the cubic polymorphous and the presence of the peak at $2\theta = 74.5°$ detectable for the tetragonal polymorph. Also $AZrCu_7$340 and $AZrCu_{14}$340 present peaks related to the formation of nanocrystals, while $NZrCu_6$340 is still amorphous as suggested by DTA results. The average dimensions of the zirconia crystallites according to the Scherrer's equation are reported in Table 3-1. For $ZrO_2$600 the narrowing of the broad peaks related to the tetragonal phase occurs with the early appearance of the two most intense peaks of the ZrO_2 monoclinic polymorph (trace (b) of Fig. 3-2), indicating the growth of the tetragonal nanocrystals (about 10 nm) and the beginning of the transition from tetragonal to monoclinic. In contrast, for $NZrCu_6$600, $AZrCu_7$600 and $AZrCu_{14}$600 the tetragonal polymorph appears to be the only crystalline phase present at this stage of annealing; moreover the peaks related to tetragonal ZrO_2 appear to be shifted to higher angle (trace (b) of Fig. 3-2) indicating that Cu^{2+} ions are being incorporated into the ZrO_2 lattice (i.e. they occupy the position of Zr^{4+}) [84,87, 92,95]. In fact, the lattice parameters evaluated from the $NZrCu_6$600 XRD profile are: a = b = 3.5924(3) Å, c = 5.1169(5) Å. These values are lower than the ones evaluated for the $ZrO_2$600 support (a = b = 3.598 Å, c = 5.152 Å) confirming that part of Zr^{4+} (ionic radius = 79 pm) are substituted by Cu^{2+} (ionic radius = 72 pm).

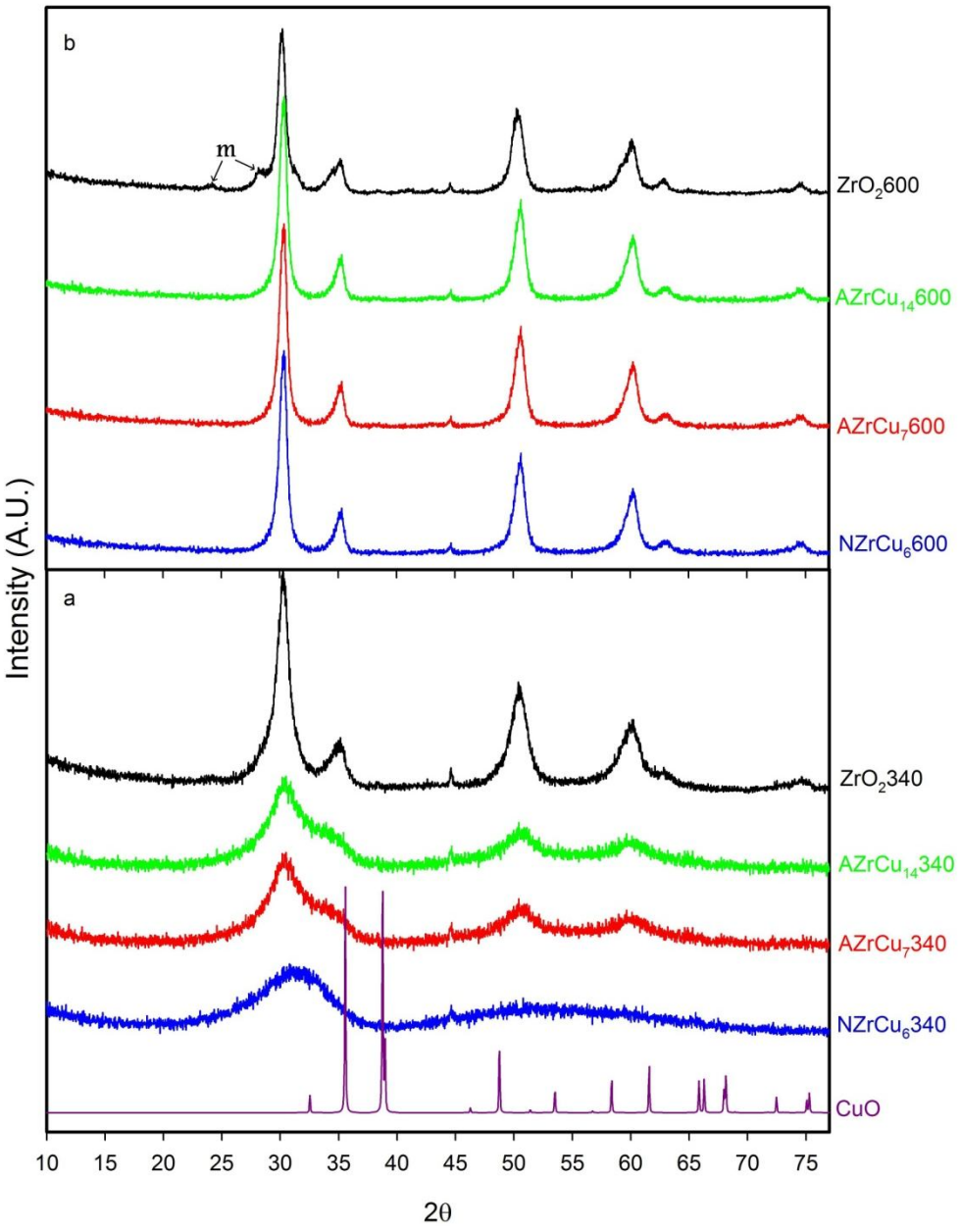

Fig.3-2. XRD patterns of gels heat treated at different temperatures: 3h at 340 °C and 30 min at 600 °C. Arrows mark small picks of monoclinic zirconia (m).

Table 3-1
Average dimensions of zirconia crystallites.

Sample	2ϑ	FWHM	Dcrist (nm)
$ZrO_2$340	50.369	1.331	6.6
$ZrO_2$600	50.302	0.888	10
NZr$Cu_6$340	-	-	-
NZr$Cu_6$600	50.489	0.887	10
AZr$Cu_7$340	50.413	1.835	4.8
AZr$Cu_7$600	50.493	0.847	10.4
AZrCu_{14}340	50.443	2.076	4.2
AZrCu_{14}600	50.490	0.847	10.4

Similar crystallisation behaviour was previously reported for zirconia based materials containing about 10 mol% CuO obtained by coprecipitation [84,95] or sol gel [87,92]. It was suggested that only a part of Cu^{2+} ions gets substituted for Zr^{4+} in the lattice while the remaining part either occupies interstitial positions of the zirconia network, acting as charge compensating ions, or exists as surface bound ions and CuO crystalline clusters.

In the present case, the XRD analysis has not evidenced peaks related to the CuO phase at any stage of annealing, indicating the presence either of very small crystalline (lower than 2 nm) or amorphous aggregates. This result suggests that a remarkable high dispersion of copper into the zirconia matrix has been obtained with the synthesis procedure used in this work. In the tetragonal polymorph, the coordination of Zr is 8-fold with oxygen anions forming two jointed tetrahedral, and the oxygen atom is shared by four adjacent Zr atoms. In the monoclinic phase, the coordination of Zr is 7-fold with oxygen anions forming two types of non-equivalent oxygen sites. The structural distortion of $[ZrO_7]$ units is greater than the $[ZrO_8]$ ones as all the Zr–O bond lengths are different [148]. The initial formation of the metastable tetragonal phase can be explained on the basis of its structural similarity with the sol-gel matrix.

3.1.3 TPR and dispersion measurements

To get a greater insight into the copper-zirconia interaction, the reducibility of the samples is studied by the TPR technique. TPR profiles of $NZrCu_6340$, $AZrCu_7340$ and $AZrCu_{14}340$ are reported in Fig.3-3 together with the curves of pure CuO and ZrO_2340. The quantitative evaluation of TPR peaks is reported in Table 3-2. ZrO_2340 gives two small TPR signals with maxima at 380 and 660 °C, the corresponding amount of H_2 consumed (Table 3-2) indicates a very limited reduction, that probably is related to the creation of Zr^{3+} ions and anionic vacancies ($VO^{\cdot\cdot}$), according to:

$$2Zr^{4+} + O^{2-} + H_2 \rightarrow 2Zr^{3+} + H_2O + VO^{\cdot\cdot} \qquad (33)$$

Anionic vacancies can be easily formed on the surface of ZrO_2 under some conditions, such as calcination at 550 °C [84].

$NZrCu_6340$, $AZrCu_7340$ and $AZrCu_{14}340$ show composite signals with two components at about 205 and 235 °C. On the other hand the TPR profile of bulk CuO shows a single reduction peak at about 400 °C with intensity corresponding to the complete reduction of Cu^{2+} to Cu^0. This suggests that most CuO is not present in the catalyst as a segregated phase and that the copper-zirconia interaction facilitates the reduction of the Cu(II) species, in agreement with previous studies [20,72,84,149]. The presence of more than one reduction signals was already observed in the TPR profiles of Cu based catalysts and explained by different effects [26,70,82,150]. Sometimes it was attributed to the stepwise reduction of copper oxide ($Cu^{2+} \rightarrow Cu^{+} \rightarrow Cu^0$) [20], but it was more often explained by the presence of Cu(II) species with different reducibility [150]. Two reduction peaks in the range 200-250 °C were also observed with copper supported zirconia materials prepared by deposition-precipitation and were attributed to different kinds of CuO species [86]. A similar behaviour was observed with copper-containing ZrO_2 systems prepared by oxalate gel coprecipitation [84]. In this case three types of CuO species were hypothesized from TPR data and their reducibility was related to the strength of the interaction with ZrO_2 [84]. On the other hand, some authors supposed that dispersed CuO particles exhibiting the weakest interaction with zirconia were most easily reduced [147]. Taking into account these data, the twinned TPR signal is probably related to two kinds of CuO species interacting with ZrO_2 with different strength.

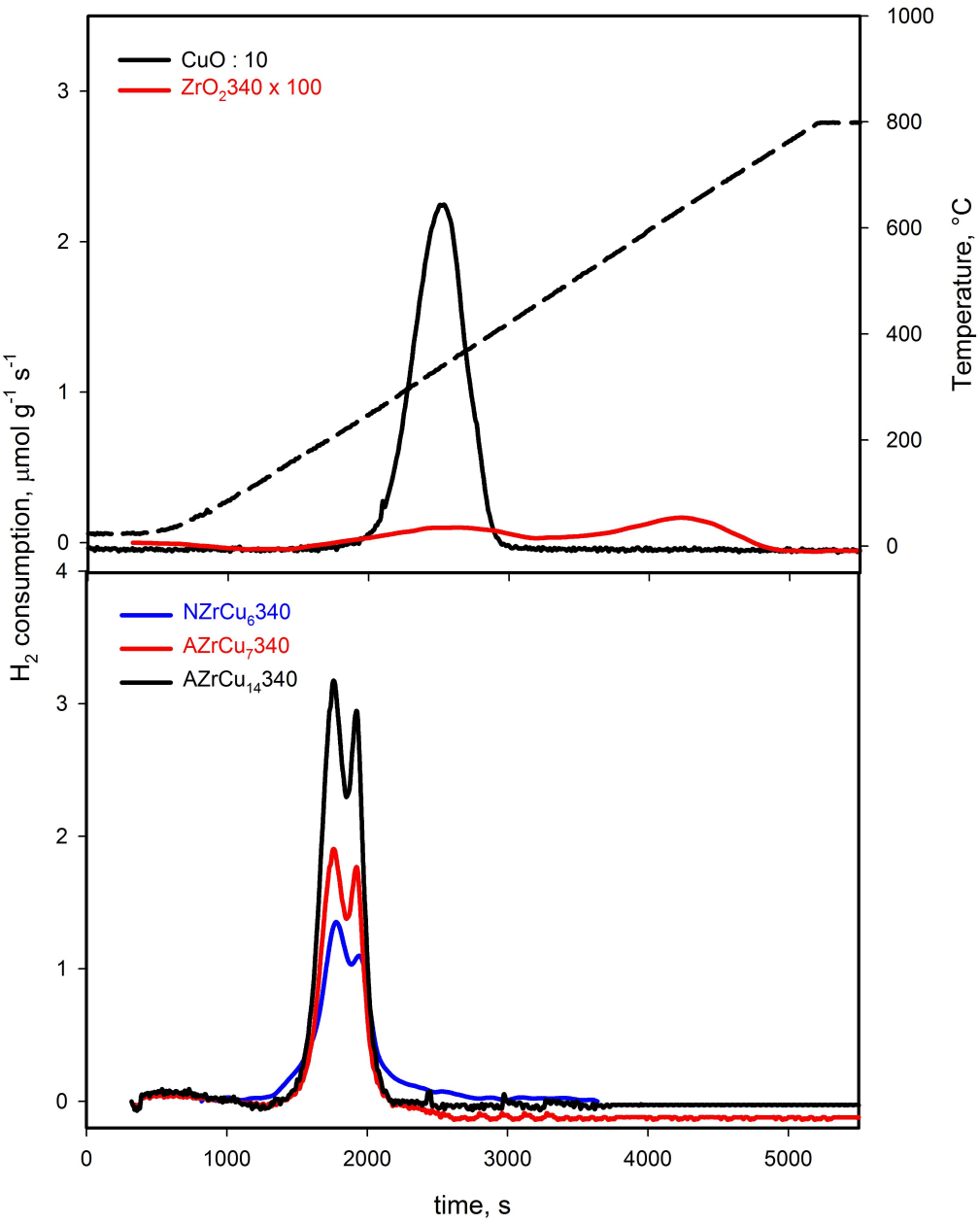

Fig.3-3. TPR spectra of the catalysts $NZrCu_6340$, $AZrCu_7340$, $AZrCu_{14}340$ and the reference CuO and ZrO_2340 samples. Note the different scales used for CuO and ZrO_2340.

Table 3-2
TPR and Cu dispersion data.

Sample	Composition (mol g^{-1} x 10^{-3}) Zr	Cu	Tmax (°C)	H_2 consumption (mol g^{-1} x 10^{-3})	Cu dispersion (%)	Cu S.A.[a] (m^2 g_{cat}^{-1})	Cu crystal size[b] (nm)
CuO	-	12.57	400	12.57	-	-	-
ZrO_2	8.1	-	380, 660	0.004	-	-	-
$NZrCu_6340$	7.7	0.71	205,235	0.58	-	-	-
$NZrCu_6R300$	7.7	0.71	200	0.30	85.0	24.5	1.2
$NZrCu_6R450$	7.7	0.71	200	0.17	47.0	13.5	2.2
$AZrCu_7340$	7.7	0.86	205,235	0.63	-	-	-
$AZrCu_7R300$	7.7	0.86	200	0.14	32.0	11.2	3.3
$AZrCu_7R450$	7.7	0.86	200	0.086	20.0	7.0	5.3
$AZrCu_{14}340$	7.2	1.73	205,235	1.10	-	-	-
$AZrCu_{14}R300$	7.2	1.73	205, 225	0.20	23.4	16.4	4.5
$AZrCu_{14}R450$	7.2	1.73	205, 225	0.11	13	9.1	8.1

[a] Calculated from Cu dispersion assuming a surface Cu concentration of 1.47×10^{19} atoms m^{-2} [82].

[b] Calculated from Cu dispersion assuming a spherical shape.

It can be noted from Table 3-2 that the amount of H_2 consumed is lower than the stoichiometric one. This fact can be explained by the presence of not reducible cupric ions that could correspond to the ones that occupy the reticular positions of the zirconia lattice or to the presence of Cu(I) before or after the reduction treatment, indicating the ability of zirconia to stabilize Cu(I).

Comparing the TPR signals reported in Fig.3-3, it appears that the redox properties depend on the preparation method, but not on the composition of samples prepared by the same method. The TPR signal obtained with $NZrCu_6340$ is in fact broader than that obtained with $AZrCu_7340$, indicating the presence of copper species more easily reducible, instead $AZrCu_7340$ and $AZrCu_{14}340$ give TPR signals with the same shape and only an intensity depending on the composition.

In Figs. 3-4, 3-5 and 3-6 the TPR profiles obtained with the catalysts $NZrCu_6340$, $AZrCu_7340$ and $AZrCu_{14}340$ reduced and treated with N_2O as described above (see *Section 2.1.4*) together with, for sake of comparison, the corresponding profile obtained with the oxidized samples $NZrCu_6340$,

$AZrCu_7340$ and $AZrCu_{14}340$ are reported. The samples reduced are identified with the suffix "R" followed by a number indicating the reduction temperature, for example $NZrCu_6R300$.

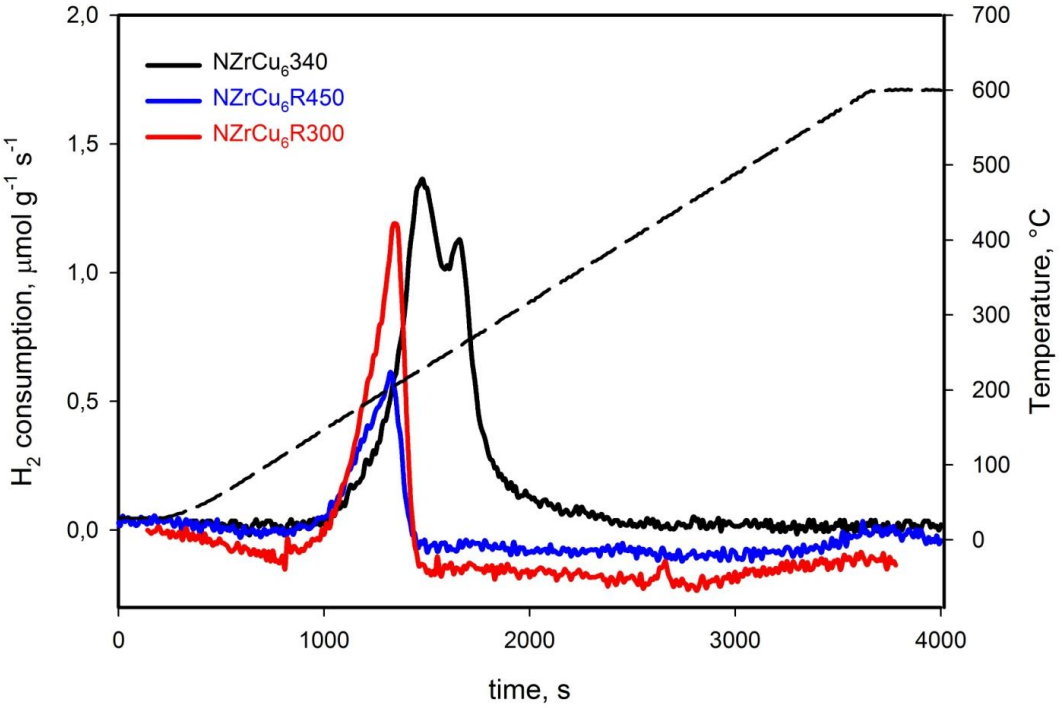

Fig.3-4. Cu dispersion measurements: TPR profiles of $NZrCu_6340$ and of the same sample after H_2 reduction at 300°C and 450°C and subsequent N_2O oxidation.

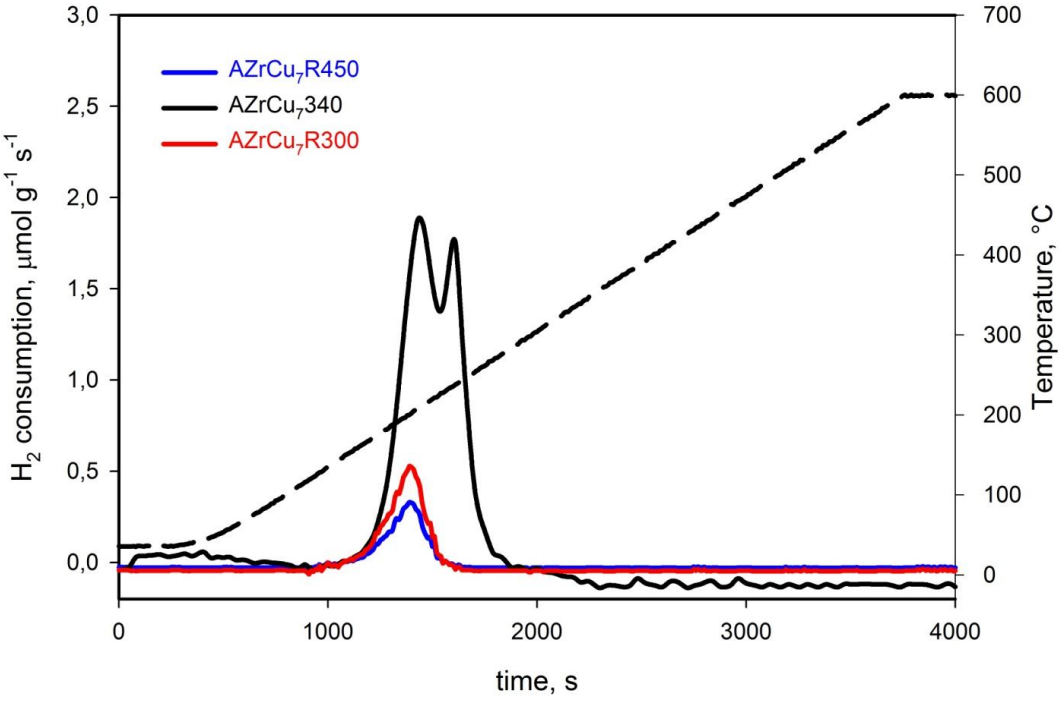

Fig.3-5. Cu dispersion measurements: TPR profiles of $AZrCu_7340$ and of the same sample after H_2 reduction at 300°C and 450°C and subsequent N_2O oxidation.

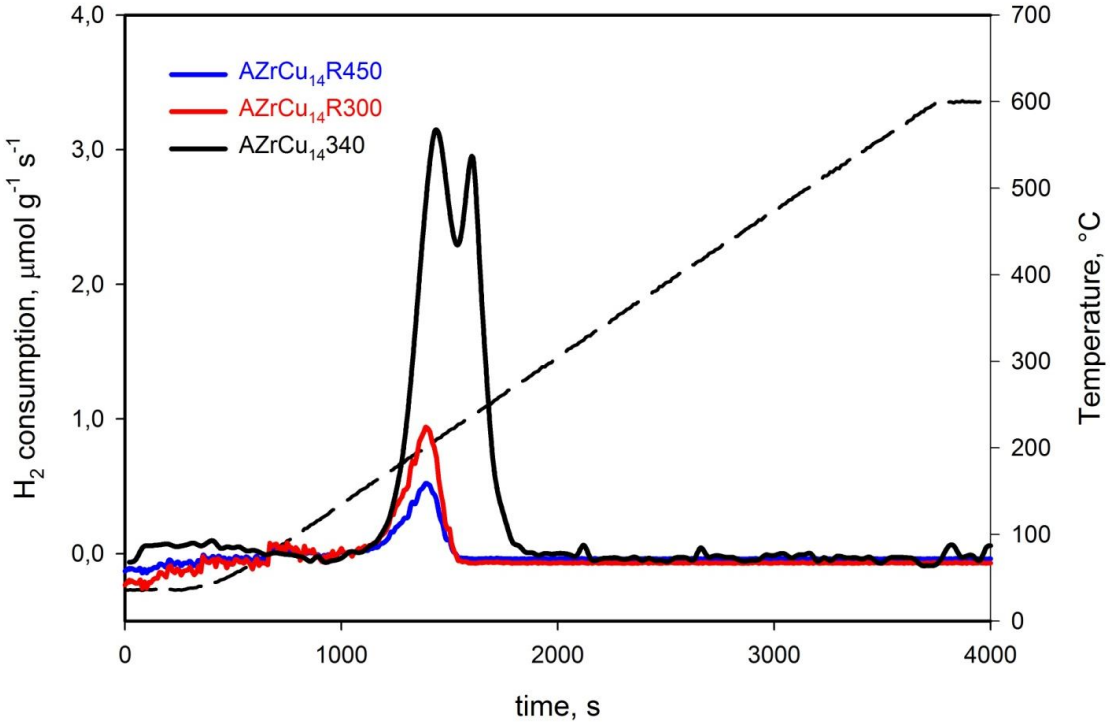

Fig.3-6. Cu dispersion measurements: TPR profiles of $AZrCu_{14}340$ and of the same sample after H_2 reduction at 300°C and 450°C and subsequent N_2O oxidation.

The presence of one reduction signal at a lower temperature in the TPR profiles obtained after H_2 reduction and treatment with N_2O is due to the reduction of only superficial Cu(I) species. The integration of the TPR peaks allows to calculate the amount of adsorbed oxygen (as Cu_2O) and so the Cu surface area from which the average size of Cu particles has been calculated hypothesizing spherical particles (Table 3-2). As it is difficult to determine the exact amount of metallic copper in the sample after the first reduction, the values of Cu dispersion have been related to the total Cu content and so can be considered as nominal. Nevertheless, these data allow to claim that the present synthetic procedure gives highly dispersed $Cu\text{-}ZrO_2$ catalysts.

Increasing the final temperature of the first TPR from 300°C to 450°C, a strong decrease of Cu dispersion is observed for all materials, that can be related to the strong tendency of coalescence of the nanosized particles. Anyhow, the $NZrCu_6$ sample shows a dispersion much higher than $AZrCu_7$, indicating the influence of the preparation method on this property. This behaviour can be explained by the strong interaction between copper and zirconia observed for $NZrCu_6$.

Based on these data, the temperature of 300°C was chosen to completely reduce the copper oxide to metallic copper, avoiding the sinterization of metallic Cu and retaining a high dispersion degree.

However also the reduction temperature of 450°C was employed because this temperature, being higher than the operating range of the OSRM tests, ensured a higher stability of the catalysts under reaction conditions.

3.1.4 N_2 physisorption

To consider materials of interest for the catalytic activity, textural properties were studied on samples treated at 340°C, $NZrCu_6340$, $AZrCu_7340$ and $AZrCu_{14}340$, but also on materials reduced at 300 and 450°C, $NZrCu_6R300$, $NZrCu_6R450$, $AZrCu_7R300$, $AZrCu_7R450$, $AZrCu_{14}R300$ and $AZrCu_{14}R450$ and the corresponding isotherms are reported respectively in Figs. 3-7, 3-8 and 3-9. Note that the representation of $AZrCu_7R450$ and $AZrCu_{14}R450$ is not possible, because of the low surface area. The corresponding BET areas are reported in Table 3-3. Micropore volumes and surface areas evaluated by the method of α-plot are also reported in Table 3-3. N_2 adsorption-desorption measurements were carried out also on the reference ZrO_2340 and reported in Fig.3-10.

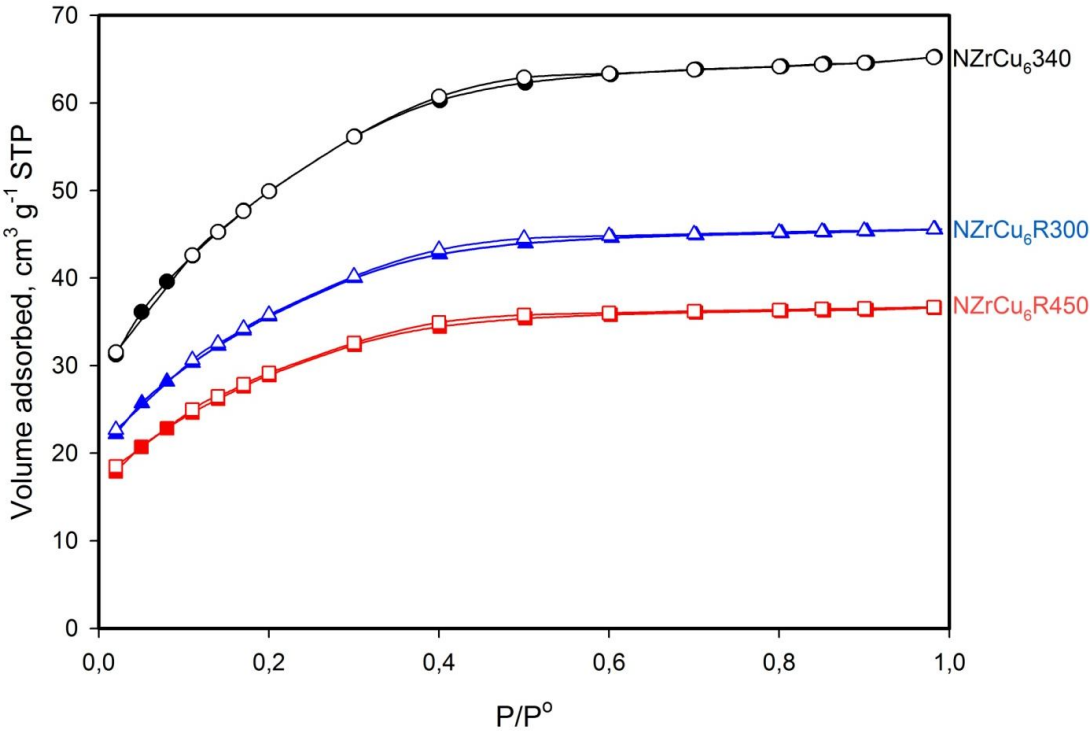

Fig.3-7. Adsorption-desorption isotherms of $NZrCu_6340$, $NZrCu_6R300$ and $NZrCu_6R450$. Full symbols: adsorption, empty symbols: desorption.

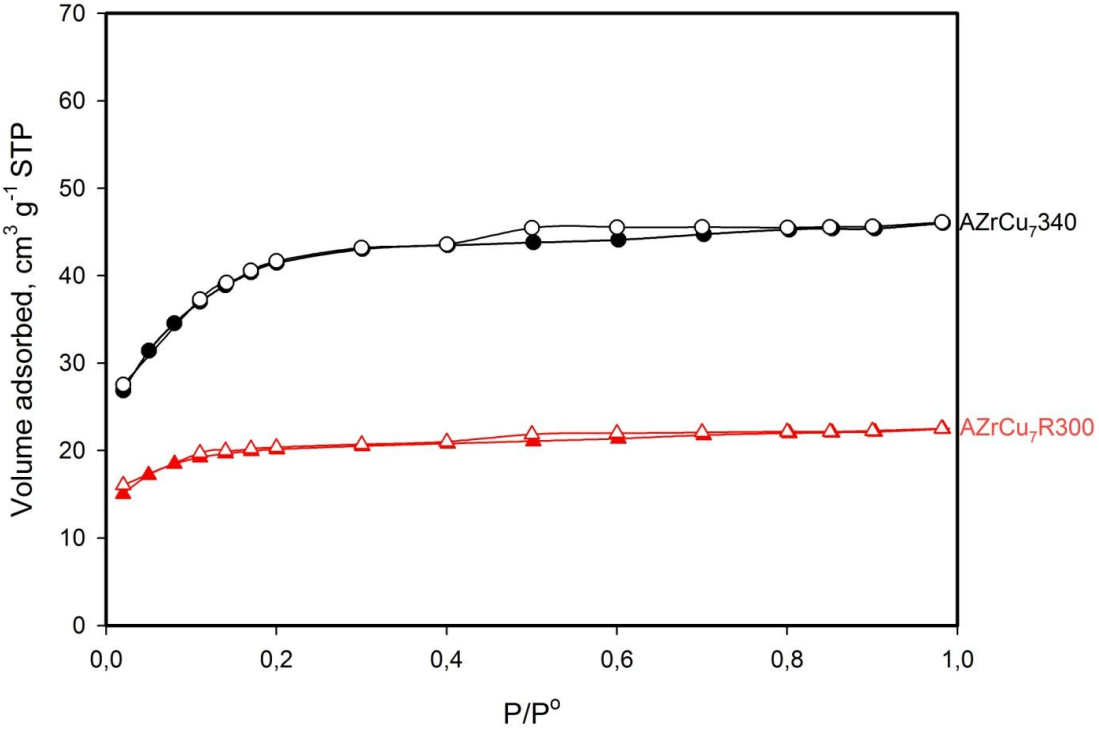

Fig.3-8. Adsorption-desorption isotherms of $AZrCu_7340$ and $AZrCu_7R300$. Full symbols: adsorption, empty symbols: desorption.

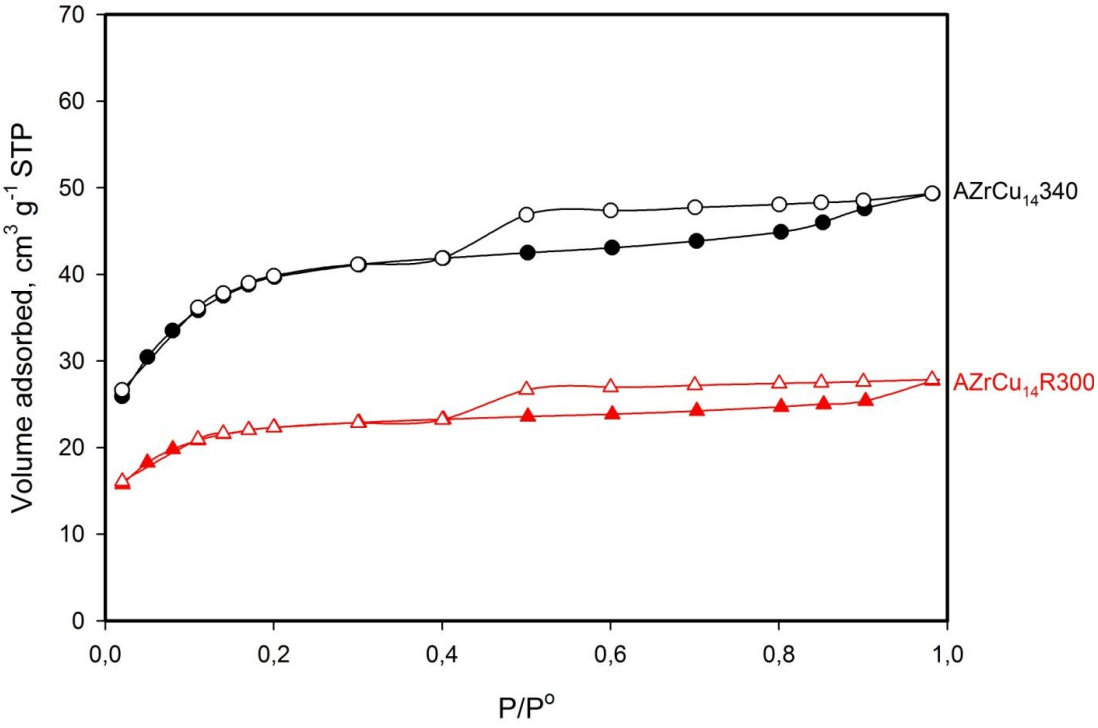

Fig.3-9. Adsorption-desorption isotherms of $AZrCu_{14}340$ and $AZrCu_{14}R300$. Full symbols: adsorption, empty symbols: desorption.

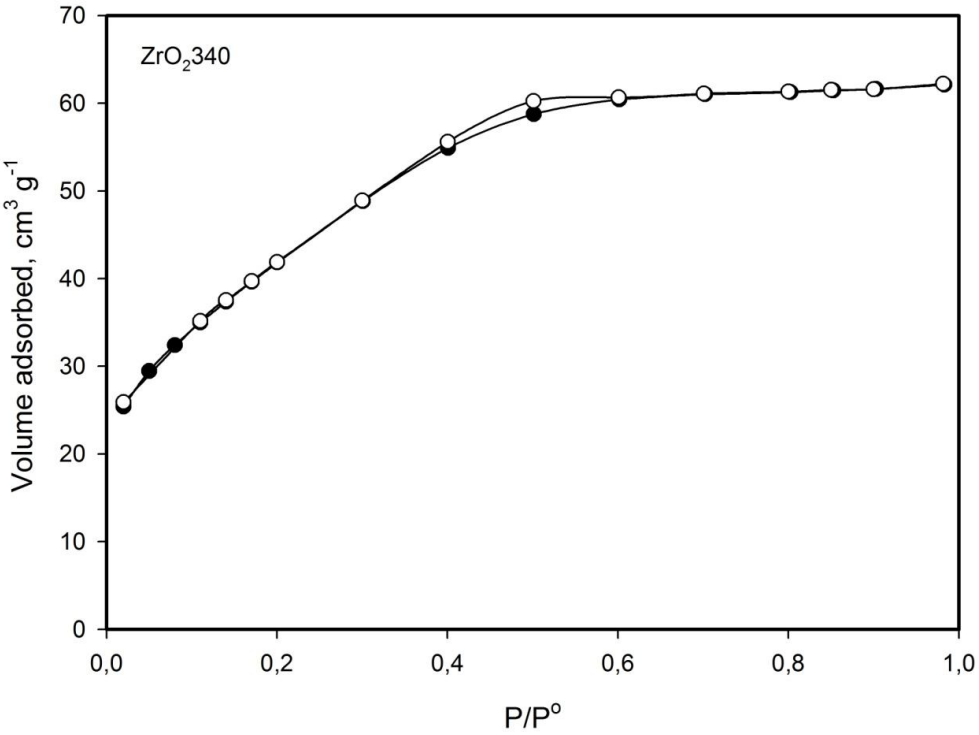

Fig.3-10. Adsorption-desorption isotherms of ZrO_2340. Full symbols: adsorption, empty symbols: desorption.

The shape of the curves of ZrO_2340, $NZrCu_6340$, $NZrCu_6R300$ and $NZrCu_6R450$ appears of type Ib according to the IUPAC classification [135], indicating the possible presence of micropores wider than molecular dimensions.

The samples $AZrCu_7340$, $AZrCu_7R300$, $AZrCu_{14}340$ and $AZrCu_{14}R300$ show a Type IV isotherm, according to the IUPAC classification [135], with a hysteresis loop typical of mesoporous materials. It is worth noting that the present preparation method produces ZrO_2 and $Cu\text{-}ZrO_2$ samples with higher surface areas in comparison with other chemically similar systems [84,147].

Table 3-3

Surface area, micropore volume, pore volume and pore diameter of ZrO_2 and $Cu\text{-}ZrO_2$ samples calcined at 340°C, reduced at 300°C and reduced at 450°C.

Sample	S_{BET}[a] (m^2g^{-1})	$S_{alfaplot}$ (m^2g^{-1})	Micropore volume ($cm^3\ g^{-1}$)	V_p[b] ($cm^3\ g^{-1}$)	D_p[c] (nm)
ZrO_2340	165	145	0.0037	0.096	2.3
$NZrCu_6340$	182	168	0.0073	0.101	2.2
$NZrCu_6R300$	131	121	0.0048	0.071	2.2
$NZrCu_6R450$	106	100	0.0033	0.057	2.1
$AZrCu_7340$	141	133	0.0080	0.071	2.0
$AZrCu_7R300$	77	61	0.0070	0.035	1.8
$AZrCu_7R450$	<5	-	-	-	-
$AZrCu_{14}340$	133	132	0.0066	0.076	2.3
$AZrCu_{14}R300$	85	71	0.0061	0.043	2.0
$AZrCu_{14}R450$	<5	-	-	-	-

[a] BET specific surface area

[b] Specific pore volume determined from the amount of N_2 adsorbed at $P/P^o = 0.98$

[c] Average pore diameter $D_p = 4V/A_{BET}$, where V is total pore volume

Compared to pure zirconia, $AZrCu_7340$ and $AZrCu_{14}340$ show, as expected, smaller N_2 adsorption and surface area, instead the sample $NZrCu_6340$ shows larger N_2 adsorption and surface area. This behaviour can be explained considering the influence of copper on the crystallisation of zirconia. In fact, as observed from XRD analysis on $NZrCu_6340$, the presence of copper leads to a shifting of the zirconia crystallization temperature to higher temperature, so the sample shows a higher surface area than ZrO_2340 probably because it is still amorphous after treatment at 340 °C, differently from pure ZrO_2.

Obviously, increasing the treatment temperature from 340 to 450 °C or taking the sample at 300°C for a long time during the reduction causes a decrease of the surface area because such treatment induces or increases the crystallisation of zirconia in all the samples.

The comparison between the XRD profiles of samples treated at 340°C and 450°C (Fig.3-11) supports the above hypothesis: the XRD profile clearly shows a more enhanced crystallization degree increasing the treatment temperature.

It can be observed that micropore volumes are very small for all samples: this ensures a satisfactory validity of the BET model and of the derived surface areas. For the same reason, surface areas calculated from α-plots, that exclude the contribution of micropores, are close to BET surface areas. The average values of pore diameter D_p calculated from the relation: $D_p = 4V/A_{BET}$ (34), where V is total pore volume, appear very similar for all samples and not much higher than 2 nm, indicating that most porosity in these samples is due to very small cavities, with size near the boundary of micropores.

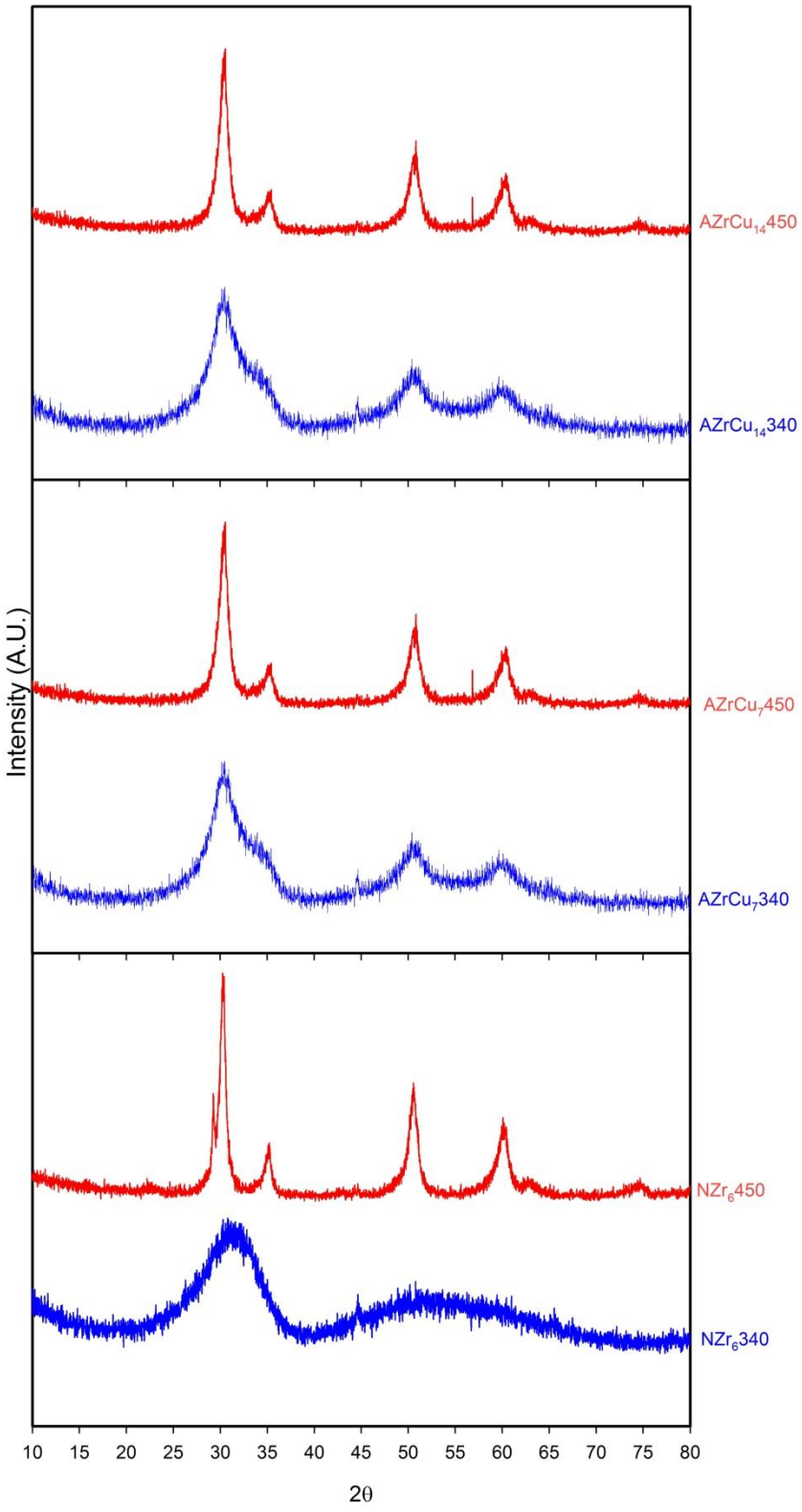

Fig.3-11. XRD patterns of $NZrCu_6340$, $NZrCu_6450$, $AZrCu_7340$, $AZrCu_7450$, $AZrCu_{14}340$ and $AZrCu_{14}450$.

3.1.5 Conclusions

The above data show that the new synthetic procedure based on the sol gel method allowed to obtain $Cu\text{-}ZrO_2$ systems with very high surface areas and remarkable Cu dispersions. Two methods based on different Cu precursors were investigated. The preparation method strongly influenced all the studied properties.

For $NZrCu_6$, prepared by *Method I*, using zirconium alkoxide as Zr source, copper (II) nitrate hydrate as copper source and acetylacetone to control the hydrolysis reaction rate of zirconium alkoxide:

- TG/DTA showed a crystallisation delay compared to pure ZrO_2 related to the introduction of Cu^{2+} ions into the zirconia matrix;
- X-ray powder diffraction confirmed the low crystallinity, due to the crystallization delay, of this system compared to pure ZrO_2;
- N_2 physisorption indicated that the crystallisation delay and the lower crystallinity allowed to obtain higher surface area (182 m^2g^{-1}), preserved after long reduction treatments (106-131 m^2g^{-1});

For $AZrCu_7$ and $AZrCu_{14}$, prepared by *Method II*, using zirconium alkoxide as Zr source, copper (II) acetate monohydrate as copper source and acetic acid glacial as alkoxide modifier to control the hydrolysis reaction rate of zirconium alkoxide:

- TG/DTA showed that the crystallisation of zirconia takes place at the same temperature of pure ZrO_2;
- X-ray powder diffraction confirmed the higher crystallinity, due to the lower crystallization temperature, compared with the sample prepared by *Method I*;
- N_2 physisorption indicated that the preparation method allowed to obtain high surface area (133-141 $m^2\ g^{-1}$), but long reduction treatments caused a strong decrease of the surface area, due to the crystallisation of zirconia (<5-85 m^2g^{-1}).

For all samples:

- X-ray powder diffraction gave no evidence of CuO, indicating a CuO phase highly dispersed on the zirconia surface;
- TPR measurements gave evidence of the stabilizing effect of ZrO_2 on the Cu^+ oxidation state;
- N_2O passivation method confirmed the results of the XRD analysis, indicating a very high dispersion of Cu oxide (13-85%), strongly influenced by the reduction temperature.

In Table 3-4 the most important properties of $Cu\text{-}ZrO_2$ samples are summarized.

Table 3-4
Summary of the most important properties of Cu/ZrO_2 systems.

Sample	$NZrCu_6$	$AZrCu_7$	$AZrCu_{14}$
Surface area (340°C), m^2g^{-1}	182	141	133
Surface area R300 (reduction at 300°C), m^2g^{-1}	131	77	85
Surface area R450 (reduction at 450°C), m^2g^{-1}	106	<5	<5
Crystallinity at 340°C	amorphous	crystalline	crystalline
Crystallinity at 450°C	crystalline	crystalline	crystalline
Reducibility, %	82	73	64
Cu dispersion R300 (reduction at 300°C), %	85	32	23
Cu dispersion R450 (reduction at 450°C), %	47	20	13

3.2 Materials $Cu/CeO_2/Al_2O_3$

3.2.1 Thermogravimetric analysis

Thermogravimetric analysis was performed in order to determinate the calcination temperature necessary to completely remove the organic phase of surfactant. All samples showed the same behaviour, reported in Fig.3-12. The weight loss up to ca. 250°C can be attributed to the removal of residual organic solvent and physisorbed and bulk water, while that starting at 250°C and ending at 550°C can be assigned to the elimination of the structure-directing agent (in the form of stearates). Based on these data, the calcination temperature of 550°C was selected.

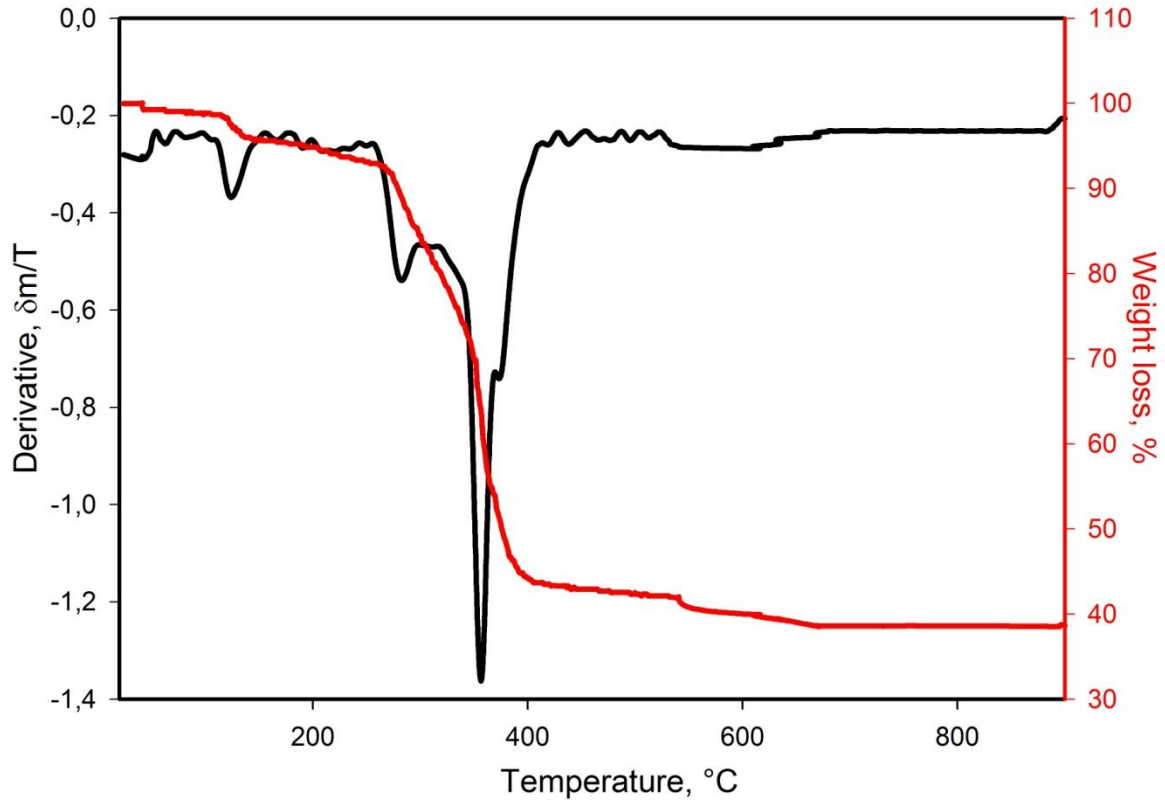

Fig.3-12. TG/DTG profiles of $EMCeCu_4$, $EMCeCu_8$ and $EMCeCu_{16}$.

3.2.2 XRD analysis

The diffractogram of all materials, treated in air at 550°C (Fig.3-13) and identified with a number indicating the temperature of the heat treatment, exhibits broad reflections due to γ-alumina, with a poorly microcrystalline structure, and peaks attributable to the presence of CeO_2 with a fluorite lattice structure. The average dimension of the ceria crystallites, calculated from the main peak at $2\theta = 28.6°$, according to the Scherrer's equation, resulted about 3.0 nm. With exception of $EMCeCu_{16}550$, the presence of a broad and very weak peak at $2\theta = 35.54°$ characteristic of the tenorite could indicate a CuO phase highly dispersed on the ceria and alumina surface with particles dimension near the XRD detection limit. As reported below, copper dispersion measured by N_2O chemisorption is very high, confirming the effectiveness of the preparation method in obtaining highly dispersed copper phases.

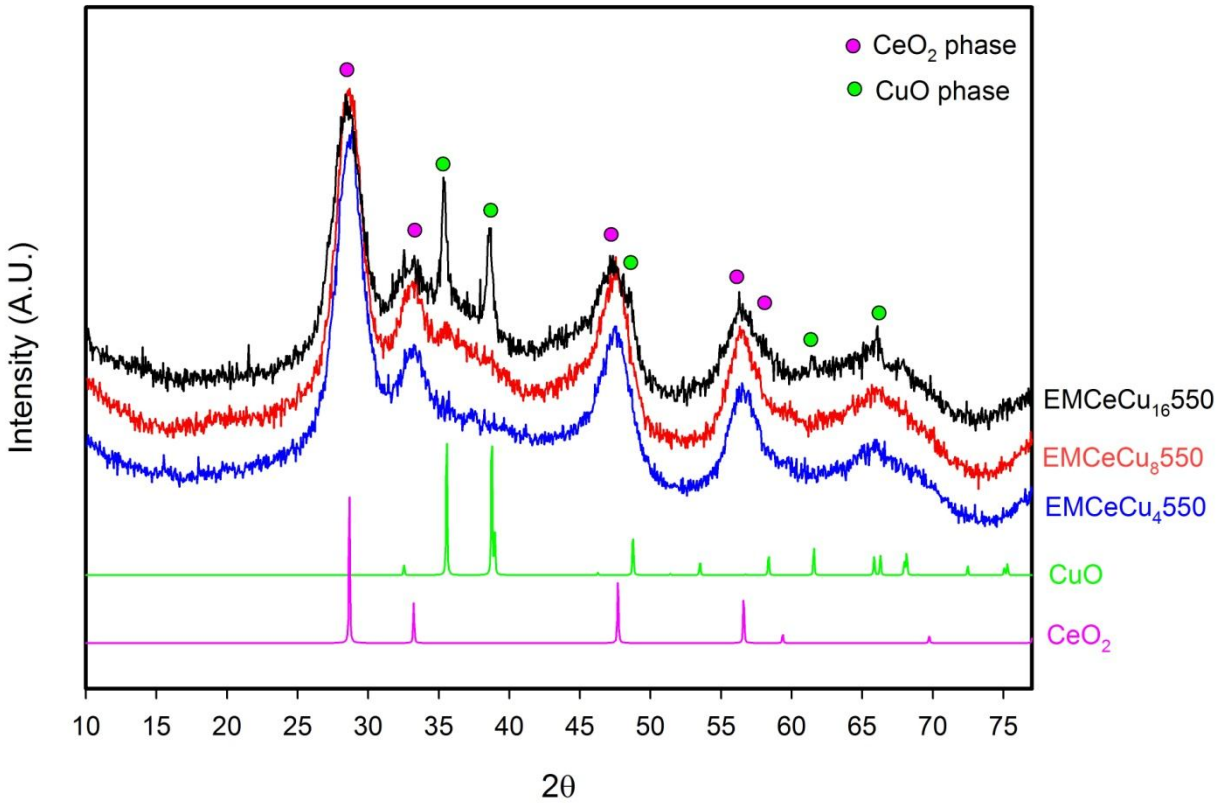

Fig.3-13. X-ray diffraction pattern of the catalysts $EMCeCu_4$, $EMCeCu_8$ and $EMCeCu_{16}$ after thermal treatment in air at 550°C.

3.2.3 N_2 physisorption

The porous nature of the prepared material was evaluated by N_2 adsorption at -196°C and the results are reported in Table 3-5. The samples show (Fig.3-14) a Type IV isotherm, according to the IUPAC classification [135], with a hysteresis loop typical of mesoporous materials and the typical inflection at low relative pressure, as expected for this type of materials [114].

The one-pot materials showed, after thermal treatment in air flow at 550°C, BET specific surface area between 316-362 m^2g^{-1}. The specific pore volumes are quite high (0.41- 0.55 cm^3g^{-1}) and the pore size distribution curves, estimated using the BJH method on the adsorption branch, are centered at 3.5 nm (Fig.3-15). The BET surface area of the calcined samples are very high and seems neither affected by the reduction with H_2 nor by operating under reaction conditions. Such treatments have also no influence on pore volume and pore size distribution.

Table 3-5

Surface area, pore volume and pore diameter of $EMCeCu_4550$, $EMCeCu_8550$ and $EMCeCu_{16}550$.

Sample	S_{BET} [a] (m^2g^{-1})	V_p [b] ($cm^3\ g^{-1}$)	D_p [c] (nm)
$EMCeCu_4550$	362	0.55	3.5
$EMCeCu_8550$	360	0.48	3.5
$EMCeCu_{16}550$	316	0.41	3.5

[a] BET specific surface area

[b] Specific pore volume determined at $P/P^o = 0.98$

[c] Pore diameter evaluated by BJH method (according to the peak of pore size distribution)

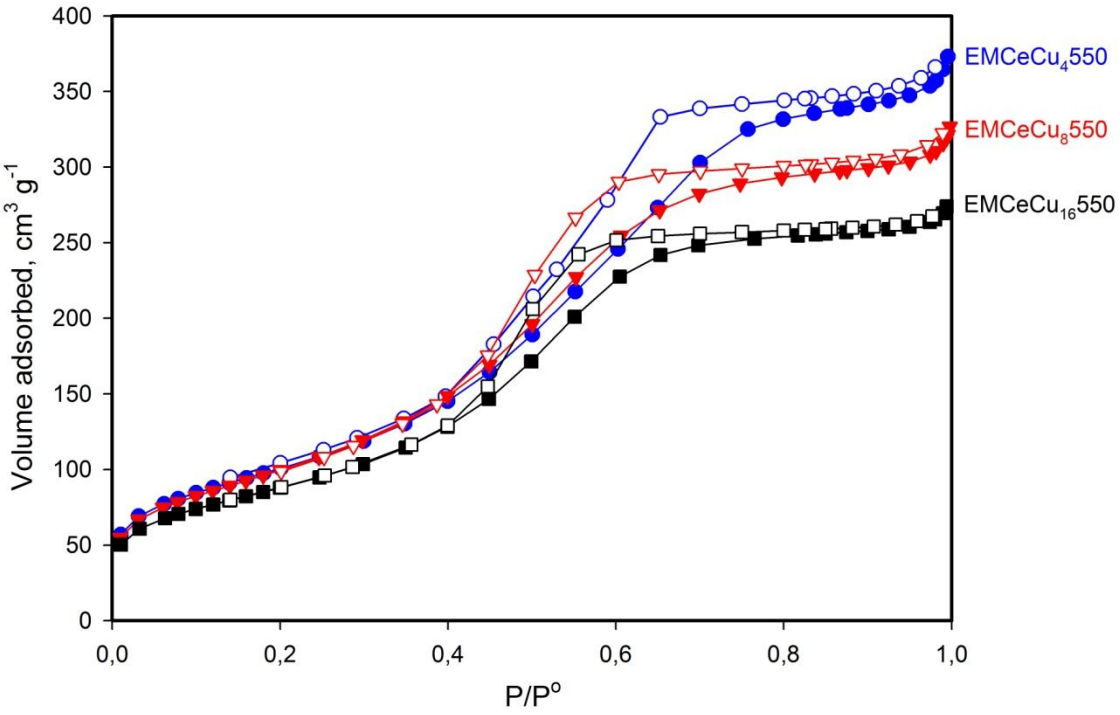

Fig.3-14. N_2 physisorption data of $EMCeCu_4550$, $EMCeCu_8550$ and $EMCECu_{16}550$ catalysts: isotherm (filled symbols for the adsorption branch and empty symbols for the desorption one).

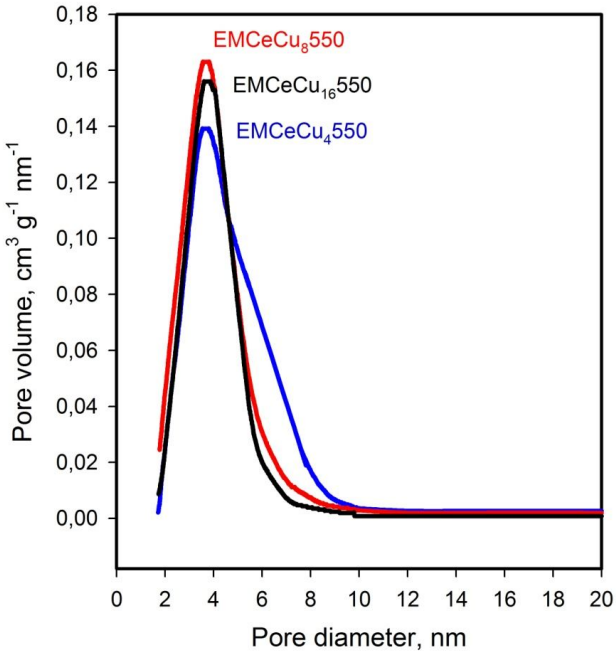

Fig.3-15. BJH pore size distribution of $EMCeCu_4550$, $EMCeCu_8550$ and $EMCECu_{16}550$ catalysts.

3.2.4 TPR and dispersion measurements

TPR measurements were carried out on the $EMCeCu_4550$, $EMCeCu_8550$ and $EMCECu_{16}550$ catalysts and on the reference materials CuO, CeO_2, CeO_2/Al_2O_3, CuO/Al_2O_3. The corresponding amounts of H_2 consumption are reported in Table 3-6.

In preliminary tests it was ascertained that under the employed experimental conditions no reaction nor adsorption of N_2O occurs on Al_2O_3, CeO_2 and CeO_2/Al_2O_3. In Fig.3-16 TPR profiles of CuO, CeO_2, CeO_2/Al_2O_3 are reported. The reference material CuO shows one peak at 400°C, with intensity corresponding to the complete reduction of Cu^{2+} to Cu^0, while CeO_2 gives a peak at about 600°C that accounts for a limited reduction (abt. 5%) of Ce^{4+} to Ce^{3+}: this can be related to a surface reaction probably forming oxygen vacancies [38,118]. The complete reduction of CeO_2 to Ce_2O_3 needs higher temperatures, thus it cannot occur under the present conditions [118,151,152]. The TPR profile of CeO_2/Al_2O_3 shows a peak broader than that of pure CeO_2 and shifted to lower temperature (450°C with a shoulder at about 300°C). The amount of consumed hydrogen is much higher than that observed for pure CeO_2 and corresponds to reduction of about 40% of Ce^{4+} to Ce^{3+}. This points to a greater reducibility of supported CeO_2, probably related to a higher dispersion. The appearance of TPR signals at lower temperature in comparison with pure CeO_2 can be explained by the formation of small ceria crystallites and isolated Ce^{4+} ions on the surface of alumina [151].

The TPR profile of CuO/Al_2O_3 is reported in Fig.3-17. The sample gives a peak with a maximum at 302°C, markedly lower than that of pure CuO, with a shoulder at about 420°C, suggesting that the redox properties of CuO are significantly affected by the interaction with alumina. Composite TPR signals were reported for CuO/Al_2O_3 materials also by other authors [153]. It can be hypothesized that small CuO clusters and/or isolated Cu^{2+} ions are reduced at lower temperature than larger CuO particles [153].

After reduction with H_2, the sample is passivated, as described in *Section 2.2.4* , and the corresponding TPR profile is shown in the same Fig.3-17. Two peaks appear at temperatures much lower than the fully oxidized sample, due to the reduction of superficial Cu(I) species. The presence of two peaks could be related to different Cu^{1+} sites linking oxygen with different strength. According to the procedure described above, the amount of superficial Cu atoms, and so the Cu dispersion, can be calculated from the H_2 consumed for reduction of superficial Cu^{1+} (Table 3-6). The calculated dispersion, 76%, corresponds to a Cu particle size of 1.4 nm (assuming a spherical

particle shape). The dispersion is very high if compared to other Cu catalysts supported on Al_2O_3 [27,154,155,156] and could be related to the textural properties of the support used.

Table 3-6
TPR and Cu dispersion data.

Sample	Composition (mol g^{-1} x 10^{-3})		Tmax (°C)	H_2 consumption (mol g^{-1} x 10^{-3})	Cu dispersion (%)	Cu S.A.[a] (m^2 g_{cat}^{-1})	Cu crystal size[b] (nm)
	Ce	Cu					
CuO	-	12.57	400	12.57	-	-	-
CeO_2	5.81	-	590	0.14	-	-	-
CeO_2/Al_2O_3	1.07	-	450	0.22	-	-	-
CuO/Al_2O_3 oxidized	-	0.79	302,420	0.67	-	-	-
CuO/Al_2O_3 passivated	-	0.79	145, 181	0.30	76	24.54	1.4
$EMCeCu_4550$	0.82	0.53	200	0.08	-	-	-
$EMCeCu_4R450$	0.82	0.53	-	-	-	-	-
$EMCeCu_8550$	0.80	1.04	195, 309, 438	0.69	-	-	-
$EMCeCu_8R450$	0.80	1.04	145, 195	0.36	69	29.45	1.5
$EMCeCu_{16}550$	0.74	2.03	183, 298,445	1.00	.	-	-
$EMCeCu_{16}R450$	0.74	2.03	126, 186	0.55	54	44.98	1.9

[a] Calculated from Cu dispersion assuming a surface Cu concentration of 1.47 x 10^{19} atoms m^{-2} [82].

[b] Calculated from Cu dispersion assuming a spherical shape.

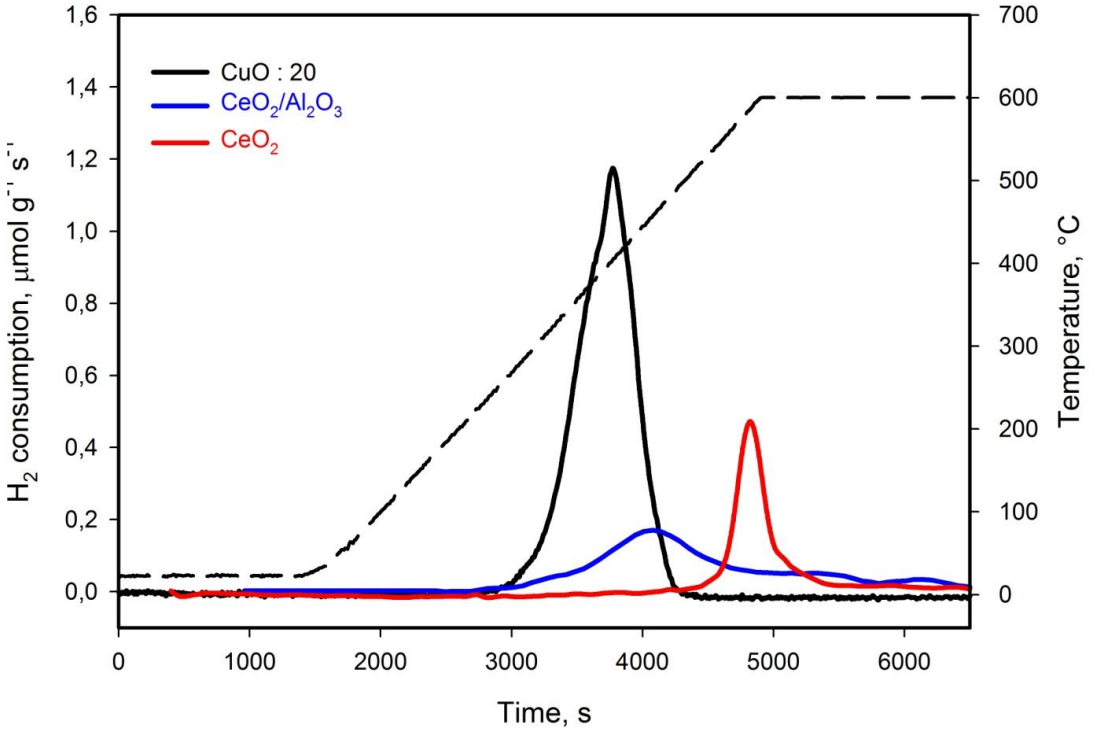

Fig.3-16. TPR profiles of reference materials CuO, CeO_2 and CeO_2/Al_2O_3.

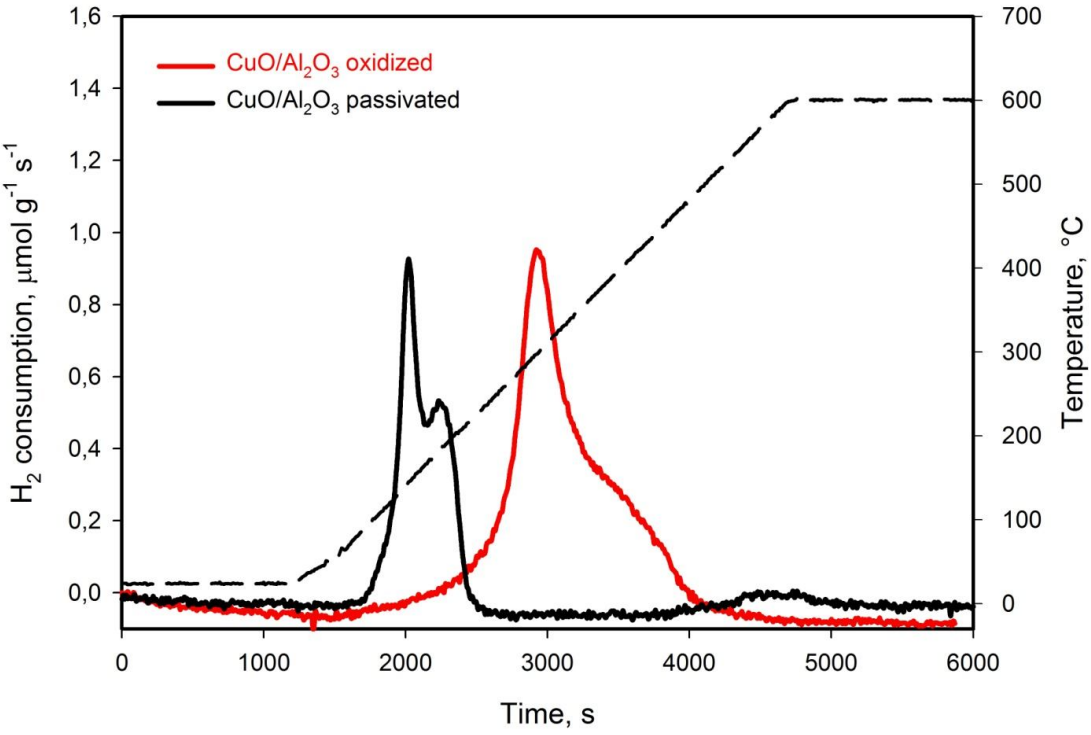

Fig.3-17. TPR profiles of CuO/Al_2O_3 oxidized and after passivation with N_2O.

The TPR spectra of the $EMCeCu_4550$, $EMCeCu_8550$ and $EMCeCu_{16}550$ oxidized are reported in Fig.3-18.

The TPR profiles of the catalysts show no signal at the temperatures usually found for CeO_2 [114, 157-159], indicating that the oxide probably is highly dispersed on alumina, and in this form can undergo a partial reduction at about 450 °C [114,159]. Moreover the TPR profiles of the catalysts indicate that most Cu is not present as bulk CuO, but as more reducible species. Taking into account the results of previous TPR measurements on a similar material [114], the appearance of three peaks is likely related to the presence of : i) Cu^{2+} ions or smaller clusters tightly bonded to CeO_2 , that are the most easily reducible, ii) a CuO phase highly dispersed in alumina and iii) larger CuO particles and a little contribution of CeO_2 dispersed in alumina.

Some tailing at high temperature could be due to the slow reduction of Cu^+ species, that are strongly stabilized by interaction with the CeO_2 phase. The presence of Cu^+ species forming part of Cu-O-Ce sites was previously observed on a similar catalyst by XPS measurements [114]. Moreover the stabilizing effect of CeO_2 on the oxidation state Cu^+ was suggested in other studies [38,154].

The $EMCeCu_4550$ sample shows only a peak at low temperature, about 200°C, related to Cu^{2+} species interacting with CeO_2 and very reducible. Instead the $EMCeCu_8550$ and the $EMCeCu_{16}550$ catalysts show also medium and high temperature signals, related respectively to well dispersed and larger CuO particles. It can be noted that mainly the low and the medium temperature signals increase with the Cu content: this suggests that increasing Cu content, instead of increasing the amount of bulk CuO, leads to an increase of the Cu fraction present as isolated Cu^{2+} ions or CuO tightly bonded to CeO_2 or dispersed on alumina.

Table 3-6 shows that the amount of consumed H_2 is always lower than that corresponding to the complete reduction of Cu^{2+} to Cu^0. Since it is unlikely that Cu is not completely reduced to the metallic state under these conditions, this means that the average initial oxidation state of Cu is lower than 2. Thus the air treated sample appears to contain both Cu^{2+} and Cu^{1+}: this can be related to the stabilizing effect of CeO_2 on the Cu^{1+} species [38].

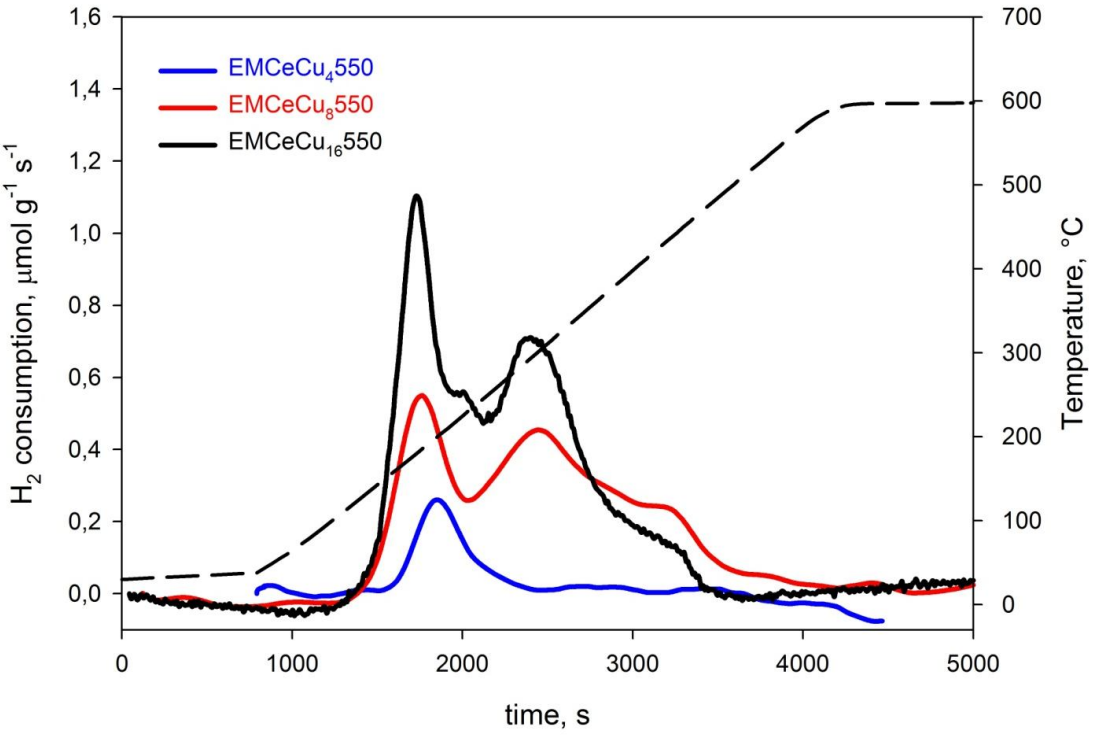

Fig.3-18. TPR profiles of $EMCeCu_4550$, $EMCeCu_8550$ and $EMCeCu_{16}550$.

In Figs. 3-19 and 3-20 the TPR profiles obtained with the catalysts $EMCeCu_8$ and $EMCeCu_{16}$ reduced and treated with N_2O as described above (see *Section 2.2.4*) together with, for sake of comparison, the corresponding profile obtained with the $EMCeCu_8$ and $EMCeCu_{16}$ sample oxidized are reported. The samples reduced and passivated are identified with the suffix "R" followed by a number indicating the reduction temperature, for example $EMCeCu_8R450$.

The TPR profiles of the passivated catalysts show two peaks at temperatures lower than those shown by the fully oxidized sample, and very close to those observed for the CuO/Al_2O_3 sample. Moreover a signal at about 600°C also appears. The low temperature signals can be attributed to the reduction of only superficial Cu^{1+} species, because the CeO_2 phase does not react with N_2O, as observed above. It is very interesting the presence of two TPR signals attributable to Cu_2O surface: such behaviour, that was observed, but with lower evidence for different Cu catalysts [150], is probably due to the presence of a mesostructured, very high surface area alumina. It can be hypothesized that water produced by reduction of Cu_2O is released from the material with a slow diffusion– adsorption sequence occurring in the tortuous mesopores system of alumina. It is likely that water vapour can re-oxidize Cu^0 under these conditions [82], so the slow H_2O desorption can

cause a delay in Cu reduction, leading to a tailing of the TPR signal or even the appearance of a further TPR signal. This effect is more pronounced with these Cu/Ce/Al materials probably because of several cooperating factors such as very high surface area, mesoporous structure, high Cu dispersion. However, it does not affect the calculation of the Cu surface area, since it is clear from an hydrogen–oxygen balance that the total amount of H_2 consumed must correspond to the oxygen originally adsorbed on Cu.

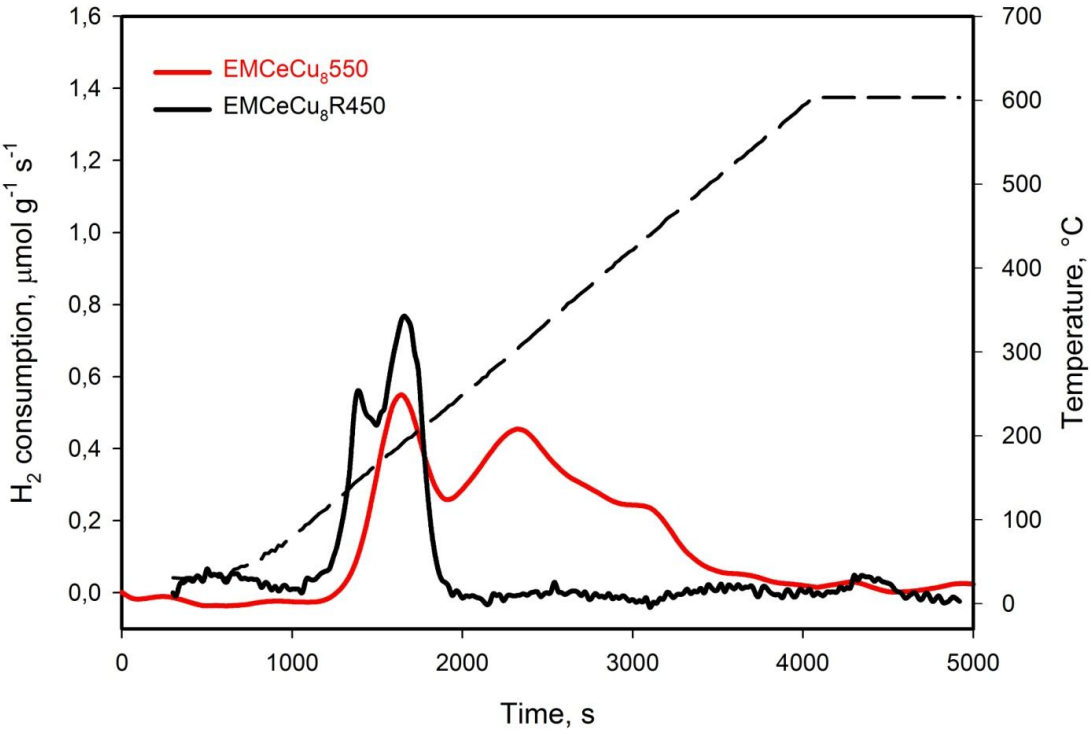

Fig.3-19. TPR profiles of $EMCeCu_8$ oxidized ($EMCeCu_8550$) and after passivation with N_2O ($EMCeCu_8R450$).

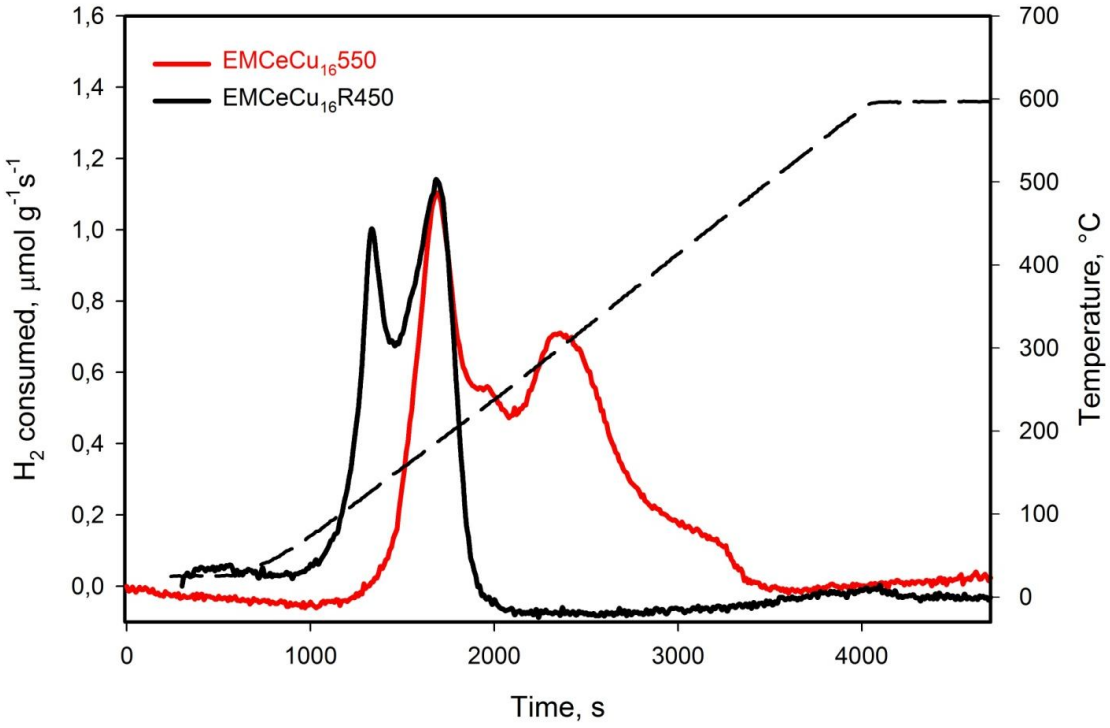

Fig.3-20. TPR profiles of $EMCeCu_{16}$ oxidized ($EMCeCu_{16}550$) and after passivation with N_2O ($EMCeCu_{16}R450$).

The Cu dispersion is 69% for the $EMCeCu_8$ sample and 54 % for the $EMCeCu_{16}$ sample, corresponding to a Cu particle size of 1.5 nm and 1.9 nm respectively, that is comparable to that of the CuO/Al_2O_3 sample. The high temperature signal can be due to Cu species that were not reduced in the first TPR limited to 450°C. These are probably Cu^{1+} species, that are hardly reducible because stabilized by CeO_2, as noted before. These data show that the presence of CeO_2 affects the reducibility of CuO supported on Al_2O_3, but does not significantly modify the dispersion of the metallic Cu phase obtained by H_2 reduction. This very high dispersion is in agreement with the results of the XRD analysis indicating very high dispersion of Cu oxide.

Based on these data, the temperature of 450°C was chosen to reduce the copper oxide to metallic copper, avoiding the sinterization of metallic Cu and retaining a high dispersion degree. This temperature, being higher than the operating range of the OSRM tests, ensured a higher stability of the catalysts under reaction conditions.

3.2.5 X-Ray Photoelectron Spectroscopy (XPS)

The results of XPS obtained for all catalysts in terms of B.E. values (in eV) and surface Ce/Al, Cu/Al and Cu/(Ce+Cu) atomic ratios are reported in Table 3-7.

Table 3-7
B.E. values (in eV) and surface Ce/Al, Cu/Al and Cu/(Ce+Cu) atomic ratios.

Sample	C 1s	O 1s	Al 2p	Cu $2p_{3/2}$	Ce/Al	Cu/Al	Cu/(Ce+Cu)
$EMCeCu_4$ fresh	284.8 (53%) 286.6 (16%) 289.1 (31%)	531.0	73.9	933.8 (86%) 935.4 (14%)	0.018	0.020	0.54
$EMCeCu_4$ used*	284.8 (68%) 286.0 (13%) 288.9 (19%)	531.3	74.3	932.7	0.009	0.012	0.56
$EMCeCu_8$ fresh	285.0 (64%) 287.2 (17%) 289.5 (19%)	531.1	74.3	932.8 (21%) 934.6 (79%)	0.015	0.032	0.68
$EMCeCu_8$ used*	284.8 (88%) 287.1 (8%) 289.3 (4%)	532.1	74.1	932.8 (83%) 934.6 (17%)	0.011	0.032	0.73
$EMCeCu_{16}$ fresh	284.0 (44%) 285.0 (26%) 289.0 (30%)	530.4	74.3	933.7	0.026	0.056	0.68
$EMCeCu_{16}$ used*	284.0 (93%) 286.0 (4%) 289.0 (3%)	532.4	74.3	932.7	0.010	0.038	0.78

* catalyst diluted in quartz powder (catalysts: quartz 1:10 wt:wt) pre-reduced at 450°C and tested in OSRM; reaction conditions: $H_2O/CH_3OH/O_2$ molar ratio = 1.1/1/0.12, CH_3OH concentration = 17.8%, GHSV = 60000 $Lg^{-1}h^{-1}$ (see *Section 2.3.1*)

Fig.3-21 shows the Ce 3*d* core level spectra for the fresh and used $EMCeCu_4$ (a), $EMCeCu_8$ (b) and $EMCeCu_{16}$ (c). The core level Ce 3*d* signal of ceria is composed of six peaks ν_0, ν_1 and ν_2 (Ce $3d_{5/2}$) and ν'_0, ν'_1 and ν'_2 (Ce $3d_{3/2}$); and four peaks u_0 and u_1 (Ce $3d_{5/2}$) and u_0' and u_1' (Ce $3d_{3/2}$) that correspond to Ce^{4+} 3d and Ce^{3+} 3d final states, respectively. A clear description of the typical Ce 3*d*

core level spectrum is reported by Qiu et al [160].

Although the Ce 3*d* spectra of cerium oxide are very complex, Ce^{4+} and Ce^{3+} can be differentiated because of the distinct line shapes, being the ν'_2 peak at 916.8 eV characteristic of Ce^{4+}, while the doublet u_1/u_1' at 885.7 and 904.1 eV, respectively, characteristic of Ce^{3+} species. In all the fresh catalysts Ce^{4+} species are clearly dominant, but after catalysis, an increase of the intensity of the doublet u_1/u_1' is observed, in addition to the decrease in the intensity of the ν'_2 peak. This indicates that some of Ce^{4+} is reduced, during the catalytic process.

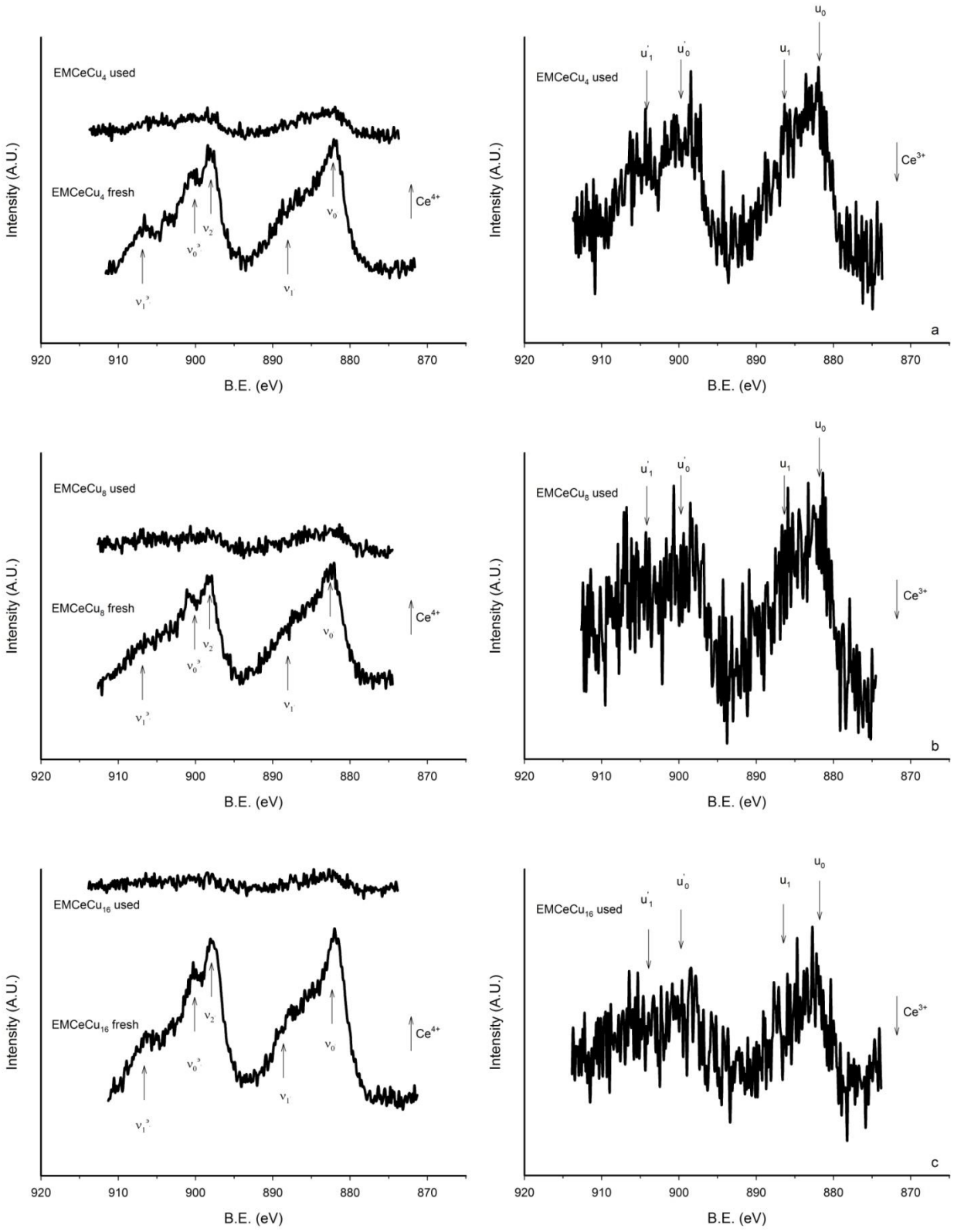

Fig.3-21. Ce 3d photoelectron profile of the fresh and used $EMCeCu_4$ (a), $EMCeCu_8$ (b) and $EMCeCu_{16}$ (c).

In Fig.3-22 a comparison between the Cu 2p photoelectron profiles for the samples $EMCeCu_4$ catalyst fresh and used is reported.

The spectrum of Cu 2*p* for the fresh $EMCeCu_4$ catalyst shows a signal centred at 933.8 eV, that can be assigned to CuO and a signal centred at 935.4 eV that can be assigned to copper basic carbonate.

The Cu 2*p* spectrum for the used catalyst shows some modifications. The two peaks at 933.8 eV and 935.4 eV disappear with their associated shake up satellites and a peak centred at 933.1 eV appears. This value is lower than the Cu $2p_{3/2}$ binding energy of CuO i.e. 933.6 eV. The lower Cu $2p_{3/2}$ binding energy and the low intensity of the shake-up satellite structure suggest the presence of reduced copper species strongly bonded to the catalysts support.

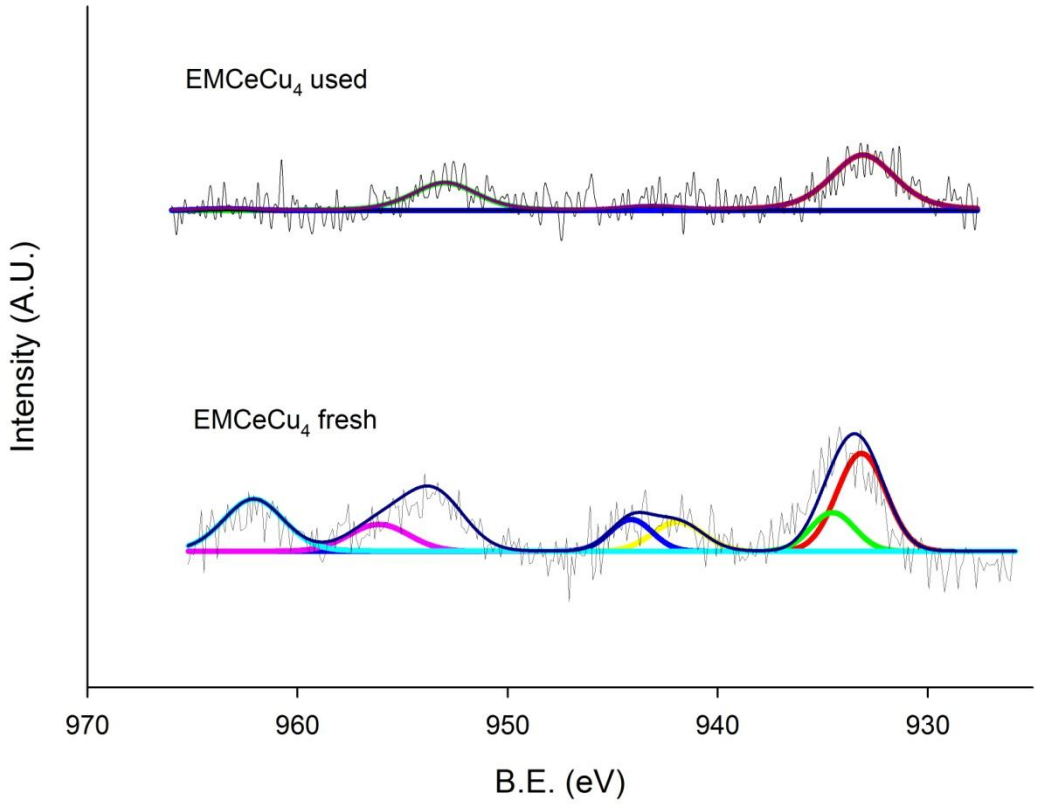

Fig.3-22. Comparison between the Cu 2p photoelectron profiles for the sample $EMCeCu_4$ fresh and used.

In Fig.3-23 a comparison between the Cu 2p photoelectron profiles for the sample $EMCeCu_8$ fresh and used is reported.

The spectrum of Cu 2*p* for the fresh $EMCeCu_8$ catalyst shows a signal centred at 932.8 eV, that can be assigned to the presence of Cu^{+1} and a signal at 934.6 eV assigned to Cu^{+2} strongly interacting with the alumina support. The intensity ratio of the shake up satellite to the corresponding principal peak (I_{sat}/I_{pp}) is 0.35, lower than 0.55, the characteristic value for Cu^{+2} species and higher than the one corresponding to Cu^{+1} species. This low I_{sat}/I_{pp} ratio suggests the probable presence of Cu^{+1} but Cu^0 species cannot be discarded.

The Cu 2*p* spectrum for the used catalyst shows many modifications. The intensity of the peak at higher binding energy assigned to $CuAl_2O_4$ decreases with a concomitant drastic decrease in intensity of its associated shake up satellites (see the low I_{sat}/I_{pp} value for the used catalyst), and the intensity of the peak assigned to Cu-O-Ce is more intense than that of $CuAl_2O_4$.

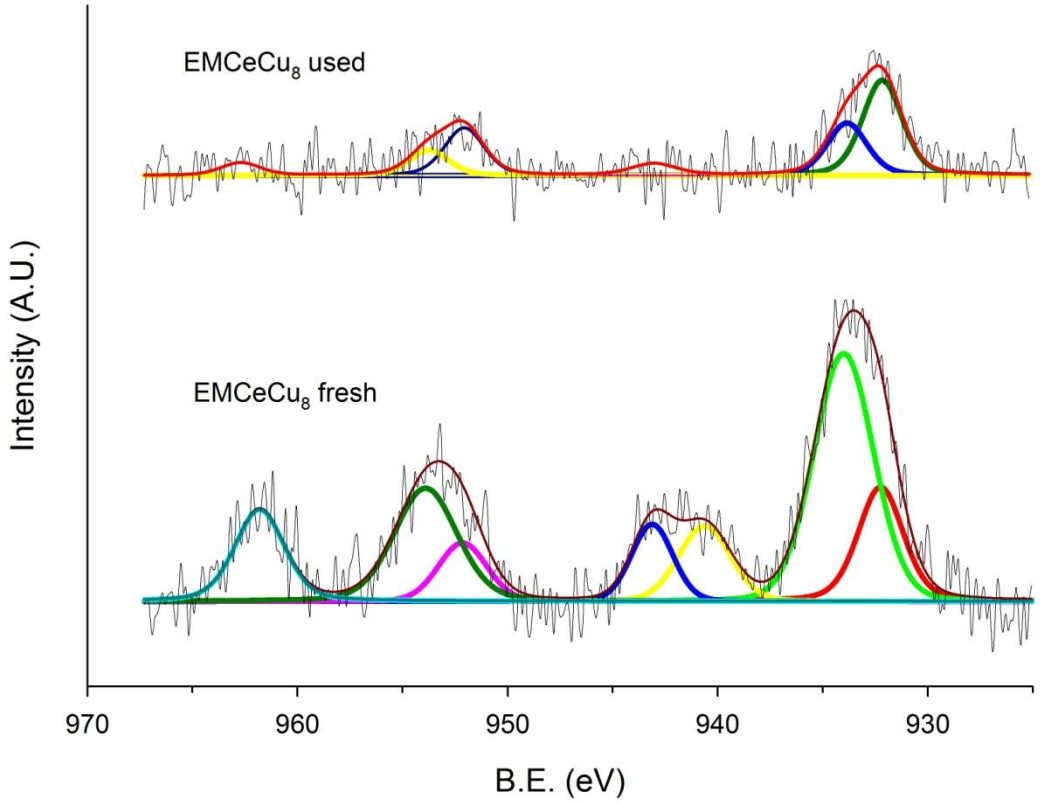

Fig.3-23. Comparison between the Cu 2p photoelectron profiles for the sample $EMCeCu_8$ fresh and used.

In Fig.3-24 a comparison between the Cu 2p photoelectron profiles for the sample $EMCeCu_{16}$ fresh and used is reported.

The spectrum of Cu 2*p* for the fresh $EMCeCu_{16}$ catalyst shows a signal centred at 933.7 eV, that can be assigned to CuO.

The Cu 2*p* spectrum for the used catalyst shows many modifications. It shows a signal shifted to 932.7 eV with its associated shake up satellites with much lower intensities. This value is lower than the Cu $2p_{3/2}$ binding energy of CuO i.e. 933.6 eV. The lower Cu $2p_{3/2}$ binding energy and the low intensity of the shake-up satellite structure suggest the presence of reduced copper species in the catalyst. The Cu $2p_{3/2}$ binding energy cannot, however, be used to distinguish between Cu_2O and Cu^0 because they are essentially identical.

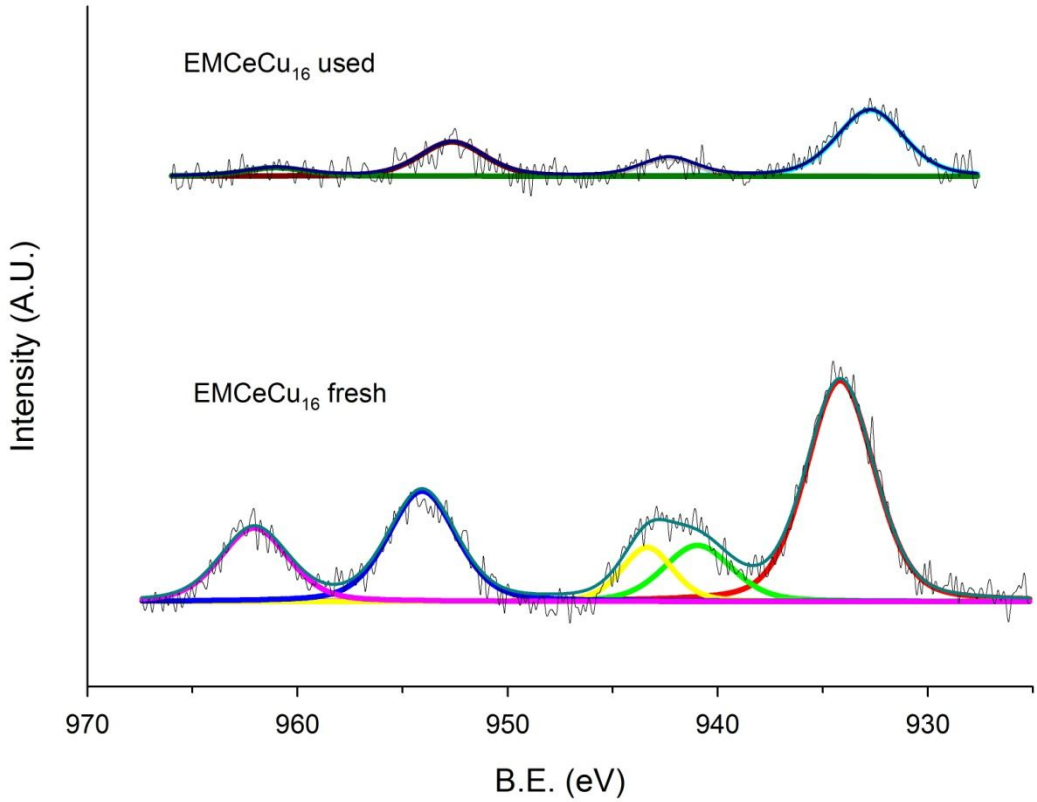

Fig.3-24. Comparison between the Cu 2p photoelectron profiles for the sample $EMCeCu_{16}$ fresh and used.

The presence of surface carbonates is detected by XPS and, in fact, a high intensity peak at about 289.0 eV in the C 1s core level spectrum of the fresh catalysts $EMCeCu_4$, $EMCeCu_8$ and $EMCeCu_{16}$ is assigned to carbonate groups. After catalysis the area of this peak decreases (Table 3-7) probably due to the catalytic reaction. The binding energies of the other constituent elements are unaffected after catalytic tests. Avgouropoulos and Ioannides [161] detected the presence of both Cu^{2+} and Cu^{1+} species in the fresh system $CuO\text{-}CeO_2$ and observed a significant enrichment of the surface with copper oxide species.

3.2.6 Conclusions

The characterization data show that mesoporous Cu-Ce-Al based materials can be prepared by a new single-step synthesis, performed in n-propanol using aluminium sec-butoxide as Al precursor and metal stearates, both as Cu-Ce sources and structural directing agents. This type of synthetic approach appears to be very efficient for the preparation of highly dispersed Cu-Ce containing particles supported on a structurally ordered alumina.
The most important results are reminded in Table 3-8.

Table 3-8
Summary of the most important properties of $Cu/CeO_2/Al_2O_3$ systems.

Sample	$EMCeCu_4$	$EMCeCu_8$	$EMCeCu_{16}$
Surface area (550°C), m^2g^{-1}	362	360	316
Crystallinity at 550°C	crystalline	crystalline	crystalline
Reducibility, %	15	66	49
Cu dispersion (reduction at 450°C), %	-	69	54

In particular the following results must be emphasized:

- N_2 physisorption showed that the samples have exceptionally high surface area (316-360 m^2g^{-1}) and quite narrow pore size distributions;

- X-ray powder diffraction indicated a CuO phase highly dispersed on the ceria and alumina surface;
- N_2O passivation method confirmed the results of the XRD analysis, indicating a very high dispersion of Cu oxide (54-69%).

Another important result regards the influence of the presence of CeO_2 on the oxidation state of Cu. As suggested by TPR measurements, the presence of CeO_2 favours the Cu^+ oxidation state. This was confirmed by XPS measurements effected on the fresh and used catalyst, that gave evidence of the presence of Cu^+ species and of the Ce^{4+} reduction during the reaction.
This last point will be further investigate in Chapter 5, where it will be shown that the presence of Cu^+ under steam reforming conditions is essential for the reaction and that CeO_2 seems to be directly involved in the Cu^0 oxidation.

4 Results and discussion

Catalytic tests: Apparatus 1

Catalytic tests performed in the Apparatus 1 (see *Section 2.3.1*) are presented.

4.1 Catalytic activity of Cu/ZrO_2 catalysts

OSRM tests are carried out both on $Cu\text{-}ZrO_2$ samples and on ZrO_2 subjected to different heat treatments.

4.1.1 ZrO_2

The results obtained with $ZrO_2$340 (Fig.4-1A) are presented as CH_3OH total conversion and partial conversions to different products. $ZrO_2$340 shows an appreciable methanol conversion that reaches about 60% at 400 °C: however the activity for OSRM is negligible, since the production of H_2 is very small in the entire temperature range and the main products are $(CH_3)_2O$ and CH_2O. The formation of $(CH_3)_2O$ indicates a dehydration activity of $ZrO_2$340, that is expected from a metal oxide having surface acid sites. On the other hand, the formation of CH_2O is due to an oxidative dehydrogenation, since H_2 is not produced. This oxidative activity is probably related to the presence of anionic vacancies, that can exist on the surface of $ZrO_2$340 [84]. The oxidation activity of the zirconia due to the oxygen vacancies was already reported [162]. OSRM tests are carried out also on ZrO_2R450. The results, reported in Fig.4-1B, are similar to those obtained with the not pre-reduced sample, indicating no OSRM activity, the only difference being the higher CH_3OH conversion in the range 300-350 °C, due to production of $(CH_3)_2O$ in larger extent. This points to a higher dehydration activity, probably related to a higher concentration of acid sites on the surface of ZrO_2 after the H_2 treatment. Thus the H_2 pre-treatment does not produce substantial modification of the catalytic properties of ZrO_2.

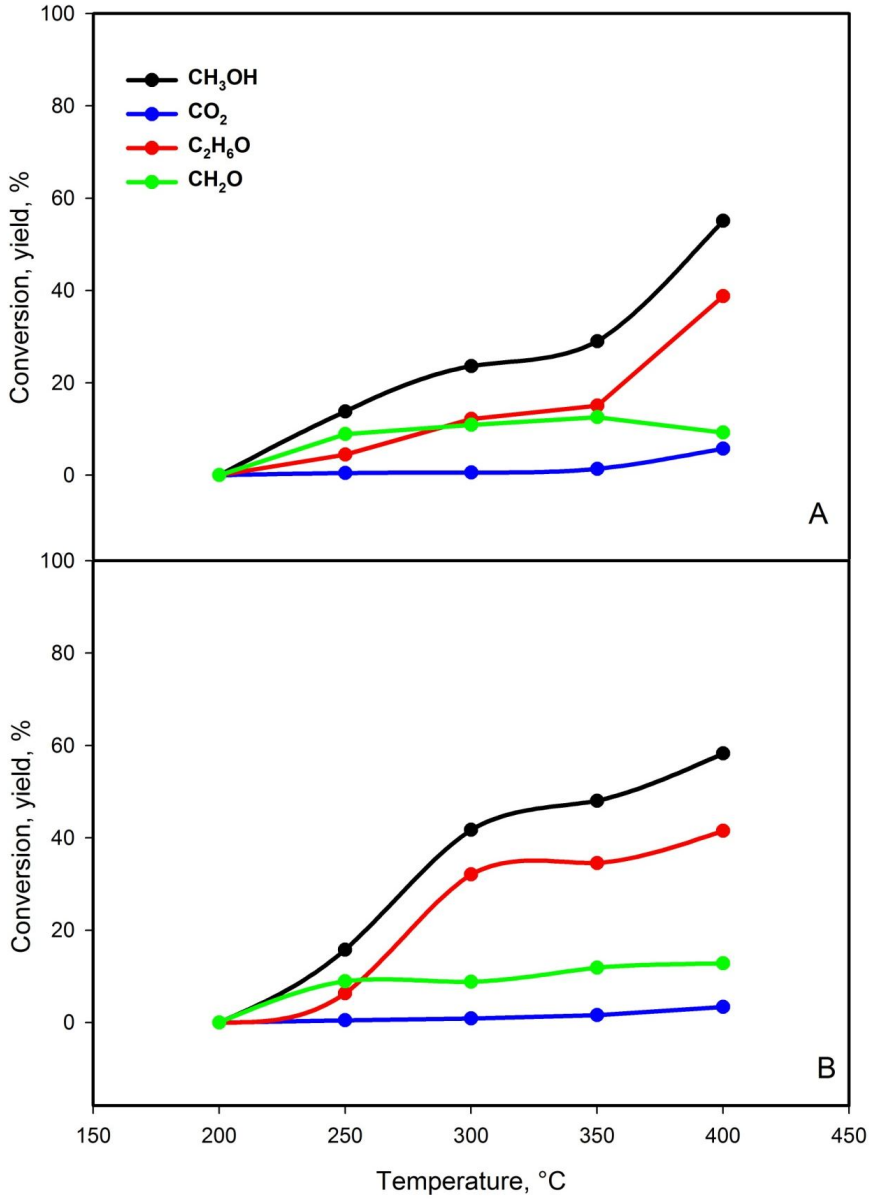

Fig.4-1. CH_3OH total conversion and partial conversions to CO_2, $(CH_3)_2O$ and CH_2O as a function of temperature on $ZrO_2$340 (A) and ZrO_2R450 (B). Reaction conditions: $H_2O/CH_3OH/O_2$ molar ratio = 1.1/1/0.12, CH_3OH concentration = 17.8%, GHSV = 60000 h^{-1}.

4.1.2 $NZrCu_6$

The results of OSRM tests carried out on $NZrCu_6$ samples pre-reduced with H_2 at 300 or 450°C as described in *Section 2.1.4* are reported in terms of methanol conversion and H_2 yield as a function of temperature (Fig.4-2). The material not reduced with H_2 ($NZrCu_6340$) has also been tested to investigate if active Cu species can be formed in the reducing atmosphere of the reaction tests. As expected, the catalytic activity is influenced by the different pre-treatments, although it is not simple to find a clear interpretation of this effect. For all catalysts methanol conversion increases with temperature reaching a maximum at 400 °C, however the complete conversion is not reached under the present conditions. Surprisingly, the not reduced $NZrCu_6340$ gives values of methanol conversion comparable and sometimes higher than those observed with the $NZrCu_6R300$: this suggests that under reaction conditions the CuO species are effectively reduced to metallic Cu due to the reducing action of methanol. The behaviour is similar to that observed for $Cu/CeO_2/Al_2O_3$ catalysts (see *Section 4.2.1*). The lowest methanol conversion is instead observed with $NZrCu_6R450$, probably due to the strong decrease of surface area caused by the more severe pre-treatment, as observed above (see Table 3-3).

As shown in Fig. 4-2, H_2 yield does not parallel methanol conversion. In fact, the highest values of H_2 yield are observed with $NZrCu_6R450$ and $NZrCu_6340$ (maxima at 400 and 350 °C respectively), while $NZrCu_6R300$ gives a higher yield at 300 °C, but shows a lower performance at higher temperatures. H_2 yield is generally lower than 2.76 mol H_2 per mol methanol, that expected on the basis of the feeding composition (see *Section 2.3.1*) and the values of methanol conversion considering only the reactions of partial oxidations and steam reforming, with the exception of the case of $NZrCu_6R450$ tested at 350-400 °C. These results indicate that secondary reactions occur in appreciable extent. The conversions to CO, CO_2, $(CH_3)_2O$ and CH_2O are reported in Figs. 4-3 and 4-4. The values of conversion to CO_2 (Fig. 4-3) appear generally lower than those of methanol conversion, with the exception cited above. Conversion to CO (Fig.4-3) is negligible at low temperatures and increases markedly above 300°C for $NZrCu_6340$ and $NZrCu_6R300$, while it increases much less for $NZrCu_6R450$. The production of $(CH_3)_2O$ and CH_2O (Fig.4-4) is appreciable for $NZrCu_6340$ or $NZrCu_6R300$, while it is much lower for $NZrCu_6R450$. The formation of the last products is probably also due to the catalytic activity of the support, as observed above (Fig.4-1).

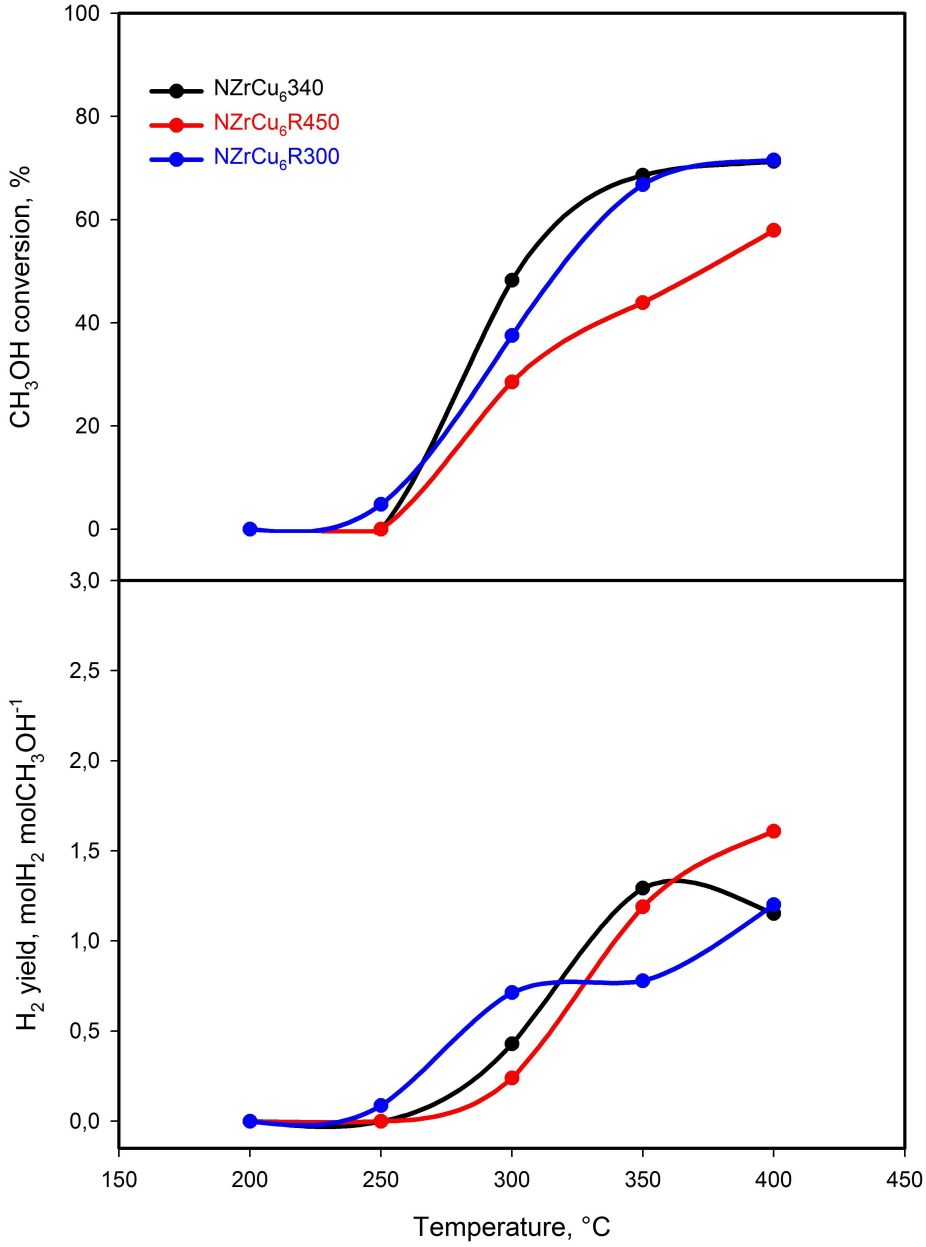

Fig.4-2. CH_3OH conversion and H_2 yield as a function of temperature in OSRM tests on $NZrCu_6340$, $NZrCu_6R300$ and $NZrCu_6R450$. Reaction conditions as in Fig.4-1.

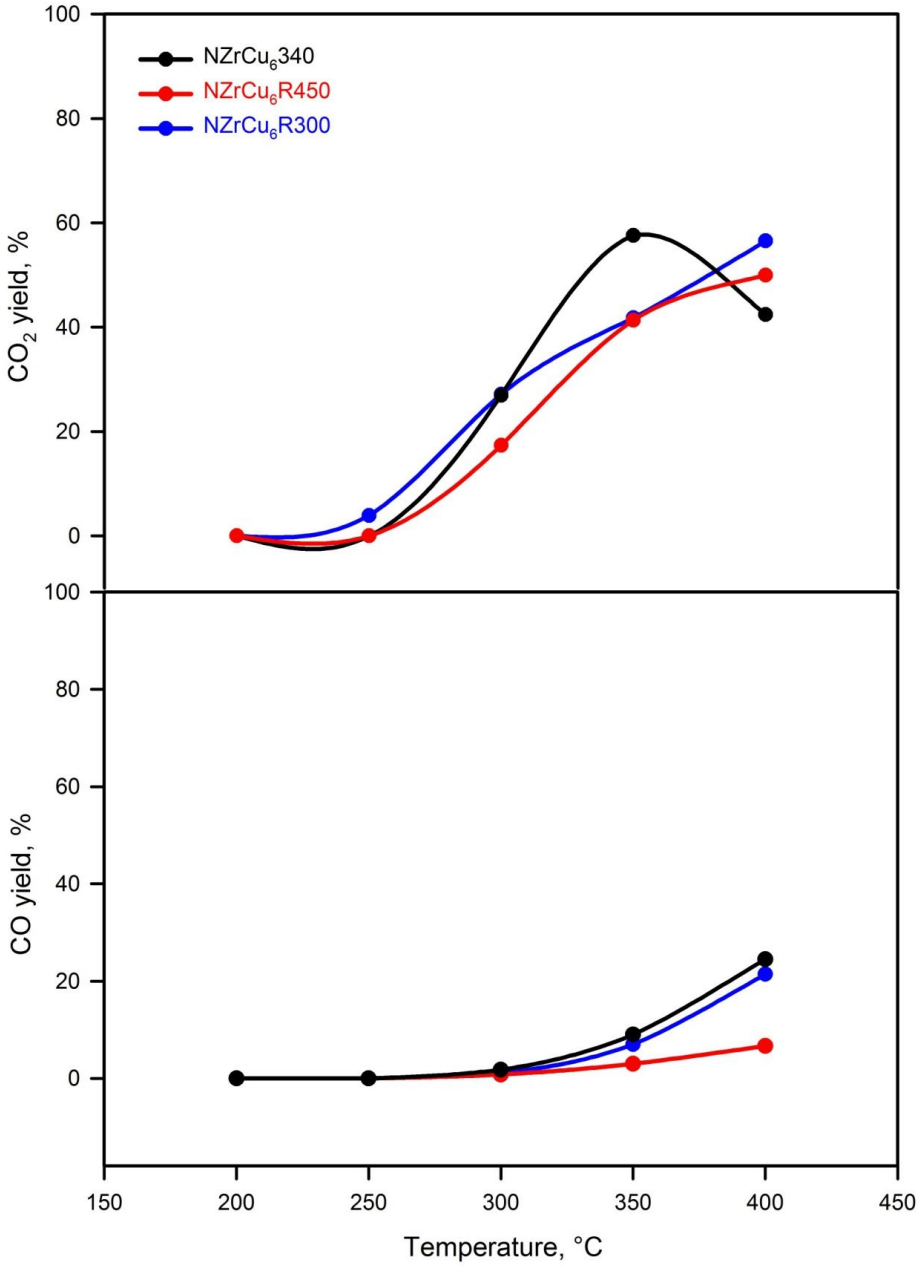

Fig.4-3. CO_2 and CO yield as a function of temperature in OSRM tests on $NZrCu_6340$, $NZrCu_6R300$ and $NZrCu_6R450$. Reaction conditions as in Fig.4-1.

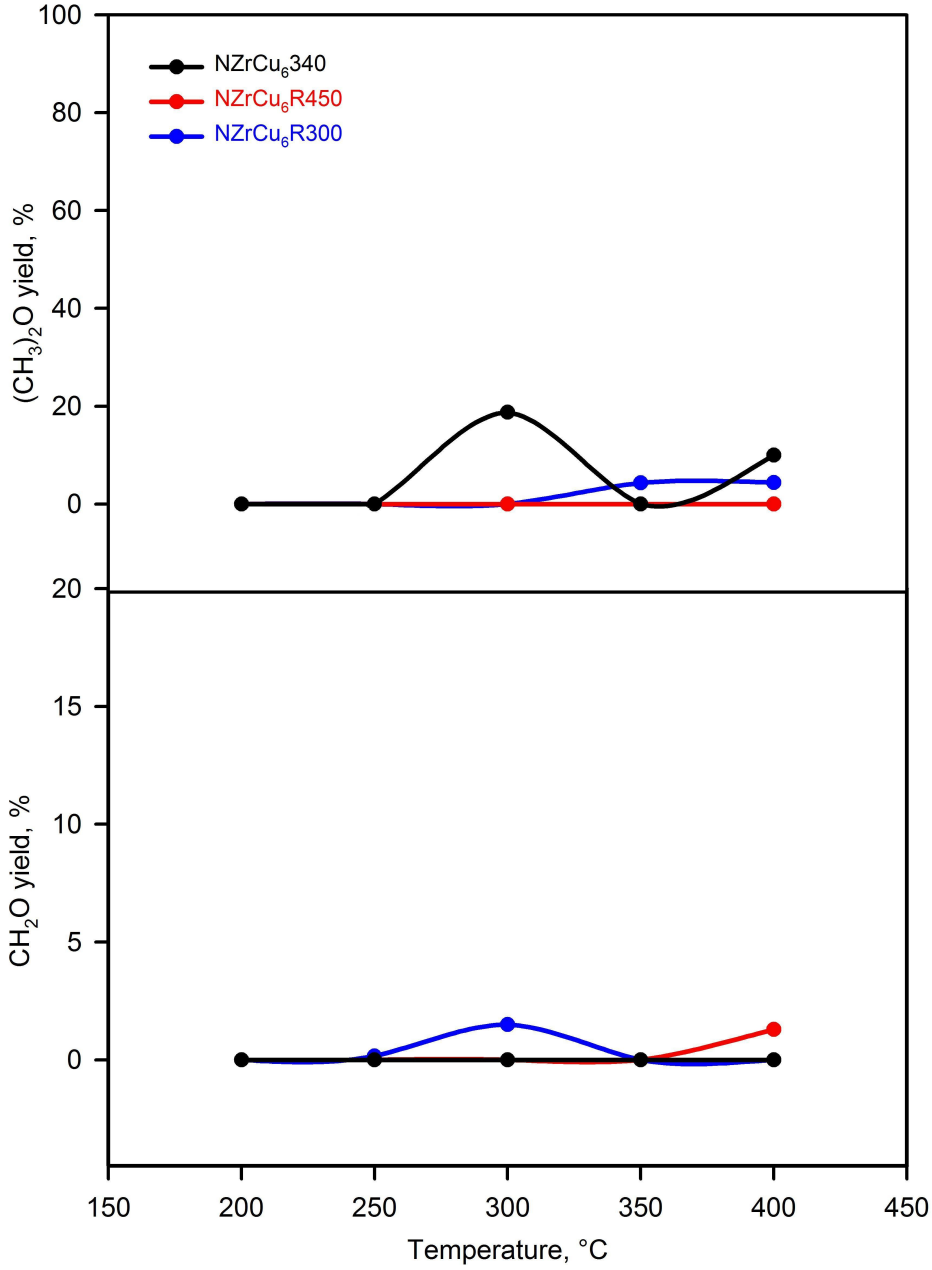

Fig.4-4. $(CH_3)_2O$ and CH_2O yield as a function of temperature in OSRM tests $NZrCu_6340$, $NZrCu_6R300$ and $NZrCu_6R450$. Reaction conditions as in Fig.4-1.

4.1.3 $AZrCu_7$

The results of OSRM tests carried out on $AZrCu_7$ not reduced with H_2 and reduced at 300°C or 450°C are reported in terms of methanol conversion and H_2 yield as a function of temperature (Fig.4-5). Also in this case, methanol conversion increases with temperature reaching a maximum at 400 °C, but the complete conversion is never reached and the not reduced $AZrCu_7340$ gives values of methanol conversion comparable with that of $AZrCu_7R300$: this confirms the hypothesis that under reaction conditions the CuO species are reduced by methanol to metallic Cu. The catalytic activity of the sample pre-reduced at 450°C is much lower than those of the not reduced and reduced at 300°C materials and this effect is much stronger than that observed with $NZrCu_6$, because of the stronger decrease of the surface area caused by the more severe pre-treatment, as observed above (see Table 3-3). H_2 yield is always lower than that expected under the catalytic conditions and, as explained above, this fact is due to the secondary reactions that occur in appreciable extent, producing $(CH_3)_2O$, CH_2O and CO and reducing CO_2 yield (Figs.4-6 and 4-7).

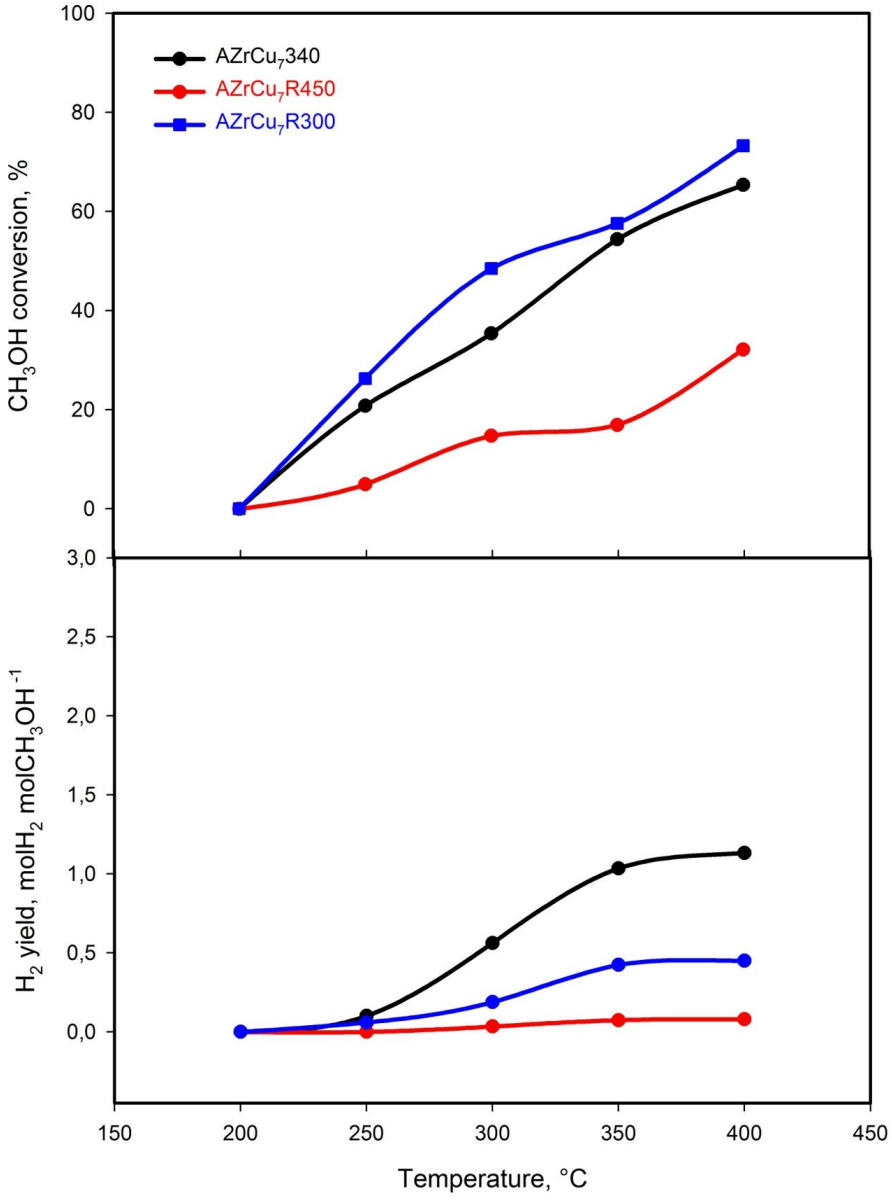

Fig.4-5. CH_3OH conversion and H_2 yield as a function of temperature in OSRM tests on $AZrCu_7340$, $AZrCu_7R300$ and $AZrCu_7R450$. Reaction conditions as in Fig.4-1.

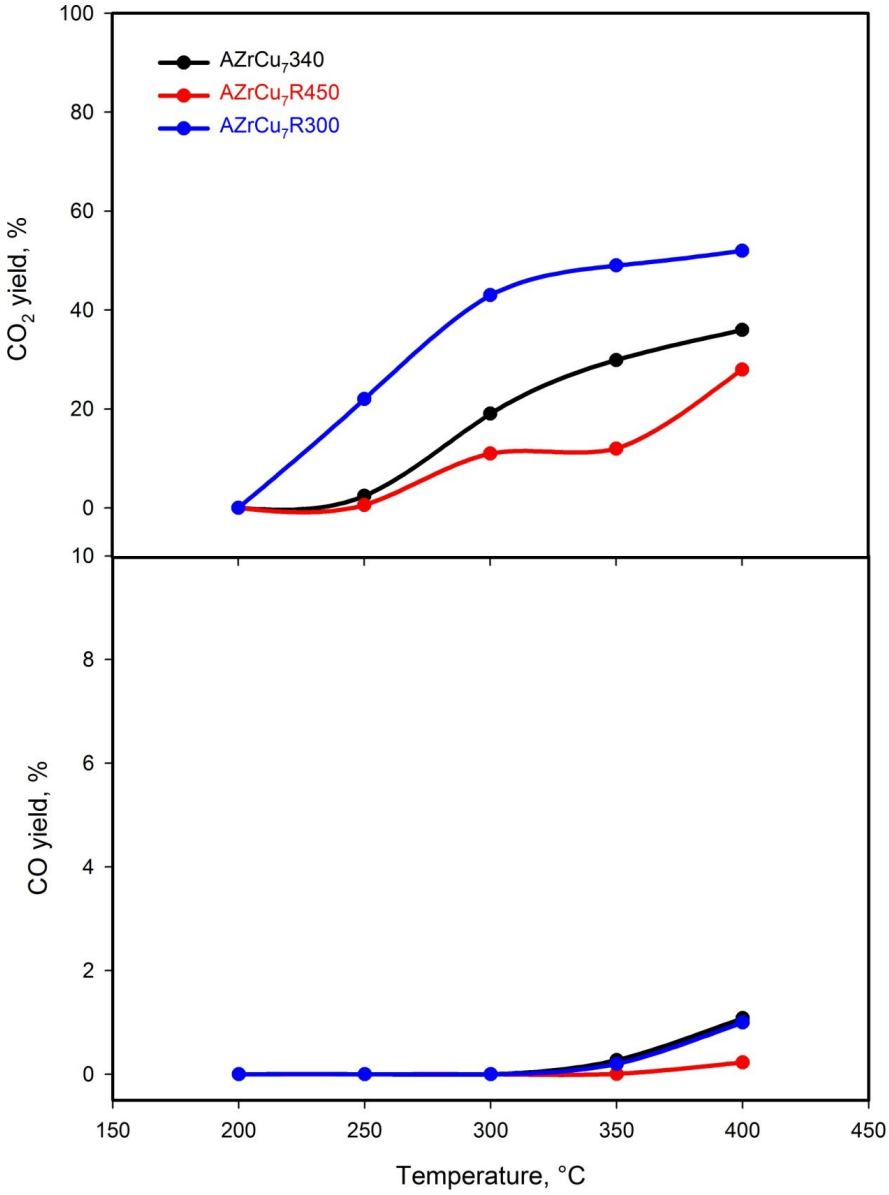

Fig.4-6. CO_2 and CO yield as a function of temperature in OSRM tests on $AZrCu_7340$, $AZrCu_7R300$ and $AZrCu_7R450$. Reaction conditions as in Fig.4- 1.

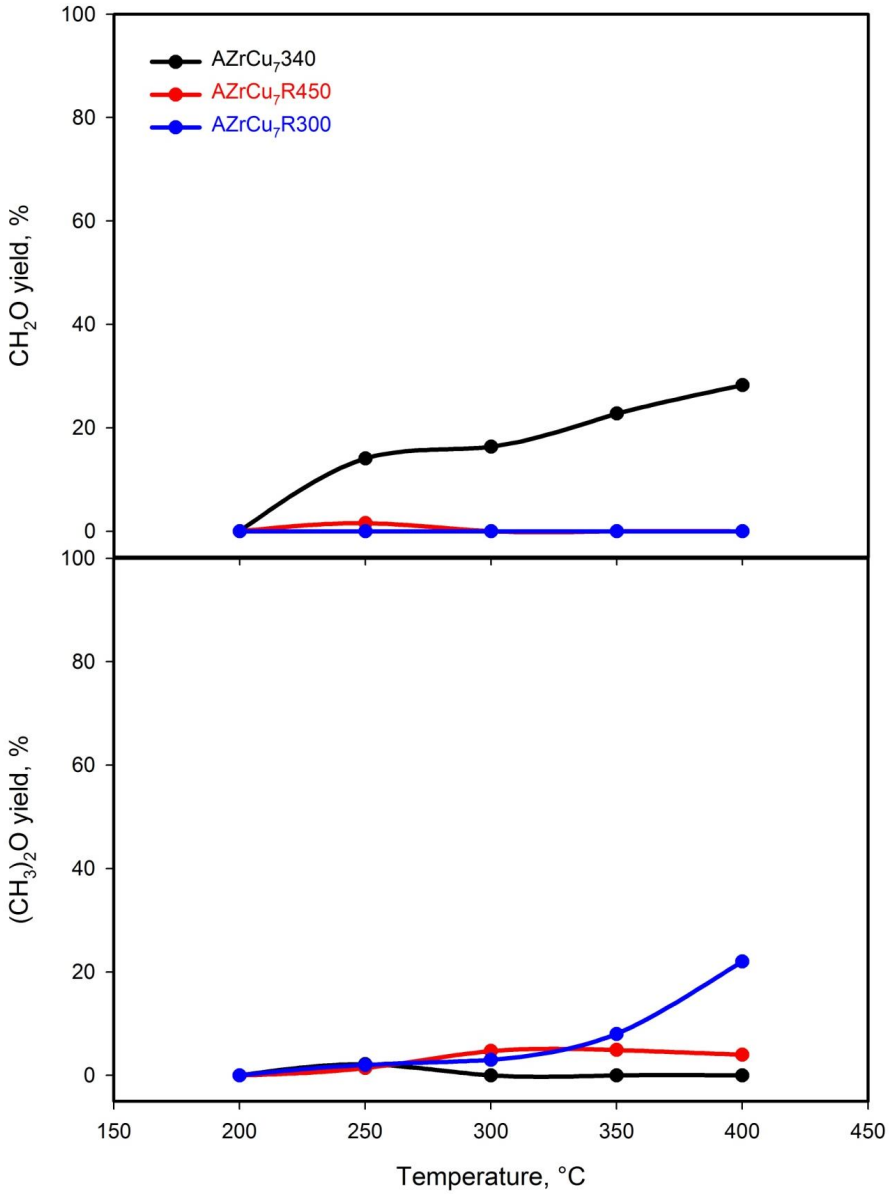

Fig.4-7. $(CH_3)_2O$ and CH_2O yield as a function of temperature in OSRM tests $AZrCu_7340$, $AZrCu_7R300$ and $AZrCu_7R450$. Reaction conditions as in Fig. 4-1.

4.1.4 $AZrCu_{14}$

OSRM tests were carried out only on the material reduced with H_2 at 450°C. In fact, the catalyst showed a very low activity, compared with $NZrCu_6$ and $AZrCu_{14}$ reduced in the same conditions, although it has a higher copper content, so a further investigation was not considered useful. In Fig.4-8 methanol conversion and yields to different products are reported. Methanol conversion is lower than 40% at 400°C and the corresponding H_2 yield is only 0.35 mol_{H_2} $mol_{CH_3OH}^{-1}$.

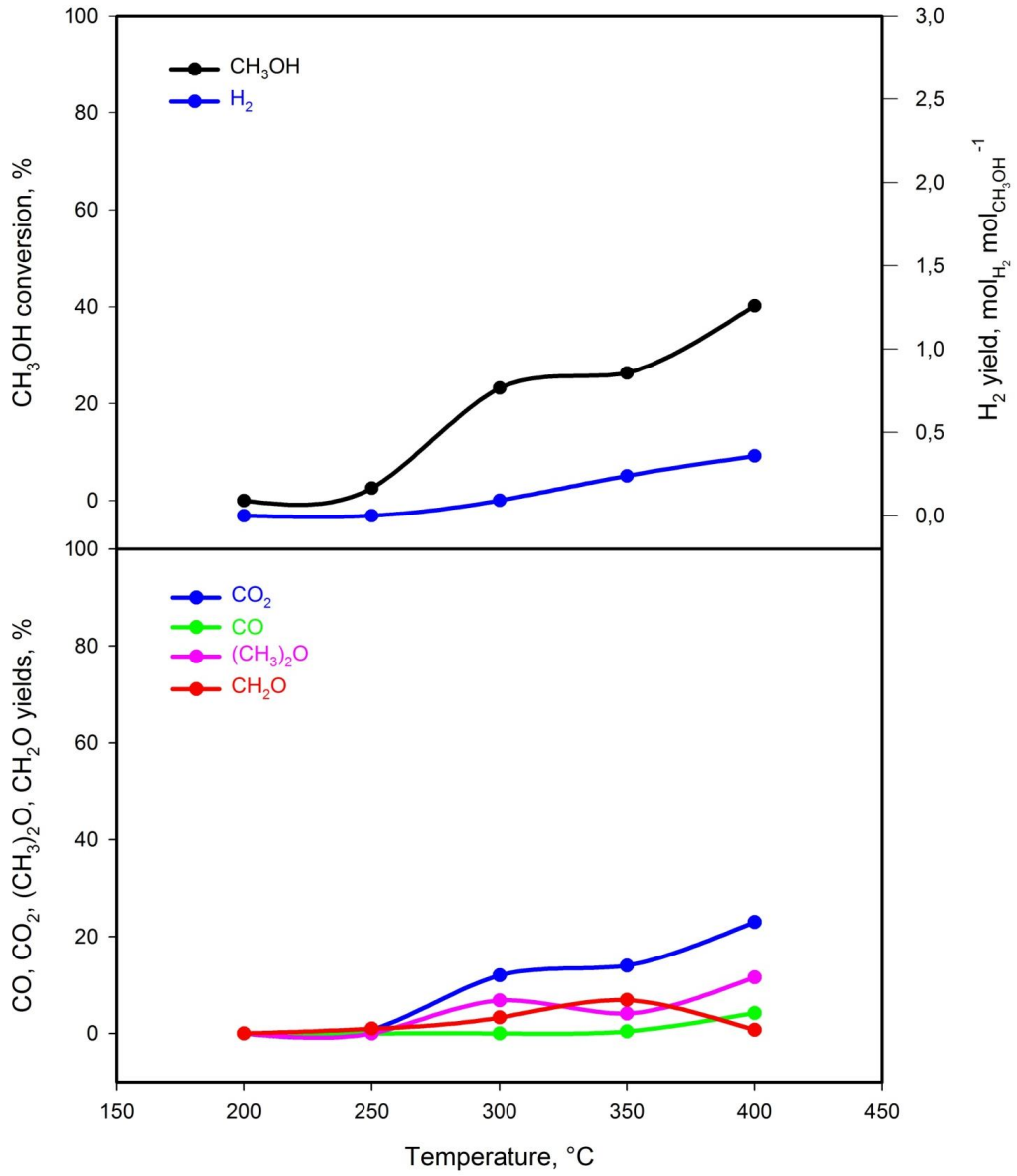

Fig.4-8. CH_3OH conversion, H_2 CO_2, CO, $(CH_3)_2O$ and CH_2O yield as a function of temperature in OSRM tests on $AZrCu_{14}R450$. Reaction conditions as in Fig. 4-1.

To compare the three catalytic systems reduced at 450°C, the H_2 production rate per mol Cu, expressed as $mol_{H2}s^{-1}mol_{Cu}^{-1}$ is reported as a function of Cu content in Fig.4-9, whilst the CO production rate per mol Cu, expressed as $mol_{CO}s^{-1}mol_{Cu}^{-1}$ is reported as a function of Cu content in Fig.4-10. If the quality of copper were the same among the three catalysts, it would be observed that the rate of H_2 and CO production per mol Cu are equal for the three systems. Instead, as expected, they change among the three catalysts and in particular the highest rates are observed with $NZrCu_6R450$. In Fig.4-11 and 4-12 respectively the H_2 production rate per m^2_{Cu}, expressed as $mol_{H2}s^{-1}m_{Cu}^{-2}$ and the CO production rate per m^2_{Cu}, expressed as $mol_{CO}^{-1}m_{Cu}^{-2}$ are reported as a function of Cu surface ($m_{Cu}^2g^{-1}$). Also in this case the rates change among the three catalysts. This fact proves that the reaction is structure sensitive and also that the copper quality is influenced by the preparation method and also by its quantity.

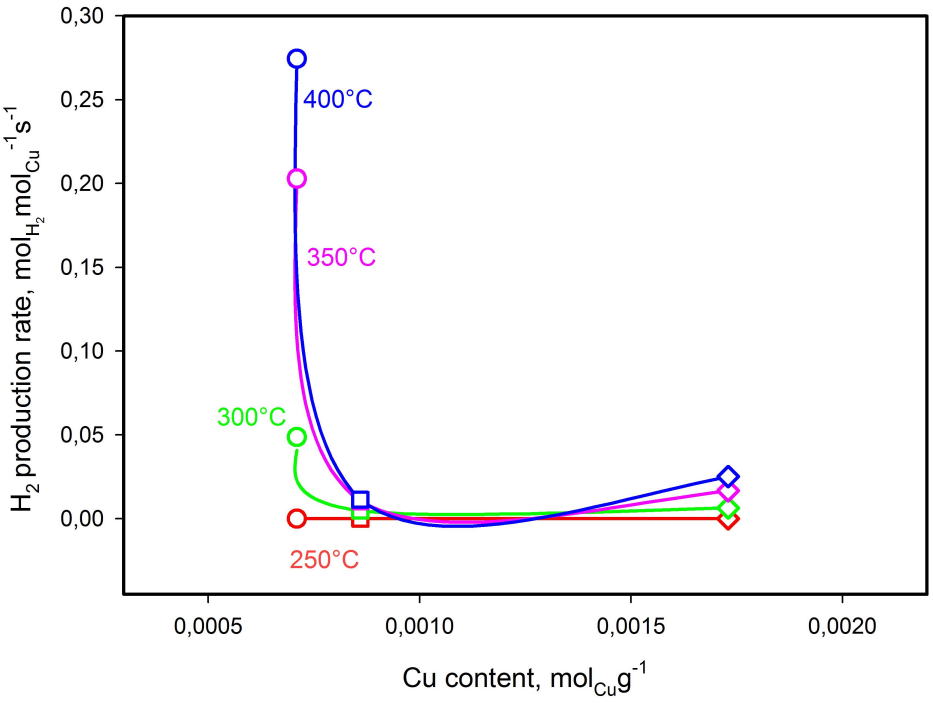

Fig.4-9. H_2 production rate as a function of Cu content, ○ $NZrCu_6R450$, ▫$AZrCu_7R450$, ◇$AZrCu_{14}R450$.

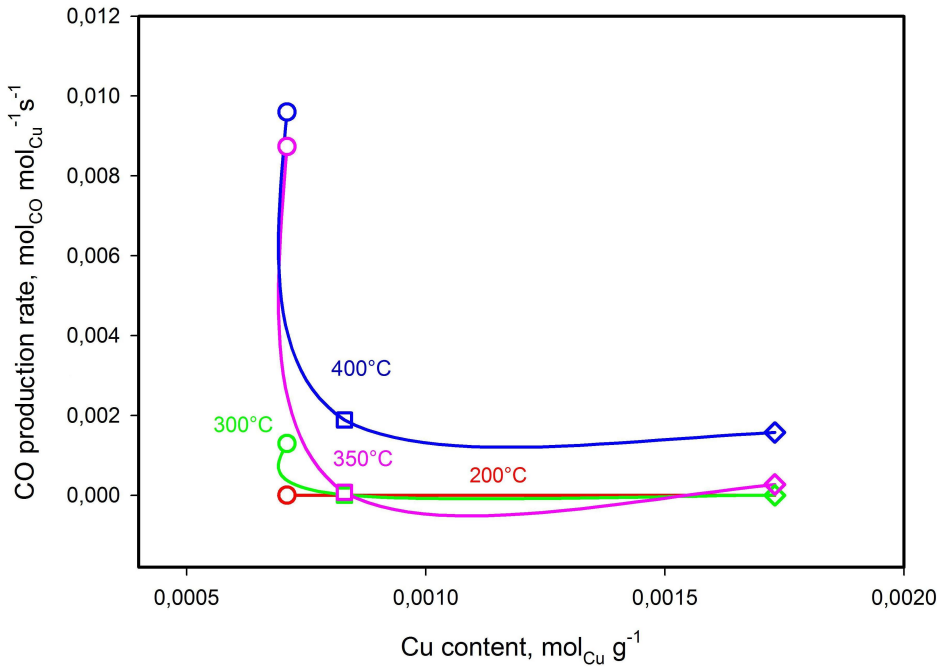

Fig.4-10. CO production rate as a function of Cu content, ○ $NZrCu_6R450$, ▫$AZrCu_7R450$, ◇$AZrCu_{14}R450$.

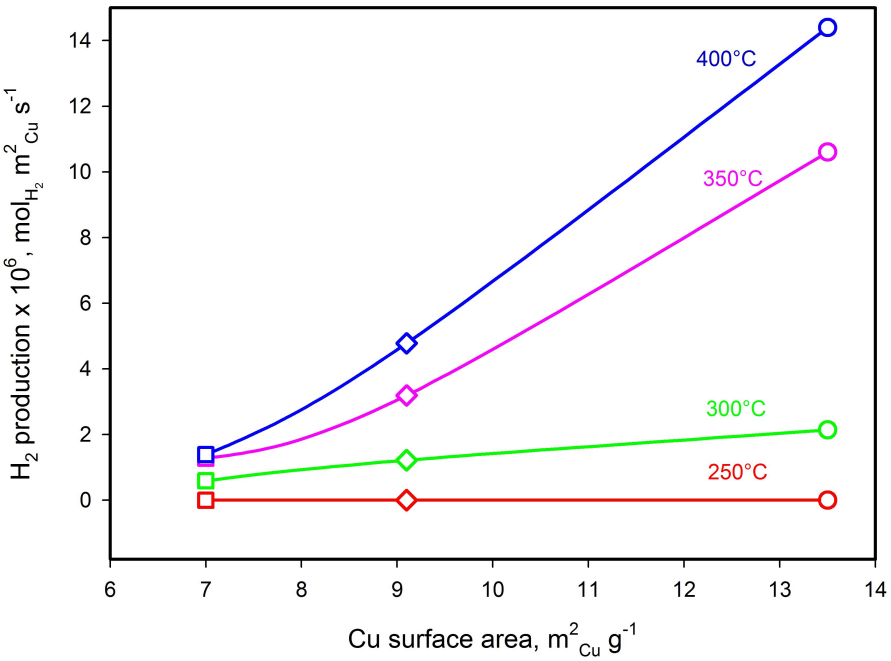

Fig.4-11. H_2 production rate as a function of m^2Cug^{-1}, ○ $NZrCu_6R450$, ▫$AZrCu_7R450$, ◇$AZrCu_{14}R450$.

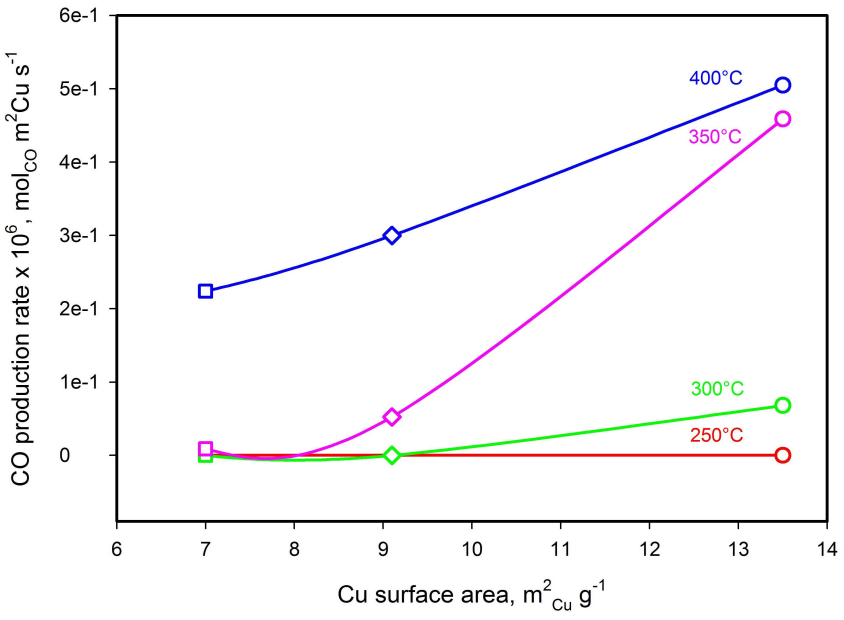

Fig.4-12. CO production rate as a function of m^2Cug^{-1}, ○ $NZrCu_6R450$, ▫$AZrCu_7R450$, ◇$AZrCu_{14}R450$.

Arrhenius plots for OSRM of catalysts pre-reduced at 450°C, evaluated from conversion data as described in *Section 2.3.3* are shown in Fig.4-13. The activation energies and the pre-exponential factors of *Eq.(31)* are reported in Table 4-1. Arrhenius plots for OSRM of catalysts not pre-reduced or pre-reduced at 300°C are not reported, since no satisfactory linear regressions were obtained with these systems, due to the not negligible contribution of parasitic reactions.

The catalysts $AZrCu_7R450$ and $AZrCu_{14}R450$ are characterized by low catalytic activity: the low conversion values suggest that the kinetics is slow so these systems work in the kinetic regime also for higher temperature ranges.

Analyzing the regression for the $NZrCu_6R450$ catalyst, a clear change in slope can be observed: the halving of slope at T > 300°C is representative of a change of regime, that is between 250°C and 300°C the regime is kinetic, whilst between 300 and 400 °C the regime is kinetic-diffusive.

$NZrCu_6R450$ is characterized by higher values of conversion and therefore by a faster kinetic which is associated with a mixed kinetic-diffusive regime.

However the role of secondary reactions in the variation of activation energy cannot be excluded.

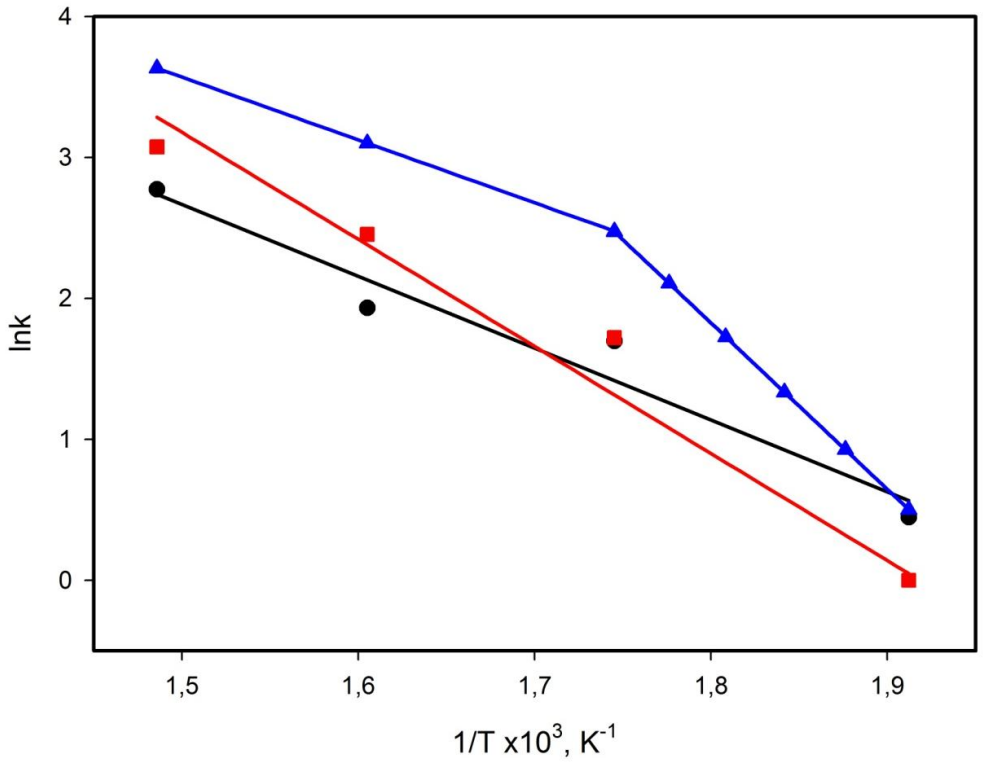

Fig.4-13. Arrhenius plot for OSRM of the Cu/ZrO_2 catalysts pre-reduced at 450°C. Blue line: $NZrCu_6R450$, black line: $AZrCu_7R450$, red line: $AZrCu_{14}R450$.

Table 4-1
Activation energy and pre-exponential factors for OSRM of the Cu/ZrO_2 catalysts pre-reduced at 450°C

T, °C	$NZrCu_6R450$		$AZrCu_7R450$		$AZrCu_{14}R450$	
	k_0, $cm^3s^{-1}g_{cat}^{-1}$	Eatt, cal mol^{-1}	k_0, $cm^3s^{-1}g_{cat}^{-1}$	Eatt, cal mol^{-1}	k_0, $cm^3s^{-1}g_{cat}^{-1}$	Eatt, cal mol^{-1}
250	$1.0 \cdot 10^{10}$	23450				
300			$3.05 \cdot 10^4$	10360	$2.48 \cdot 10^6$	15350
350	$2.8 \cdot 10^4$	9850				
400						

4.1.5 Comparison between $NZrCu_6$ and $AZrCu_7$

To understand the influence of the preparation method and pre-treatments on the catalytic properties, a comparison between $NZrCu_6$ and $AZrCu_7$, prepared by different methods, respectively *Method I* and *Method II* (see *Section 2.1.2*), but with a similar composition, is considered.
For a clearer comparison, taking also into consideration the different pre-treatments, the distribution of reaction products obtained with the different catalysts is reported in Table 4-2. The comparison is made at temperature of 400°C, at which the highest conversions are observed.
For both catalysts a clear effect of the pre-reduction treatment can be noted: the selectivity for OSRM, measured by the ratio between the product of the main reaction CO_2 and the products of other reactions, is the lowest for the not pre-reduced samples, that give noticeable amounts of CO and CH_2O. The secondary products are inhibited with the catalyst pre-reduced at 300°C and even more with that pre-reduced at 450°C.

Table 4-2
Product distribution in OSRM tests*.

	Conversion/yield, %					
	$NZrCu_6340$	$NZrCu_6R300$	$NZrCu_6R450$	$AZrCu_7340$	$AZrCu_7R300$	$AZrCu_7R450$
CH_3OH	71.3	71.5	57.9	65.0	73	32
CO_2	40.0	54.5	50.0	37.0	52	28.0
CO	21.0	12.6	6.7	1.0	1.0	0.0
CH_4	0.3	0.0	0.0	0.0	0.0	0.0
$(CH_3)_2O$	0.0	4.4	1.2	0.0	22.0	4.0
CH_2O	10.0	0.0	0.0	27.0	0.0	0.0

* T = 400°C, reaction conditions as in Fig. 4-1.

These data show that, even if the influence of the pre-treatment is not simple, the highest selectivity for OSRM is obtained with the reduced materials. The explanation of this behaviour could be in the contribution of the catalytic activity of the support. As shown above, the support is appreciably active for methanol dehydration to dimethylether and oxydehydration to formaldehyde, but it can be involved also in the formation of CO. This product, that is inevitably observed during SRM or OSRM on Cu based catalysts, is often explained by the reverse water gas shift (RWGS) reaction:

$$CO_2 + H_2 \leftrightarrows CO + H_2O$$

occurring as series reaction after SRM. Since RWGS is favoured by increasing temperature for both thermodynamic and kinetic reasons, it can explain the steady increase of CO with temperature that is generally observed. However in the present case, considering the higher selectivity of the catalysts reduced, the formation of CO can be related also to an effect of the ZrO_2 support on the main reaction mechanism. Methanol steam reforming on Cu catalysts probably involves adsorbed formate species as intermediate [150], and these can be easily decomposed to CO in the presence of an acid support such as Al_2O_3 [150] or ZrO_2 [163]. Since the reduced materials contain a more crystalline ZrO_2 phase with a lower surface area, this can lead to a lower activity towards secondary reactions occurring on the surface of ZrO_2, including methanol dehydration to dimethylether and oxydehydration to formaldehyde and decomposition of adsorbed formate species.

To understand the influence of preparation method a comparison between $NZrCu_6$ and $AZrCu_7$ pre-treated under the same conditions can be considered.

The catalyst $NZrCu_6R450$ showed a much higher activity in terms of methanol conversion than $AZrCu_7R450$. This behaviour can be easily explained considering that the surface area of $AZrCu_7R450$ (<5 m^2g^{-1}) is much lower than that of $NZrCu_6R450$ (106 m^2g^{-1}), as observed in *Section 3.1.4*

Comparing $NZrCu_6340$ with $AZrCu_7340$ and $NZrCu_6R300$ with $AZrCu_7R300$, they showed respectively a very similar activity in terms of methanol conversion and selectivity, measured by the ratio between the product of the main reaction CO_2 and the products of other reactions, but the distribution of secondary products was completely different. $NZrCu_6$ produced a lot of CO, while $AZrCu_7$ gave essentially CH_2O and $(CH_3)_2O$. This fact could be explained hypothesizing that the copper present in $NZrCu_6$ is more active towards SRM and RWGS. These two reactions occur in series, so SRM produces much more CO_2 but this is converted into CO by RWGS. On the other hand, copper present in $AZrCu_7$ is less active, so the secondary reactions occurring on the surface of ZrO_2, including methanol dehydration to dimethylether and oxydehydration to formaldehyde, are favoured. The different activity of copper present in the two catalysts could be related to the different copper dispersion, since $NZrCu_6$ has a copper surface higher than $AZrCu_7$, as observed above (see Table 3-2).

It is worth comparing the OSRM activity of these catalysts with that of other Cu based systems that were studied for the same process. There are no $Cu\text{-}ZrO_2$ systems investigated in the literature for this process under reasonably similar conditions, so a comparison is possible only with systems based on different supports. Such comparison is made in terms of H_2 production rate in Table 4-3, where the catalyst that showed the best activity, $NZrCu_6$, both pre-reduced with H_2 at 300°C and not pre-reduced is considered.

Table 4-3
Comparison data from OSRM.

Sample [ref.]	Cu content mol %	Feed ratio $O_2/H_2O/CH_3OH$	GHSV L g^{-1} h^{-1}	Temperature °C	H_2 production rate μmol s^{-1} g_{cat}^{-1}
$NZrCu_6R300$	8.3	0.12/1.1/1	60	300	93
$NZrCu_6340$	8.3	0.12/1.1/1	60	300	55
$Cu/ZnO/CeO_2/Al_2O_3$ [164] [a]	19	0.15/1.5/1	7.8[b]	300	240
CuZnAl [150][a]	18	0.12/1.1/1	60	300	260
Cu/CeO_2 [68][c]	10	0.3/1.3/1	20	300	110

[a] catalyst pre-reduced with H_2
[b] referred to CH_3OH flow
[c] catalyst not pre-reduced

The performances of the studied $Cu\text{-}ZrO_2$ catalysts, notwithstanding the very high Cu dispersions, appear lower than those of other systems. However, if the different Cu contents are taken into account, it appears that the results obtained are almost comparable and encouraging, since it is expected that significant improvements can be obtained by addition of suitable promoters.

4.1.6 Conclusions

The catalytic activity of Cu/ZrO_2 systems for the oxidative steam reforming of methanol appears interesting compared to that of previous Cu based catalysts, taking into account the absence of any promoter.

H_2 pre-reduction is not strictly required for catalytic activity and this confirms the hypothesis that under reaction conditions the CuO species are reduced by methanol to metallic Cu. This behaviour will be further investigated in Chapter 5. However the H_2 pre-reduction is advisable to obtain a higher selectivity.

A serious drawback of these systems is the noticeable activity of the zirconia support towards the production of undesired compounds, such as dimethylether and formaldehyde.

The catalytic activity is strongly influenced by the preparation method, since copper dispersion and surface area, changing noticeably with the preparation method, can influence the reaction network.

It is expected that the performance of the catalyst would be greatly improved by using suitable promoters and pre-treatment conditions that depress the adverse activity of the support.

4.2 Catalytic activity of $Cu/CeO_2/Al_2O_3$ catalysts

OSRM and SRM tests are carried on $Cu/CeO_2/Al_2O_3$ samples subjected to different heat treatments.

4.2.1 OSRM and SRM tests on $EMCeCu_4$, $EMCeCu_8$, $EMCeCu_{16}$

Methanol conversion and H_2 yield observed in the OSRM tests on $Cu/CeO_2/Al_2O_3$ catalysts pre-reduced with H_2 are reported in Fig.4-14. For all catalysts the conversion increases strongly with temperature, but the activity varies markedly among the different catalysts. The methanol conversion on the $EMCeCu_8R450$ catalyst is always lower than that on $EMCeCu_4R450$ and $EMCeCu_{16}R450$, except at 400°C, on the other hand the lowest H_2 yield is observed with the $EMCeCu_4R450$ catalyst and the highest H_2 yield with $EMCeCu_8R450$ in the whole temperature range, with values close to the maximum expected according to the feeding composition (2.76 $mol_{H2}\, mol_{CH3OH}^{-1}$).

As shown in Fig.4-15, the values of conversion to CO_2 are close to those of CH_3OH conversion for the $EMCeCu_8R450$ catalyst, indicating that the contribution of side reactions is low, while for $EMCeCu_4R450$ and $EMCeCu_{16}R450$ conversions to CO_2 are significantly lower than CH_3OH conversions. Side reactions are responsible for the production of CO, $(CH_3)_2O$ and CH_2O. For all catalysts, as shown in Fig.4-15, the conversion to CO is negligible at T< 300°C and increases strongly at higher temperatures, reaching a maximum at 400°C (7% for $EMCeCu_8R450$).

Since the RWGS reaction occurs in small extent under OSRM conditions [82], CO is produced mainly from methanol decomposition, probably through the formation of intermediate oxygenated species, such as adsorbed formaldehyde or dioxymethylene that are bonded to metallic Cu or to cationic sites of the oxide matrix [24,82]. These intermediate species are probably common also to the mechanism of SRM, as explained in details below, and can be desorbed as gaseous formaldehyde or, if retained on the catalytic surface, further dehydrogenated giving rise to CO or CO_2. Thus it is expected that if the catalyst retains these intermediates strongly, it will favour the formation of CO. This points to a role of the oxide matrix in the reaction mechanism, probably through the adsorption of intermediate species. The presence of $(CH_3)_2O$ and CH_2O in the reaction products indicates that the catalysts are active for the reactions of methanol condensation, probably due to acid sites of Al_2O_3 and/or aluminates, and dehydrogenation, probably due to the metallic Cu phase [82,165].

The production of $(CH_3)_2O$ (Fig.4-16) is observed in noticeable amounts with $EMCeCu_4R450$ and $EMCeCu_{16}R450$, while it is not observed with the $EMCeCu_8R450$. No CH_2O (Fig.4-16) is observed with $EMCeCu_4R450$, while both $EMCeCu_8R450$ and $EMCeCu_{16}R450$ produce this compound at 400°C.

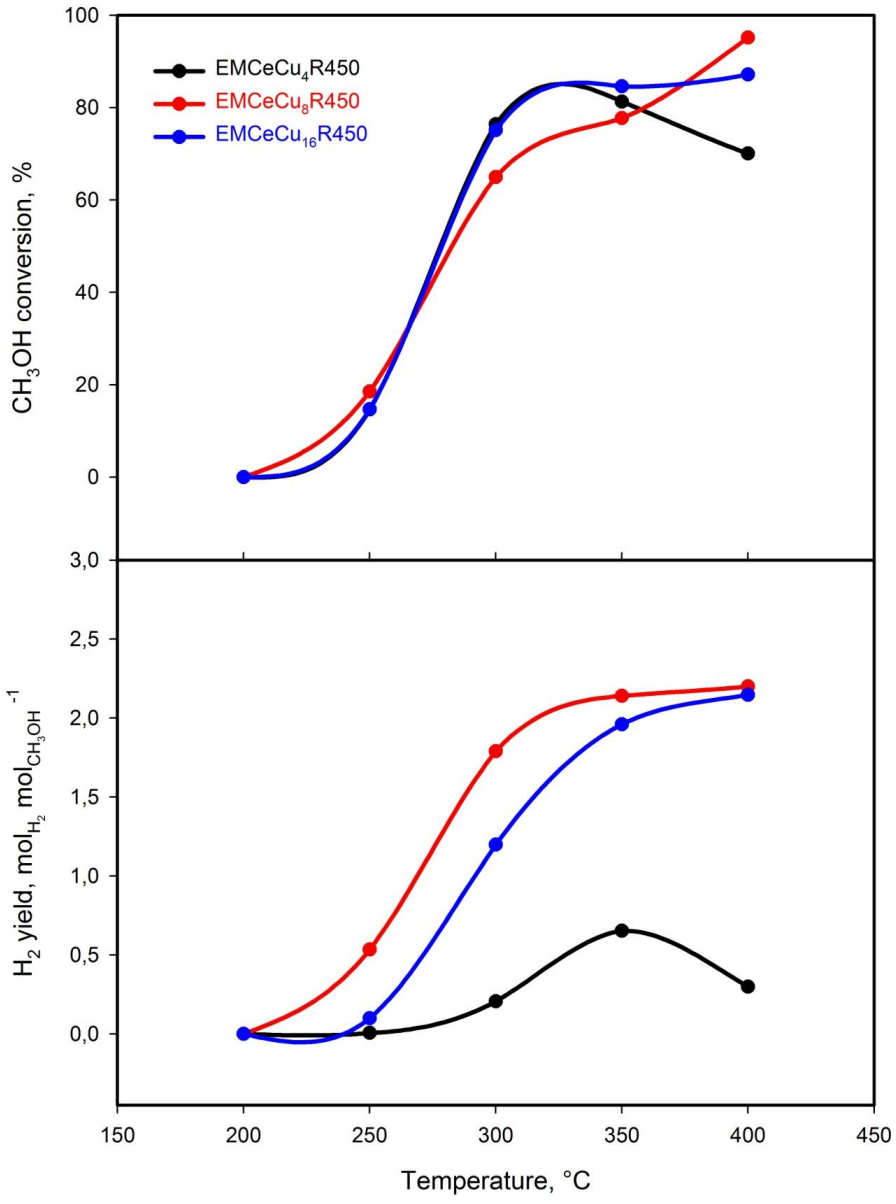

Fig.4-14. CH_3OH conversion and H_2 yield in the OSRM tests on $EMCeCu_4R450$, $EMCeCu_8R450$ and $EMCeCu_{16}R450$. Reaction conditions as in Fig. 4-1.

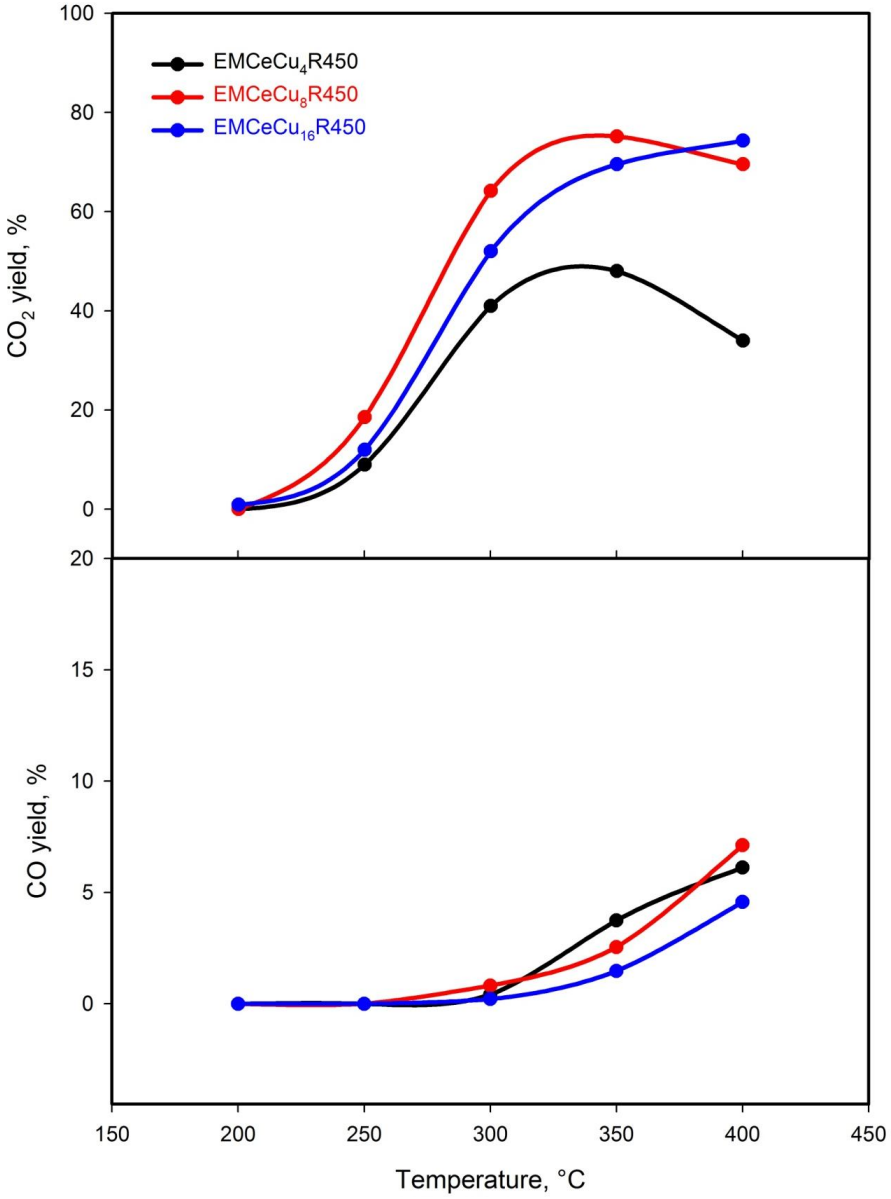

Fig.4-15. CO_2 and CO yield in the OSRM tests on $EMCeCu_4R450$, $EMCeCu_8R450$ and $EMCeCu_{16}R450$. Reaction conditions as in Fig. 4-1.

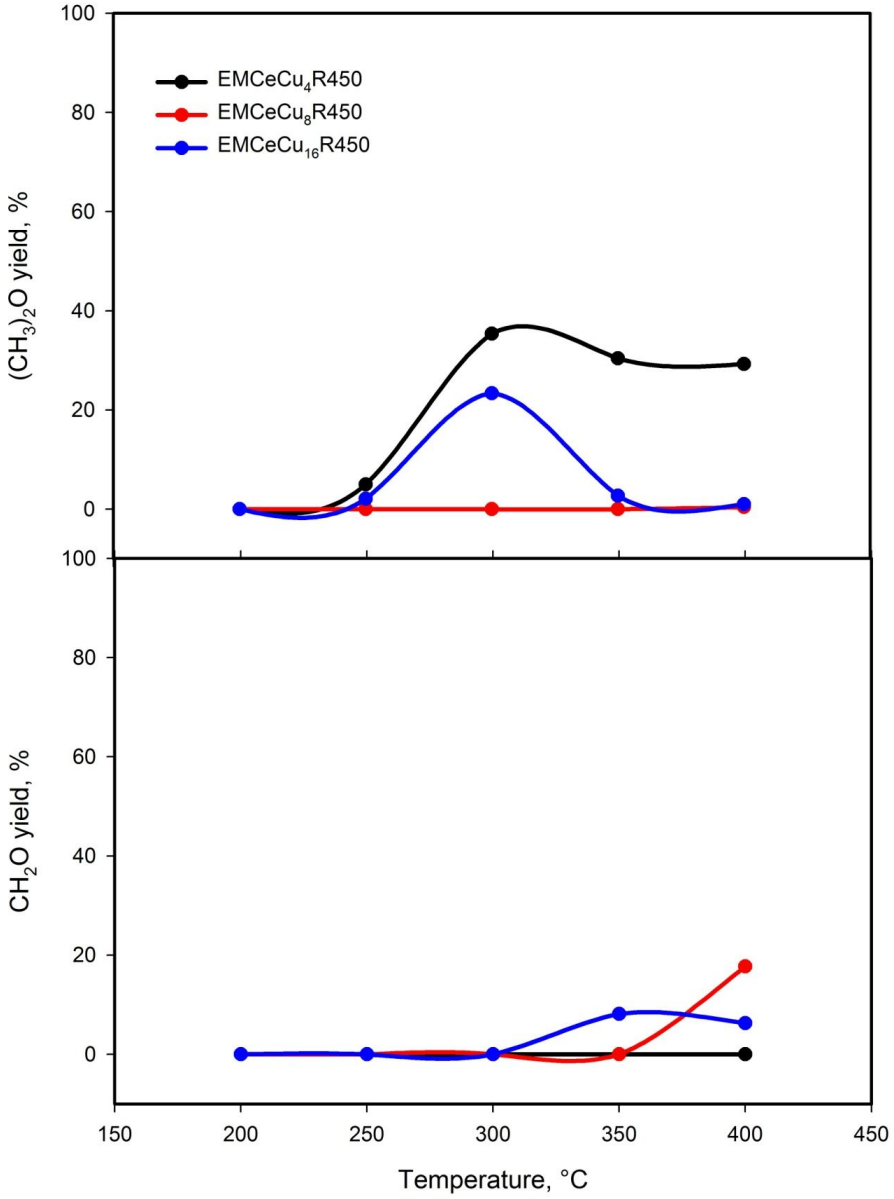

Fig.4-16. $(CH_3)_2O$ and CH_2O yield in the OSRM tests on $EMCeCu_4R450$, $EMCeCu_8R450$ and $EMCeCu_{16}R450$. Reaction conditions as in Fig. 4-1.

The series of OSRM tests was repeated in the same sequence 200-400 °C, obtaining the same values of activity as in the first cycle: this allows to exclude deactivation phenomena, at least during the time of catalytic tests.

It is interesting to compare the OSRM activity of these catalysts with that of similar Cu and Ce based systems presented in the literature, although the number of such studies is very limited. The most suitable for this comparison are those by Patel and Pant [103,164] reported in Table 4-4, that

refer to H_2 pre-reduced catalysts. The activity of the catalyst $EMCeCu_8R450$ appears high if compared with these data, considering that the catalyst in Ref. [164] contains also Zn as promoter.

Table 4-4
Comparison of data from OSRM.

Sample [ref.]	Catalyst composition Cu/Ce/Al atom%	Feed ratio $O_2/H_2O/CH_3OH$	WHSV L g^{-1} h^{-1}	Temperature °C	H_2 production rate µmol s^{-1} g_{cat}^{-1}
$EMCeCu_4R450$	3/5/92	0.12/1.1/1	60	300	60
$EMCeCu_8R450$	6/5/89	0.12/1.1/1	60	300	210
$EMCeCu_8550$[a]	6/5/89	0.12/1.1/1	60	300	135
$EMCeCu_{16}R450$	12/4/84	0.12/1.1/1	60	300	180
$Cu/CeO_2/Al_2O_3$[103]	19/6/75	0.15/1.1/1	5.7[b]	280	180
$Cu/ZnO/CeO_2/Al_2O_3$ [164]	19/3/64[c]	0.15/1.1/1	7.8[b]	300	240
Cu/CeO_2[68][a]	10/90/0	0.3/1.3/1	20	300	110

[a] catalyst not pre-reduced
[b] referred to CH_3OH flow
[c] containing 13 mol% Zn

The irregular variation of the activity with Cu content and the maximum of activity observed for the catalyst $EMCeCu_8R450$ suggest that the properties of the active phase are not simply related to its quantity and that the reaction is structure-sensitive.

To highlight this point, in Fig.4-17 and 4-18 respectively the H_2 production rate, expressed as $molH_2s^{-1}molCu^{-1}$, and the the CO production rate, expressed as $mol_{CO}s^{-1}mol_{Cu}^{-1}$ are reported as a function of Cu content. If the quality of copper were the same among the three catalysts, it would be observed that the rate of H_2 production per mol Cu is equal for the three systems. Instead, as

expected, the H_2 production rate per mol Cu changes among the three catalysts and in particular the highest rate is observed with $EMCeCu_8R450$. This fact proves that the reaction is structure sensitive and also that the copper quality is influenced by its concentration. In Chapter 3 we have already seen that the reducibility and the copper dispersion changed among the three systems and that it was just $EMCeCu_8$ that showed the best properties.

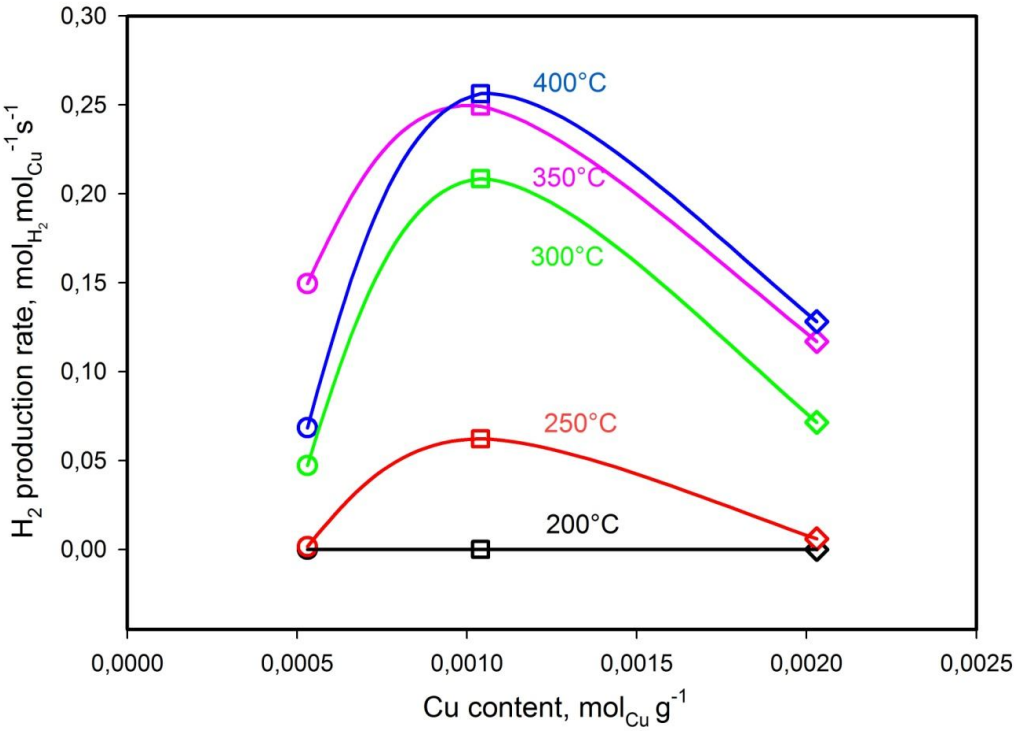

Fig.4-17. H_2 production rate as a function of Cu content, ○: $EMCeCu_4$, □: $EMCeCu_8$, ◇: $EMCeCu_{16}$

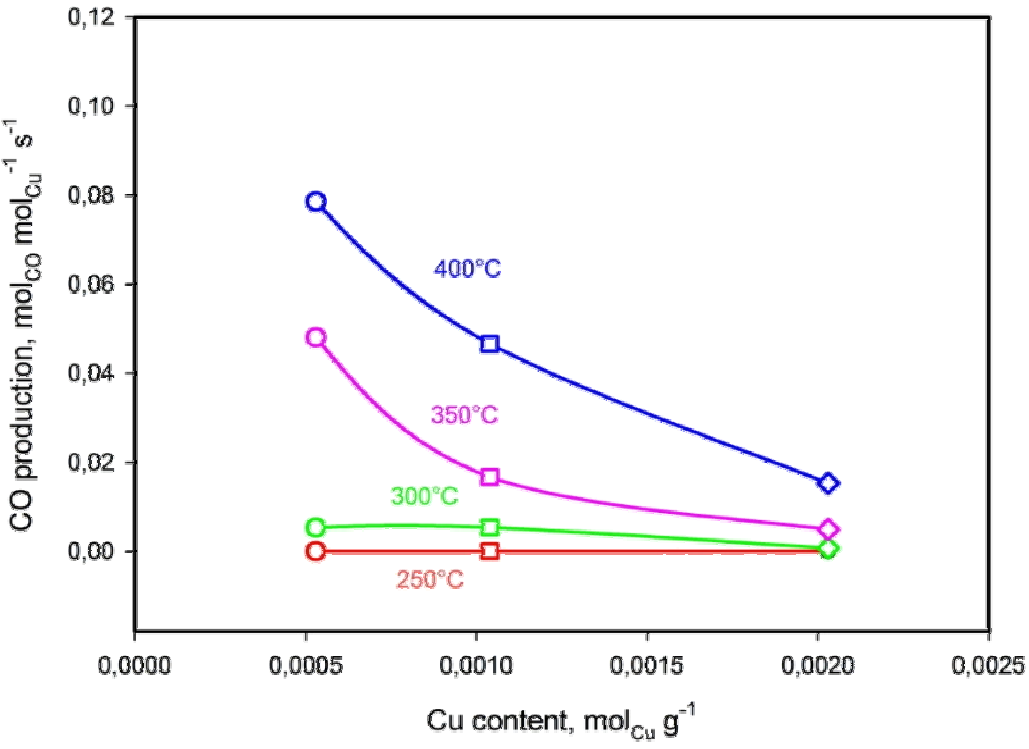

Fig.4-18. CO production rate as a function of Cu content, ○: $EMCeCu_4$, □: $EMCeCu_8$, ◇: $EMCeCu_{16}$

The best catalytic activity results were obtained for $EMCeCu_8R450$, so this catalyst was selected for a further investigation. OSRM were carried out also on the $EMCeCu_8$ not pre-reduced with hydrogen, only pre-treated in air at 550°C, identified as $EMCeCu_8550$. In Fig.4-19 a comparison between $EMCeCu_8R450$ and $EMCeCu_8550$ is reported in terms of methanol conversion and H_2 yield. It can be observed that also for the not pre-reduced catalyst the methanol conversion increases regularly with temperature according to S-shaped curves, but it is slightly higher for the pre-reduced catalyst. The pre-reduction of the catalyst has a more evident effect on the H_2 yield: for the pre-reduced catalyst H_2 yield increases with temperature up to a value of 2.2 mol_{H2} mol_{CH3OH}^{-1} at 400 °C, while for the not pre-reduced one it reaches at the same temperature the value of only 1.75 mol_{H2} mol_{CH3OH}^{-1}. In the case of the not pre-reduced sample, the conversion to CO_2 (Fig.4-20) parallels but is appreciably lower than CH_3OH conversion, indicating that the contribution of secondary reactions is not negligible: also for this catalyst the conversion to CO increases rapidly with the temperature above 300 °C, reaching about 4% at 400 °C.

Both the pre-reduced and not pre-reduced samples produce CH_2O only at 400 °C, the amount of this product being higher for the not pre-reduced one. No $(CH_3)_2O$ is observed with the pre-reduced catalyst, while this compound is observed in noticeable amounts with the not pre-reduced sample in the 300–350 °C range, being, on the other hand, negligible at lower and higher temperatures (Fig.4-21).

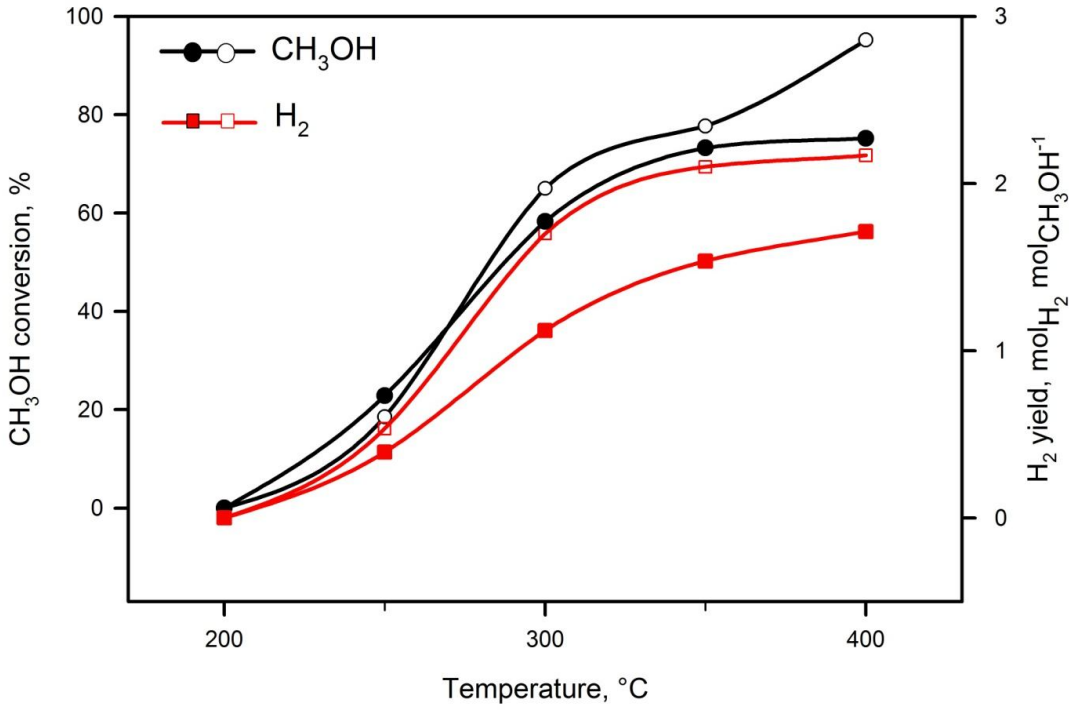

Fig.4-19. CH_3OH conversion and H_2 yield in the OSRM tests on $EMCeCu_8$. Empty symbols (○,□): catalyst pre-reduced with H_2; full symbols (•,▪): catalyst not pre-reduced. Reaction conditions as in Fig. 4-1.

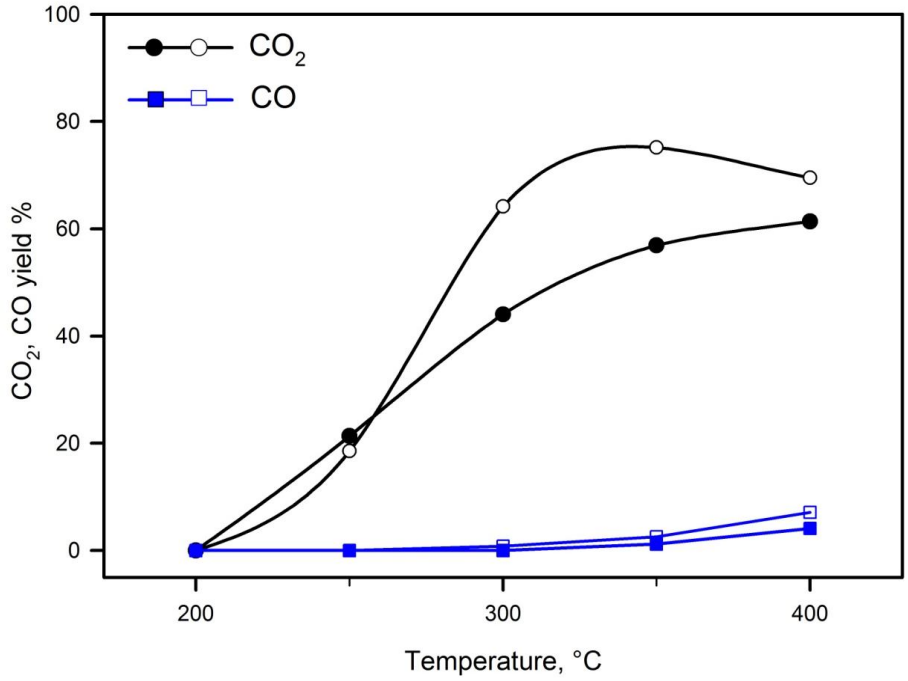

Fig.4-20. CO_2 and CO yield in the OSRM tests on $EMCeCu_8$. Empty symbols (○,□): catalyst pre-reduced with H_2; full symbols (•,▪): catalyst not pre-reduced. Reaction conditions as in Fig. 4-1.

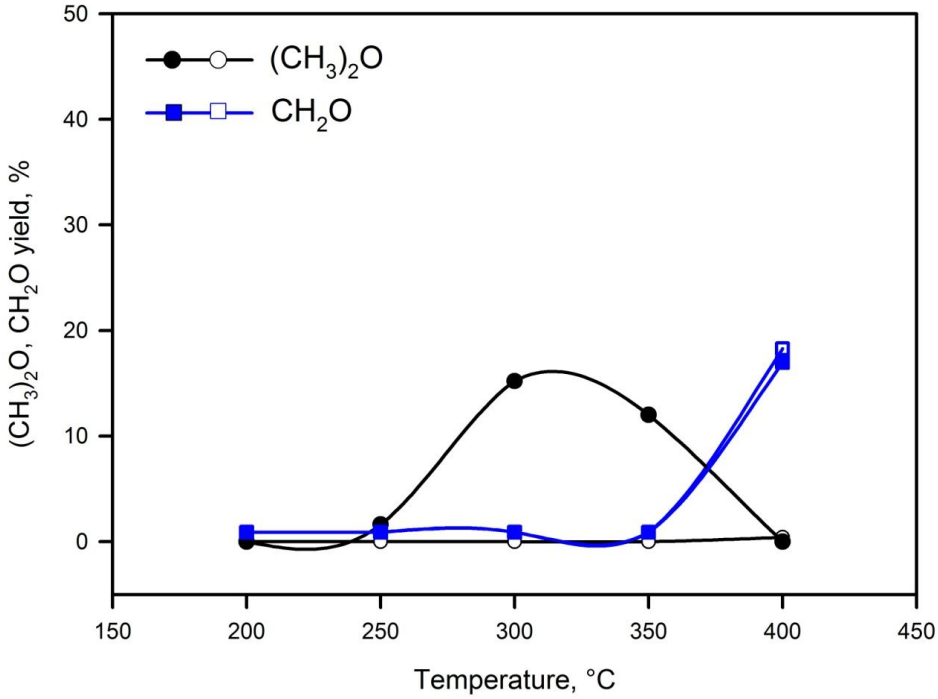

Fig.4-21. $(CH_3)_2O$ and CH_2O yield in the OSRM tests on $EMCeCu_8$. Empty symbols (○,□): catalyst pre-reduced with H_2; full symbols (•,▪):catalyst not pre-reduced. Reaction conditions as in Fig.4-1

Shan et al. [68] studied OSRM over a not reduced Cu/Ce catalyst that can be compared with the not reduced $EMCeCu_8$ sample. As shown in Table 4-4, the comparison favours $EMCeCu_8$ also in this case, and even more if the lower Cu content is taken into account. Since it is known that metallic copper is required for methanol reforming [150], the significant reforming activity found on the not pre-reduced catalyst indicates that, even if metallic Cu is not present initially in the catalyst, it is formed under reaction conditions. It can be hypothesized that the reduction of Cu oxide to the metallic state occurs simply through the reducing effect of methanol, analogously to what occurs in the so called ''polyol'' reduction of copper cations [166,167]. Another explanation can be that the initially present Cu oxide activates the partial oxidation of methanol producing H_2, and then H_2 reduces Cu oxide to metallic Cu. However the Cu^0 phase obtained in this way is less active than that formed by the H_2 reducing pre-treatment, as pointed by the lower H_2 yield. This can be due either to not complete reduction of Cu oxide or to formation of a less dispersed metallic phase.

The catalyst, in order to obtain a better knowledge of its properties, was tested also for the simple steam reforming of methanol (SRM), that is with the same flow rates of CH_3OH and H_2O, but in the absence of oxygen in the reaction system. The results of these tests, that were carried out both on the catalyst reduced with H_2 and on the not reduced one, are shown in Figs. 4-22, 4-23 and 4-24.

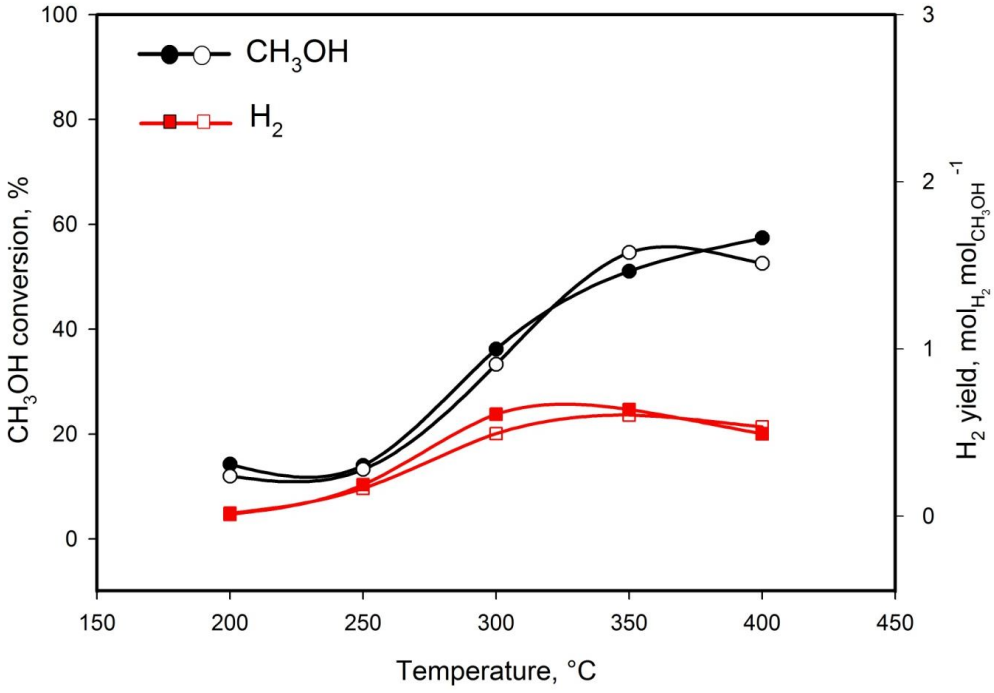

Fig.4-22. CH_3OH conversion and H_2 yield in the SRM tests on $EMCeCu_8$. Empty symbols (○,▫): catalyst pre-reduced with H_2; full symbols (•,▪): catalyst not pre-reduced.

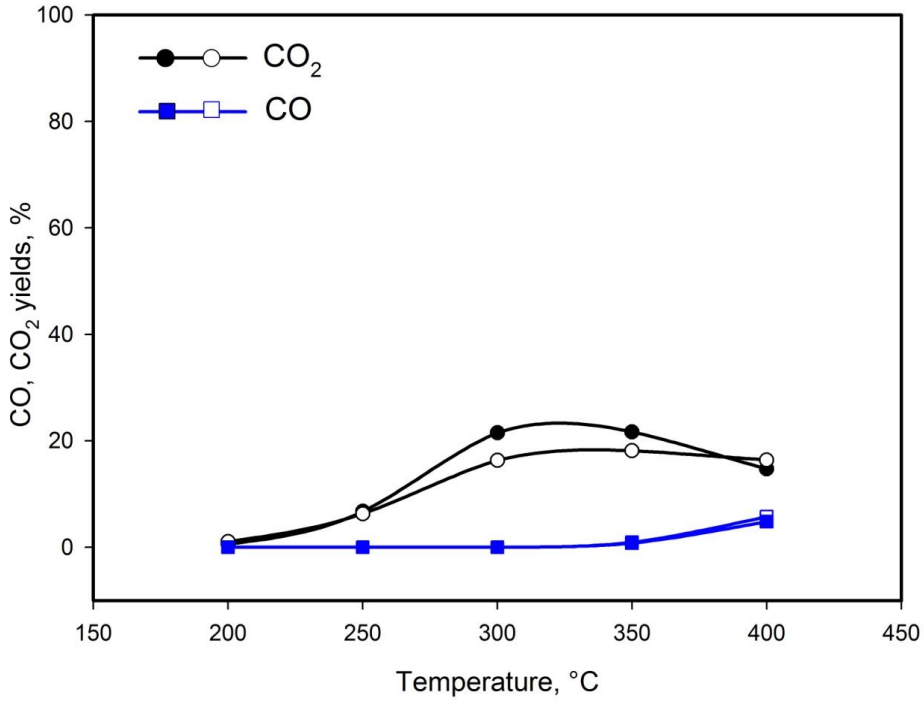

Fig.4-23. CH_3OH conversion to CO_2 and CO in the SRM tests on $EMCeCu_8$. Empty symbols (○,▫): catalyst pre-reduced with H_2; full symbols (•,▪): catalyst not pre-reduced.

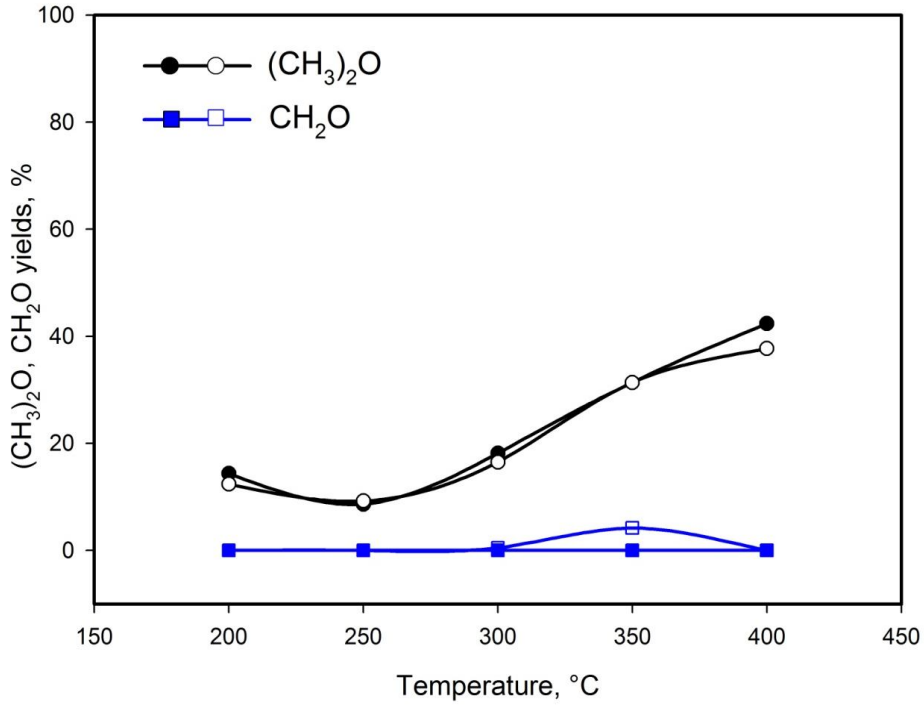

Fig.4-24. $(CH_3)_2O$ and CH_2O yield in the SRM tests on $EMCeCu_8$. Empty symbols (○,▫): catalyst pre-reduced with H_2; full symbols (•,▪): catalyst not pre-reduced.

It appears evident that under SRM conditions the behaviour of the H_2 pre-reduced catalyst is the same as that of the not pre-reduced sample. Moreover Fig. 4-22 shows that the methanol conversion is always lower than under OSRM conditions (Fig.4-19). In particular the H_2 yield appears much lower, indicating very low SRM activity. It can be noted that the maximum H_2 yield (0.5 mol_{H2} mol_{CH3OH}^{-1}) corresponds to only 16% conversion of methanol through steam reforming. This low activity is confirmed by the low values of conversion to CO_2, as appears from Fig. 4-23. Conversion to CO starts above 300 °C and reaches a noticeable value at 400 °C (Fig. 4-23). In Fig. 4-24 the conversion of methanol to formaldehyde and dimethyleter under SRM conditions is shown.

The conversion to CH_2O is negligible in the entire temperature range for both samples, while the conversion to $(CH_3)_2O$ is less than 20% at 200–250 °C and increases with temperature up to 40% at 400 °C. Thus it clearly appears that under SRM conditions the main product is dimethylether. This means that under these conditions the methanol dehydration largely prevails on steam reforming both with the pre-reduced catalyst and with the not pre-reduced one. The high activity for methanol dehydration can be attributed to the alumina phase, that is present in high amount and to the high surface area of the sample, since it is known that acid sites of alumina greatly activate the dehydration of methanol [99]. This reaction occurs in lower extent under OSRM conditions due to the competition with steam reforming. It can be supposed that also in this case metallic Cu is present even in the not pre-reduced sample, due to the reducing action of the reaction medium, but the activity of metallic Cu is so low under these conditions that no influence of the previous H_2 treatment can be detected. On the other hand, the activity of $EMCeCu_8$ under SRM conditions is not very different from that observed with other Cu/Ce/(Al) catalysts cited in the literature, although a precise comparison is hindered by differences in space velocities and catalyst compositions. From data in Table 4-5, the activity for simple SRM of $EMCeCu_8$ appears comparable to that of Cu/Ce/Al catalysts previously reported, if differences in Cu loading and partial pressures of the reactants are taken into account.

Table 4-5
Comparison data from SRM.

Sample [ref.]	Catalyst composition Cu/Ce/Al atom%	Feed ratio H_2O/CH_3OH	WHSV L g^{-1} h^{-1}	Temperature °C	H_2 production rate µmol s^{-1} g_{cat}^{-1}
$EMCeCu_8$	6/5/89	1.1/1	60	250	20
Cu/CeO_2[37]	10/90/0	1.1	5	240	40
$Cu/CeO_2/Al_2O_3$ [115]	25/8/67	1.1	8	250	83

The present results, in agreement with literature data, indicate that when oxygen is absent from the feed, the activity of the $EMCeCu_8$ catalyst for SRM is lower than that of more traditional $Cu/ZnO/(Al_2O_3)$ systems. This difference can be due to the effect of the ZnO phase. It is known that ZnO is an effective promoter of Cu based catalysts for synthesis or reforming of CH_3OH: different interpretations of such effect are given, such as stabilization of Cu(I) in a mixed Cu/Zn oxide [77], formation of a surface Cu/Zn alloy [78], increase of disorder and microstrain in Cu particles [34], H spillover effects [168]. It clearly appears that CeO_2 is not able to give a similar promoter effect under SRM conditions. On the other hand, when O_2 is present in the feed, the activity of $EMCeCu_8$ for methanol reforming is highly enhanced and becomes similar to that of traditional $Cu/ZnO/Al_2O_3$ systems. A possible explanation of this behaviour is that ceria promotes the reaction through a mechanism of H spillover. The rate determining step of methanol reforming is probably the abstraction of H atoms from adsorbed methanol or some other adsorbed species [150], so the reaction rate can be increased if a hydrogen spillover effect occurs on the oxide matrix. Such effect was observed with other CeO_2 supported catalysts, such as Pt/CeO_2 or Cu/CeO_2 [169,170] and can most probably occur on the present system due to the very high dispersion of metallic Cu. The adsorption of H atoms on CeO_2 can lead to the reaction:

$$Ce^{4+} - O - Ce^{4+} + H \leftrightarrow Ce^{3+} - O(H) - Ce^{4+} \qquad (35)$$

The last species can be considered a storage form of H, from which H can be obtained by the reverse reaction. When the catalyst is exposed to a reducing system such as the SRM feed, reaction (35) can lead to complete reduction of Ce^{4+} to Ce^{3+}, in this way the spillover effect is impaired and the rate of reforming decreases. On the other hand, when some O_2 is present in the feed, cerium can be maintained, at least partially, in the oxidized Ce^{4+} state and spillover can occur.
A different explanation is based on the possible oxidation of Cu in the presence of CeO_2, according to the reaction (36) [37]:

$$Ce^{4+} + Cu \rightarrow Ce^{3+} + Cu^{+} \qquad (36)$$

The above TPR data suggest that CeO_2 favours the Cu^+ oxidation state, in agreement with previous works [38,154]. Moreover XPS measurements effected on the used catalysts gives evidence of the presence of Cu^+ species (see *Section 3.2.5)*. The presence of Cu^+ under steam reforming conditions was also reported for other Cu based catalysts and found essential for the reaction [171,172]. It is possible that Cu^+, together with Cu^0, has an active role in the steam reforming of methanol [26,59, 150], probably through the formation of Cu^+–O–Cu^+ sites on the surface of metallic Cu. Such sites are involved in methanol chemisorption, that is a key step in the mechanism of methanol reforming [150]. It can be supposed that oxygen re-oxidizes Ce^{3+} to Ce^{4+}, thus allowing reaction (36) to proceed, this leads to a faster restoring of Cu^+ sites and can explain a much higher activity for SRM in the presence of O_2.
Arrhenius plots for OSRM and SRM evaluated from conversion data as described in *Section 2.3.3* are shown in Fig.4-25, the activation energies and the kinetic constants are reported in Table 4-6. The Arrhenius plots show a satisfactory linear regression. Table 4-6 shows that kinetic constants for OSRM are much higher than those for SRM: the higher activity in the presence of O_2 has been explained in the above discussion on the reaction mechanism.

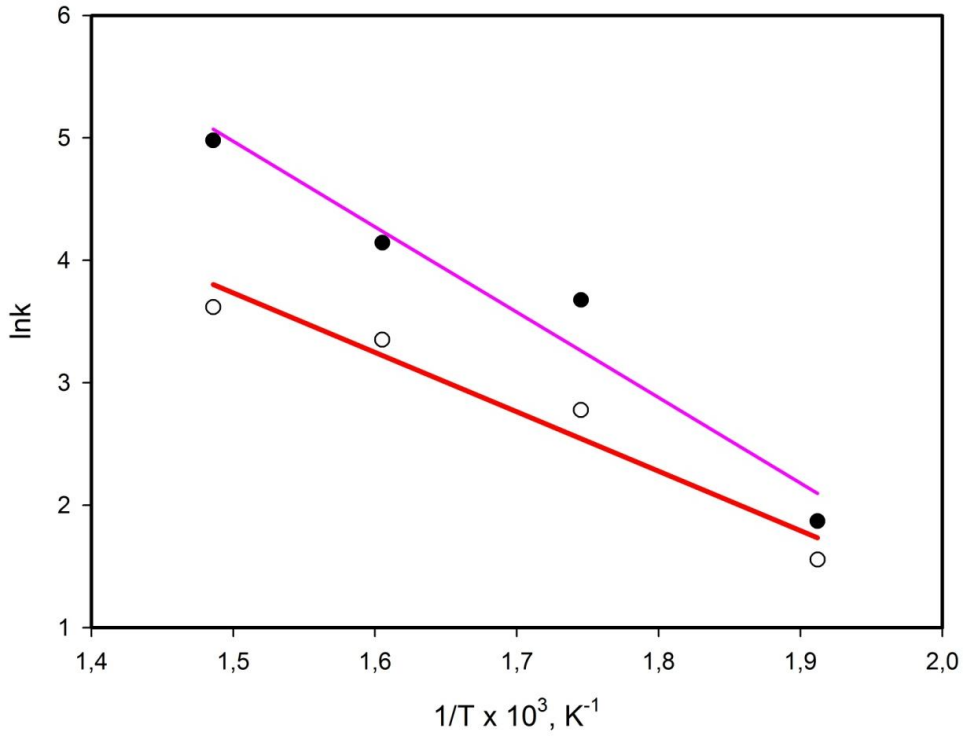

Fig.4-25. Arrhenius plot for OSRM (full symbols) and SRM (empty symbols).

Table 4-6
Activation energy for OSRM and SRM on the $EMCeCu_8$ catalyst.

	OSRM		SRM	
T, °C	k, $cm^3s^{-1}g_{cat}^{-1}$	Eatt, cal mol^{-1}	k, $cm^3s^{-1}g_{cat}^{-1}$	Eatt, cal mol^{-1}
		13860		9638
250	6.48		4.74	
300	39.43		16.07	
350	62.83		28.54	
400	144.71		37.24	

4.2.2 Conclusions

The results of OSRM and SRM tests on $Cu/CeO_2/Al_2O_3$ catalysts can be briefly summarized.

The activity of pre-reduced $Cu/CeO_2/Al_2O_3$ catalysts for the OSRM process depends on the composition of the catalysts, but no simple correlation with Cu content or Cu area can be found. This points to a role of the oxide matrix on the catalytic properties. The most active catalyst is $EMCeCu_8$ that, as shown in Chapter 3, has the higher reducibility and copper dispersion among the studied catalysts. However the activity of all pre-reduced catalysts resulted high, in terms of hydrogen production rate, if compared with data on similar Cu/Ce/Al systems, notwithstanding the absence of the well known promoter ZnO.

Also the unreduced material $EMCeCu_8$ shows a noticeable activity for the OSRM process, indicating that the metallic phase, although with lower activity, can be formed directly under reaction conditions. This very interesting aspect will be further investigated in the Chapter 5.

The different catalytic performances observed in OSRM and SRM tests on $EMCeCu_8$ indicate a strong influence of the presence of O_2 in the reaction system. This has been explained hypothesizing that CeO_2 plays an important role in the methanol reforming catalytic process considering the occurrence of the CeO_2 assisted oxidation of Cu to Cu^+ and that O_2 is needed to maintain the Ce^{4+} oxidation state.

5 Results and discussion

Catalytic tests: Apparatus 2

Catalytic tests performed in the Apparatus 2 (see *Section.2.3.2*) are presented.

5.1 Results and discussion

The best OSRM catalytic activity results were obtained on EMCeCu$_8$ (see *Section 4.2.1*), so this catalyst was selected for a further investigation in the experimental plant described in *Section 2.3.2* . SRM tests were performed both on the oxidized and the pre-reduced catalyst in order to assess the effect of the reaction conditions on the Cu reduction, the ability of copper to take part to a redox cycle and to identify the copper species involved in the reaction mechanism. In fact, as observed in *Section 4.2.1* , also the unreduced material EMCeCu$_8$ showed a noticeable activity for the OSRM process, although with lower activity compared to the pre-reduced EMCeCu$_8$, whilst the activity of the two catalysts is the same under SRM, indicating that the metallic phase can be formed directly under reaction conditions. It can be hypothesized that the reduction of Cu oxide to the metallic state occurs simply through the reducing effect of methanol, analogously to what occurs in the so called ‘‘polyol’’ reduction of copper cations [166,167].

First the results of SRM tests on the oxidized catalyst will be shown.

Fig.5-1 reports MS data representative of methanol concentration, that is masses 32, 31, 30 and 29 as a function of time. All these signals show similar variations with time. Methanol adsorption on the catalyst occurs at low temperature, as shown by the drop of concentration soon after the feed flow is introduced into the reactor. The peak at about 70°C can be attributed to the release of adsorbed methanol due to the temperature rise. Starting from 260°C, the concentration of CH_3OH decreases rapidly with temperature and disappears at 350°C. This indicates the onset of CH_3OH reforming at about 260°C. The mass profiles indicate that a 50% CH_3OH conversion is reached at 305°C. The signals of masses 30 and 29 derive from methanol but can be representative also of formaldehyde: however, since in this case they vary precisely in line with the other signals of methanol, it is likely that the amount of formaldehyde produced is negligible.

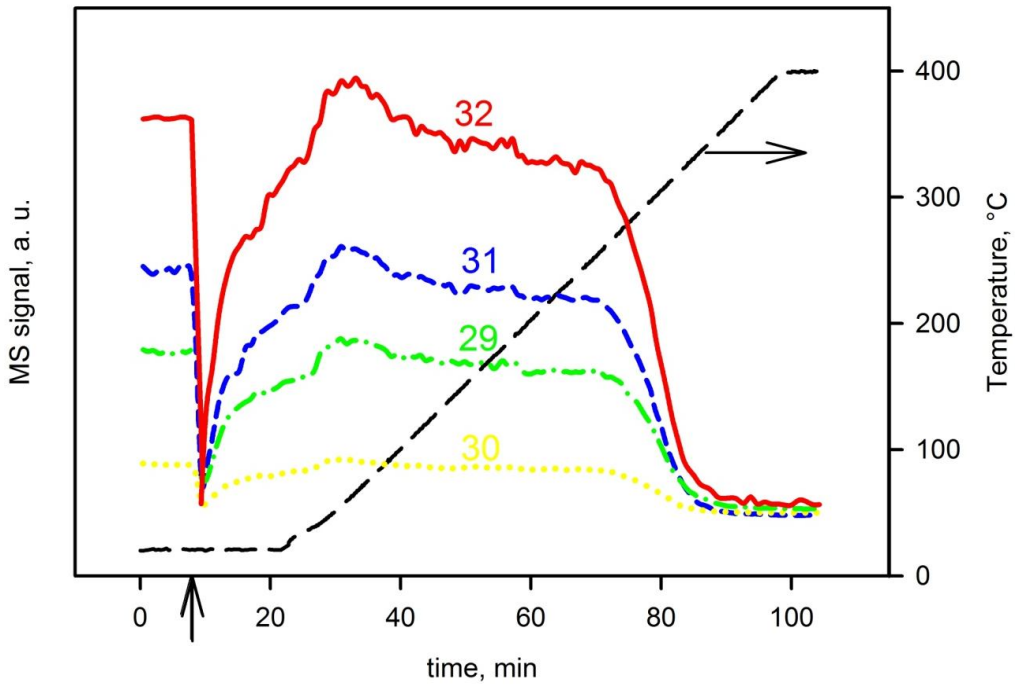

Fig.5-1 signals in the SRM test on oxidized EMCeCu$_8$: masses 32, 31, 30, 29. The arrow on the time axis indicates the introduction of the feed flow into the reactor.

The signals of water, reported in Fig.5-2 (masses 18 and 17) also indicate adsorption at low temperature, followed by release of a large amount of water as the temperature is raised: the broad desorption peak reaches a maximum around 175°C. A shoulder is observed at about 270°C and, at T > 300°C, the H_2O signal drops below the value corresponding to the feed concentration. Although the signals of water are clearly influenced by adsorption phenomena more than those of methanol, the consumption of water is evident at high temperatures, and the shoulder observed at about 270°C is probably related to the onset of the SRM reaction, since it corresponds to the beginning of the CH_3OH consumption.

This is confirmed by the appearance of the signal of mass 2 (Fig.5-2) that increases abruptly going out of range at about 300°C. The concentration of H_2 in the products can be determined more conveniently with the TCD detector, that allows a quantitative evaluation, as observed above (see *Section 2.3.2*).

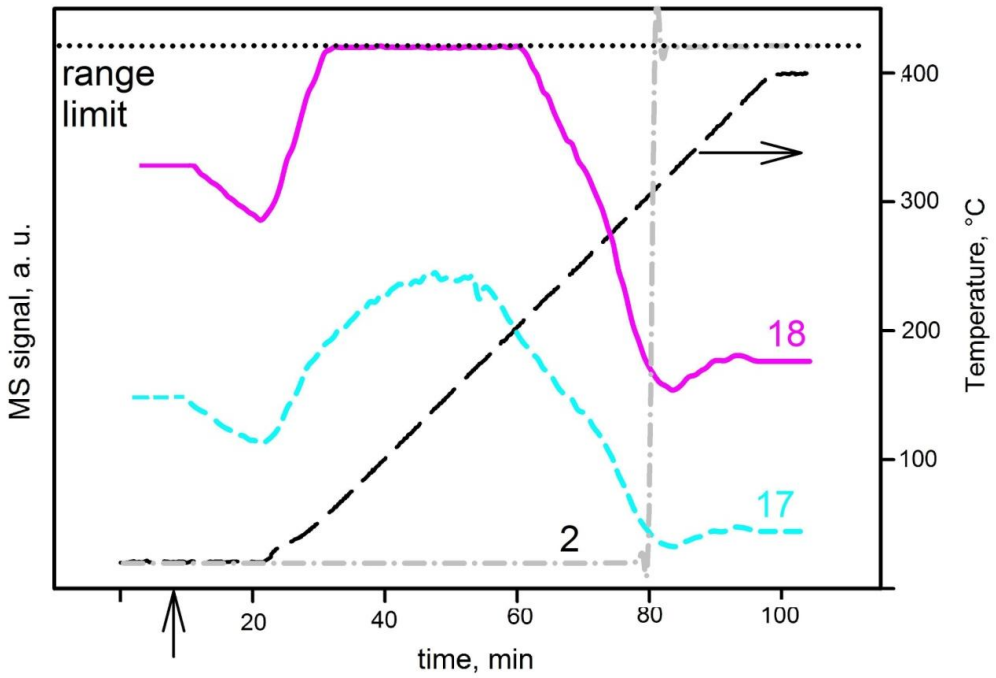

Fig.5-2. MS signals in the SRM test on oxidized EMCeCu$_8$: masses 2, 18, 17. The arrow on the time axis indicates the introduction of the feed flow into the reactor.

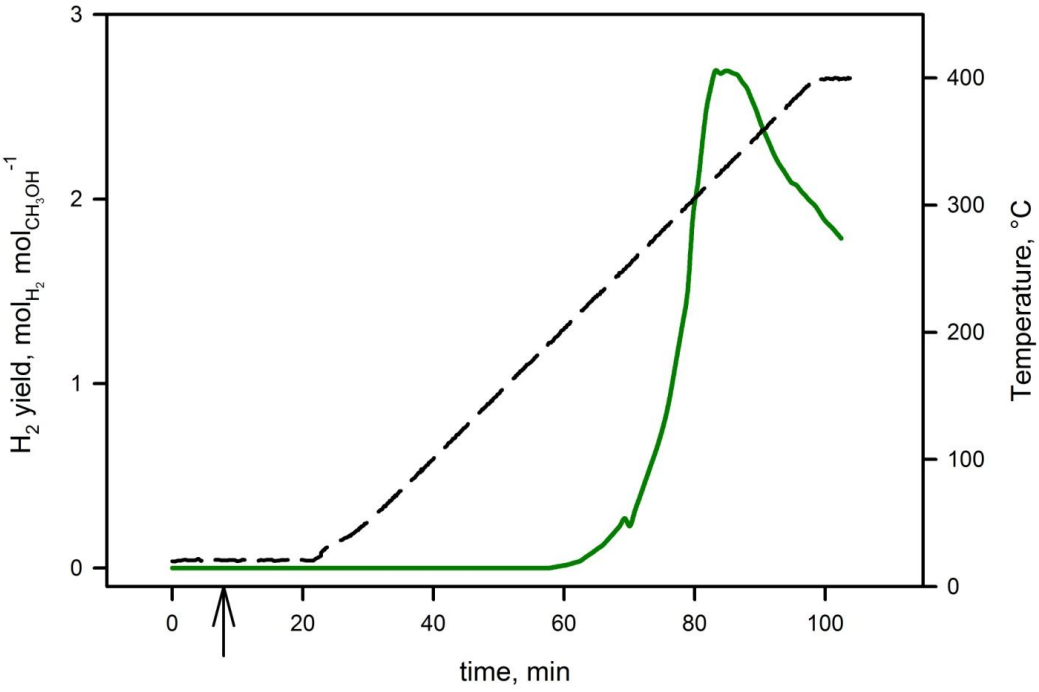

Fig.5-3 H_2 yield as a function of time in the SRM test on oxidized EMCeCu$_8$. The arrow on the time axis indicates the introduction of the feed flow into the reactor.

The TCD data, reported in Fig.5-3, show that the production of H_2 starts abruptly from 250°C and reaches a maximum at 300°C, then it decreases with further increase of temperature. This trend substantially agrees with MS data of CH_3OH and H_2O, suggesting that SRM starts at 250°C on this catalyst. The maximum value of H_2 concentration observed at 300°C corresponds to a yield of 2.7 mol H_2 per mol CH_3OH, that is close to the maximum expected from reaction (Eq.3).

The MS signals of CO_2 and CO are reported in Fig. 5-4 together with the corresponding quantitative data determined by means of the IR spectrophotometer. The CO_2 concentration shows two peaks with maxima at 170 and 330°C, with close correspondence between MS and IR data. It is unlikely that the first peak derives from SRM, as it occurs in a temperature range where the SRM reaction, as noted above, seems not yet activated. It can be supposed that some CO_2 derives from methanol that reacts with CuO present in the oxidized catalyst, according to a reaction of partial or total oxidation, represented by Eq.37 or 38 respectively.

$$CH_3OH + CuO \rightarrow CO_2 + 2H_2 + Cu \qquad (37)$$

$$CH_3OH + 3CuO \rightarrow CO_2 + 2H_2O \qquad (38)$$

These reactions can also involve methanol that was adsorbed at low temperature. The absence of H_2 in the products at temperatures lower than 250°C seems to exclude reaction (37). The amount of CO_2 corresponding to the peak at 170°C has been evaluated by integration as $7.3 \cdot 10^{-5}$ mol: since the amount of Cu present in the catalyst is $2.1 \cdot 10^{-4}$ mol, the amount of CO_2 corresponds to that expected from eq. (38).

The second CO_2 peak, extending from 250 to 400°C, follows the variation of H_2 concentration (Fig.5-3), so it can be related to the SRM reaction, that occurs in this temperature range because Cu is in the metallic state above 250°C. The temperature of 50% CH_3OH conversion to CO_2, determined from the curve of CO_2 concentration, is 295°C.

Moreover it can be observed the presence in the products of CO, that starts from about the same temperature as CO_2 and increases noticeably with temperature up to 0.2% at 400°C, indicating that SRM is not the only reaction, but a reaction such as methanol decomposition (Eq.1) or the reverse WGS (Eq.39) must be considered.

$$CO_2 + H_2 \rightarrow CO + H_2O \qquad (39)$$

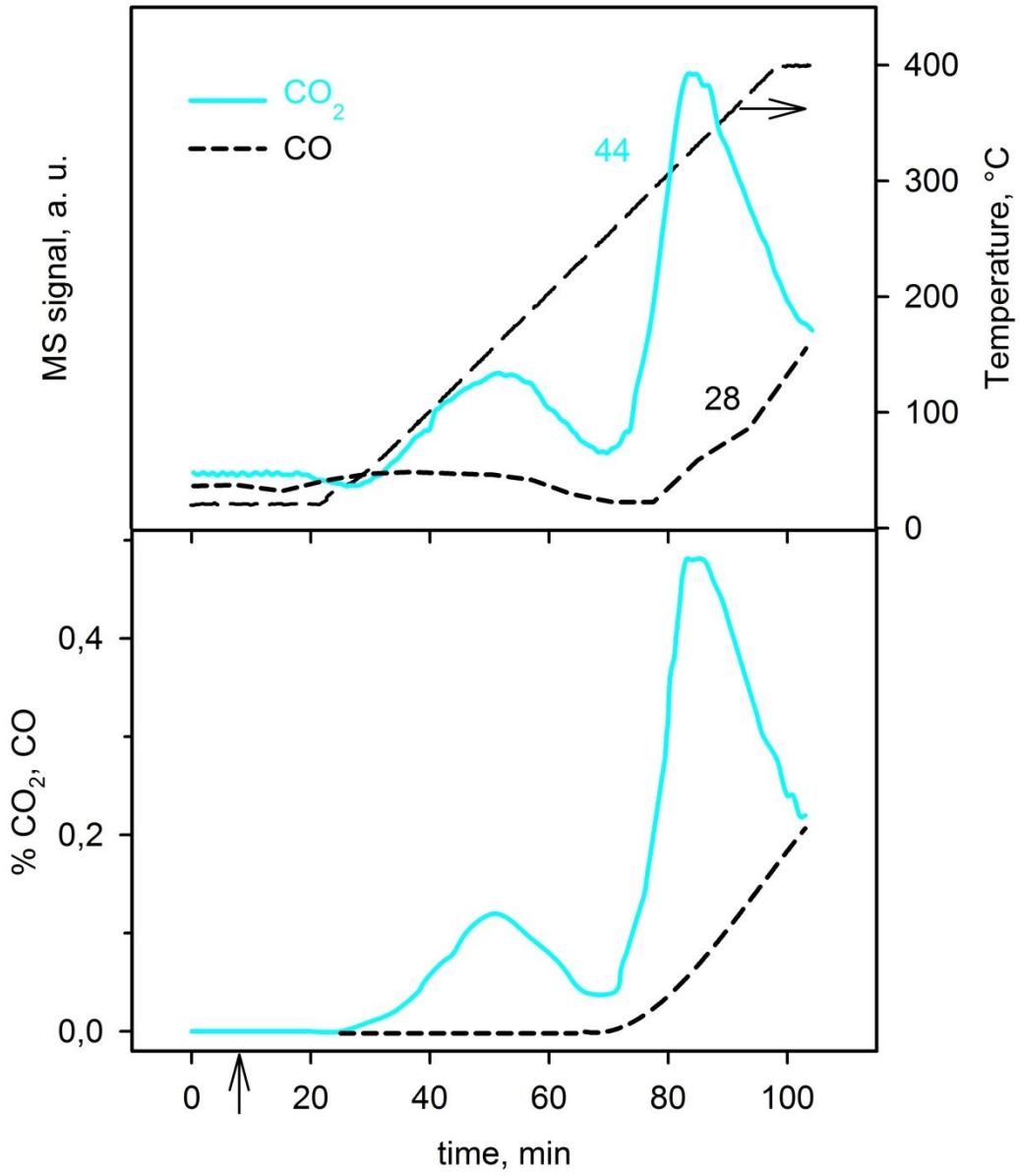

Fig. 5-4. MS signals of masses 44 and 28 (top) and concentration of CO_2 and CO measured with the IR analyzer (bottom) as a function of time in the SRM test on oxidized EMCeCu$_8$. The arrow on the time axis indicates the introduction of the feed flow into the reactor.

Methanol conversions to CO_2 and CO have been calculated from the values of CO_2 and CO concentrations. The sum of conversions to CO_2 and to CO, reported in Fig. 5-5, reaches a maximum at 310-340°C, when it accounts for total methanol conversion, while it decreases increasing the temperature above 340°C. Since this diminution cannot be balanced by any other side reactions not producing CO_x, a decrease of CH_3OH conversion must occur at high temperatures. This behaviour

is not evidenced by the MS profile of CH_3OH (Fig. 5-1), probably due to the semi-quantitative value of MS data. On the other hand it agrees with the variation of CH_3OH conversion with temperature observed in the other plant (see *Section 4.2.1*).

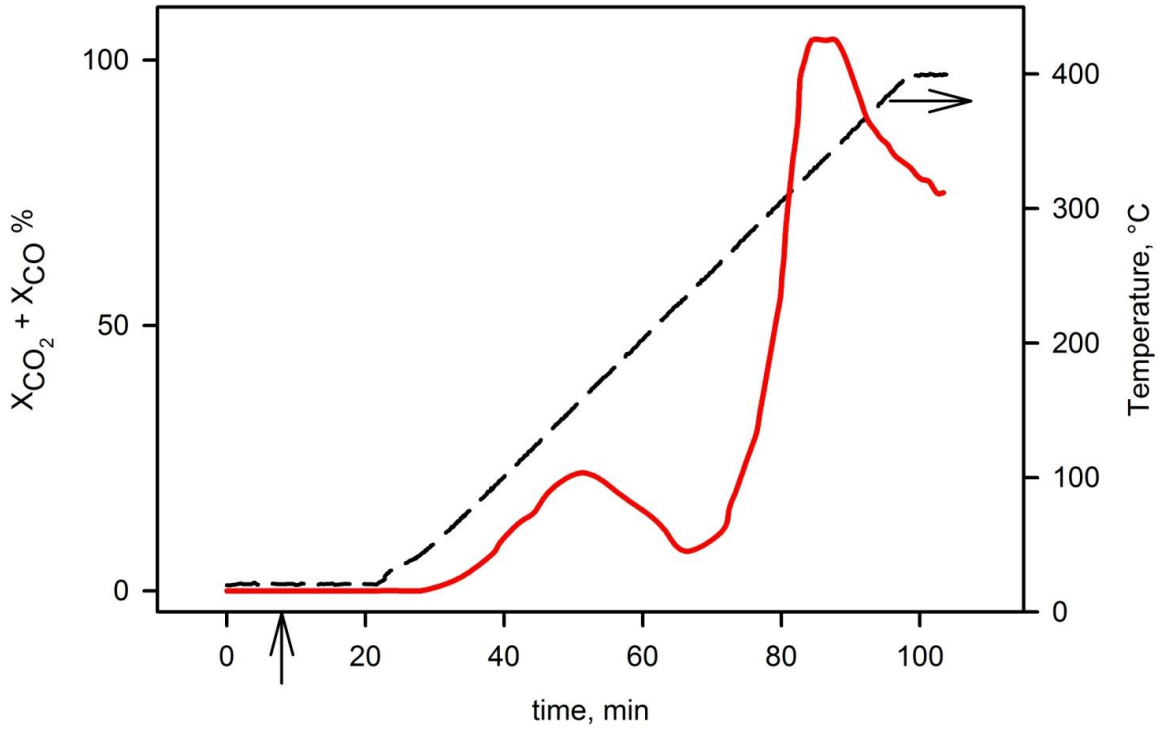

Fig. 5-5. Sum of conversions of methanol to CO_2 and CO as a function of time in the SRM test on oxidized EMCeCu$_8$. The arrow on the time axis indicates the introduction of the feed flow into the reactor.

Another product detected by MS is $(CH_3)_2O$, represented by the signal of mass 46 reported in Fig. 5-6. The signal appears weaker than those of the other components. The concentration of $(CH_3)_2O$ increases with temperature starting from 205°C and reaches a maximum at about 300°C, then it decreases rapidly at higher temperatures. The formation of $(CH_3)_2O$ can be attributed to reaction (40) that is catalyzed by the acid sites of alumina, as already observed in previous works [173] and *Section 4.2.1* The decrease observed at high temperature is not due to thermodynamic limitation because the equilibrium constant of CH_3OH dehydration is only slightly influenced by temperature (K decreases from 4.8 at 200°C to 1.8 at 400°C): it is probably due to competition with the SRM reaction, that is more favoured thermodynamically at these temperatures.

$2CH_3OH \rightarrow (CH_3)_2O + H_2O$ (40)

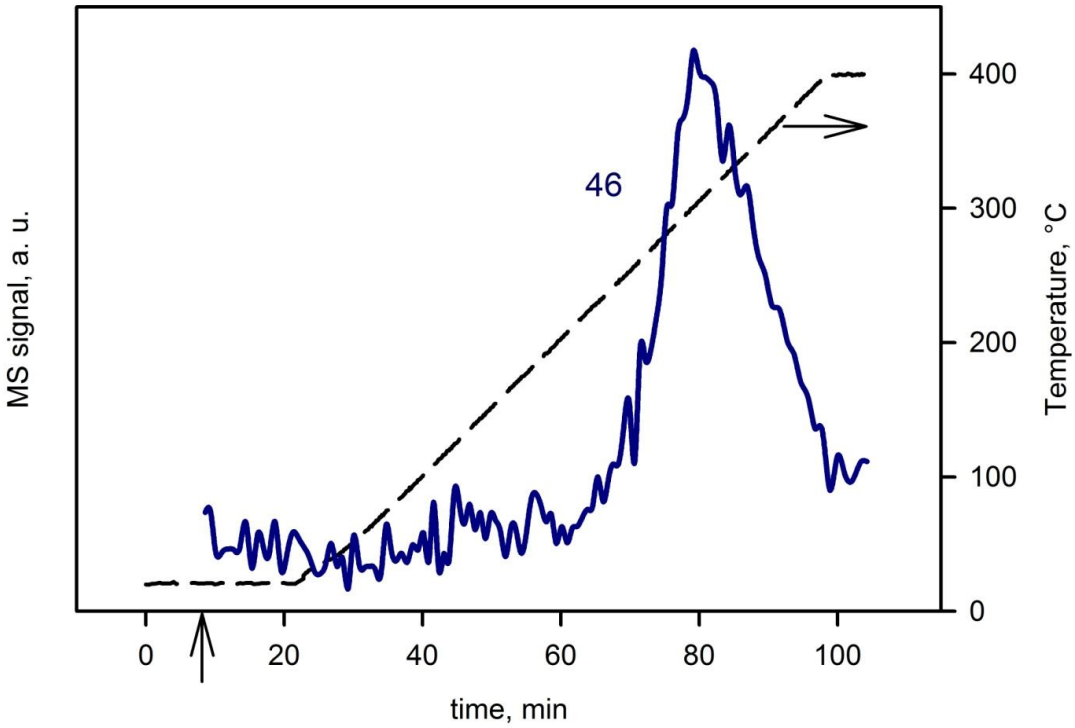

Fig. 5-6. MS signal of mass 46 in the SRM test on oxidized EMCeCu$_8$. The arrow on the time axis indicates the introduction of the feed flow into the reactor.

Now the results of SRM tests on the catalyst pre-reduced in H_2 will be shown. The MS profiles representative of methanol are reported in Fig. 5-7. Also in this case adsorption of a noticeable amount of methanol is observed as soon as the feed flow is introduced into the reactor and a clear desorption signal (peak at 76°C) appears when the temperature programming begins. The SRM reaction starts at about 180°C, as indicated by decrease of the MS signals. A 50% CH_3OH conversion is reached at 210°C and complete conversion is observed above 300°C. Also in this case the production of formaldehyde is not detectable, since the signals of masses 30 and 29 are not distinguished from those of methanol.

The signals of masses 18, 17 and 2 are reported in Fig. 5-8. After a desorption peak at 110°C, the H_2O signal drop due to the SRM reaction begins at about 180°C, in agreement with the variation of CH_3OH concentration (Fig.5-7). The signal of mass 2 indicates that H_2 production starts at 190°C, confirming the above result.

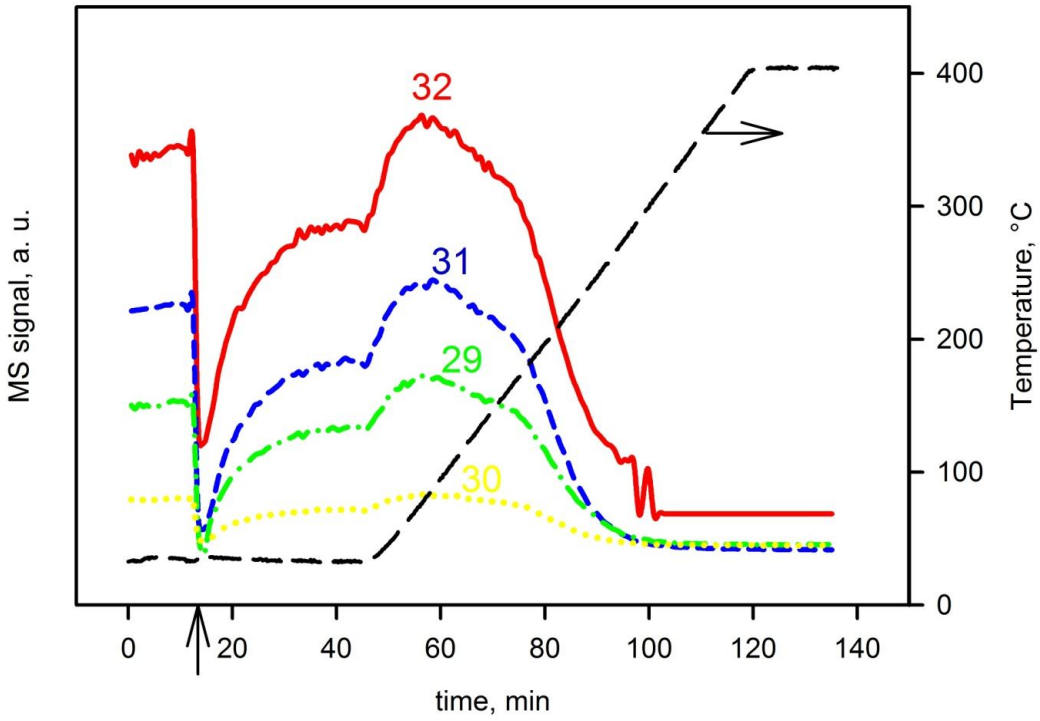

Fig. 5-7. MS signals in the SRM test on EMCeCu$_8$ pre-reduced in H_2: masses 32, 31, 30, 29. The arrow on the time axis indicates the introduction of the feed flow into the reactor.

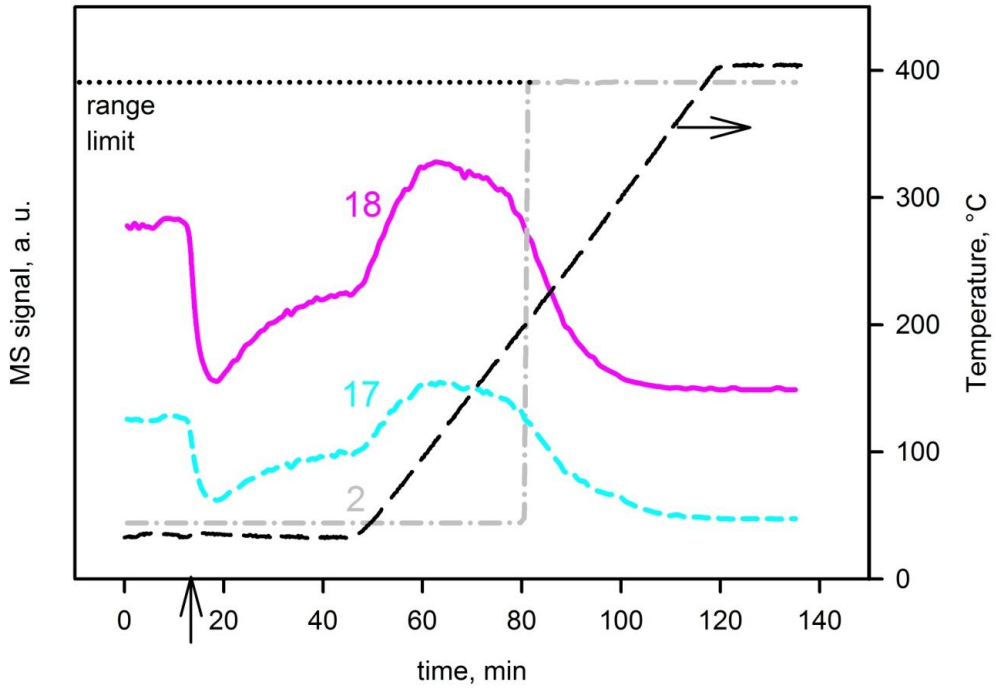

Fig. 5-8. MS signals in the SRM test on EMCeCu$_8$ pre-reduced in H_2: masses 18, 17, 2. The arrow on the time axis indicates the introduction of the feed flow into the reactor.

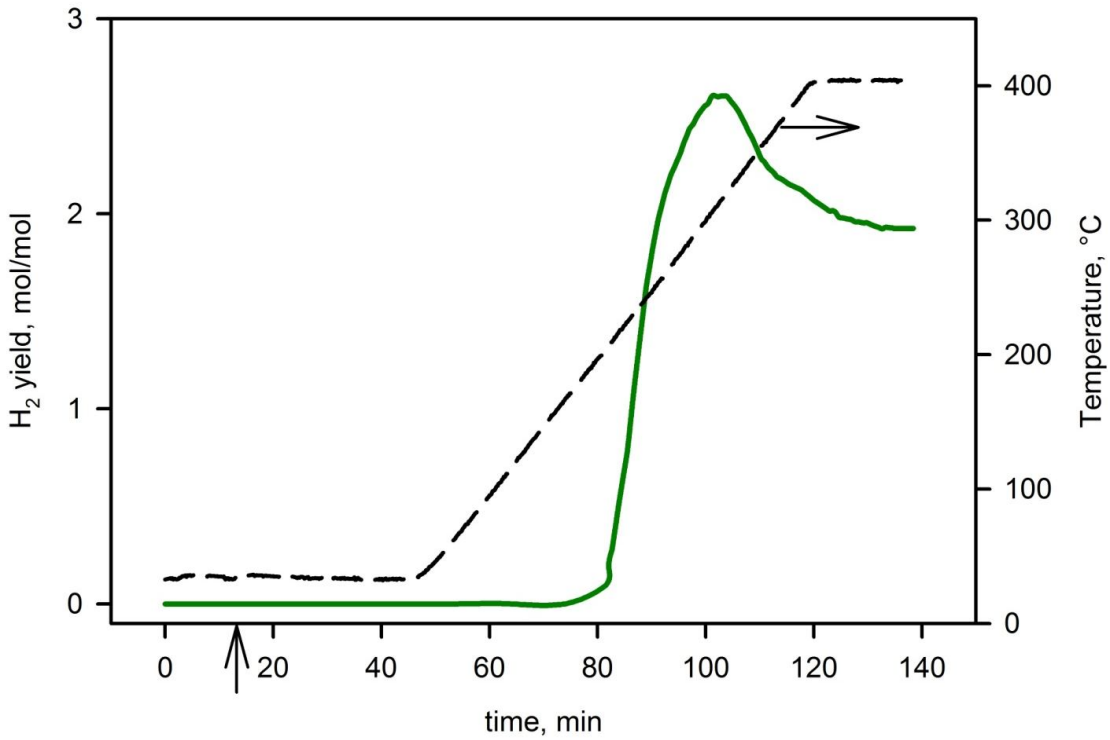

Fig. 5-9. H_2 yield as a function of time in the SRM test on $EMCeCu_8$ pre-reduced in H_2. The arrow on the time axis indicates the introduction of the feed flow into the reactor.

The concentration of H_2 determined with the TCD (Fig. 5-9) starts from 190°C, and reaches a maximum at 300°C corresponding to a yield of 2.7 molH_2 per mol CH_3OH, then it decreases at higher temperatures.

The concentrations of CO_2 and CO, determined from both MS and the IR analyzer, are reported in Fig. 5-10. Again the data obtained from the two techniques agree. In this case one peak of CO_2 concentration is observed. The CO_2 production starts from the temperature of 160-170°C and reaches a maximum of 0.45% at 260-270°C: 50% CH_3OH conversion to CO_2 is obtained at 200-220°C. Carbon monoxide is detected from 225°C and increases steadily with temperature up to 0.1% at 400°C. From these data methanol conversions to CO_2 and CO have been calculated. The sum of methanol conversions to CO_2 and to CO reported in Fig. 5-11 reaches a maximum at 280°C corresponding to almost complete methanol conversion.

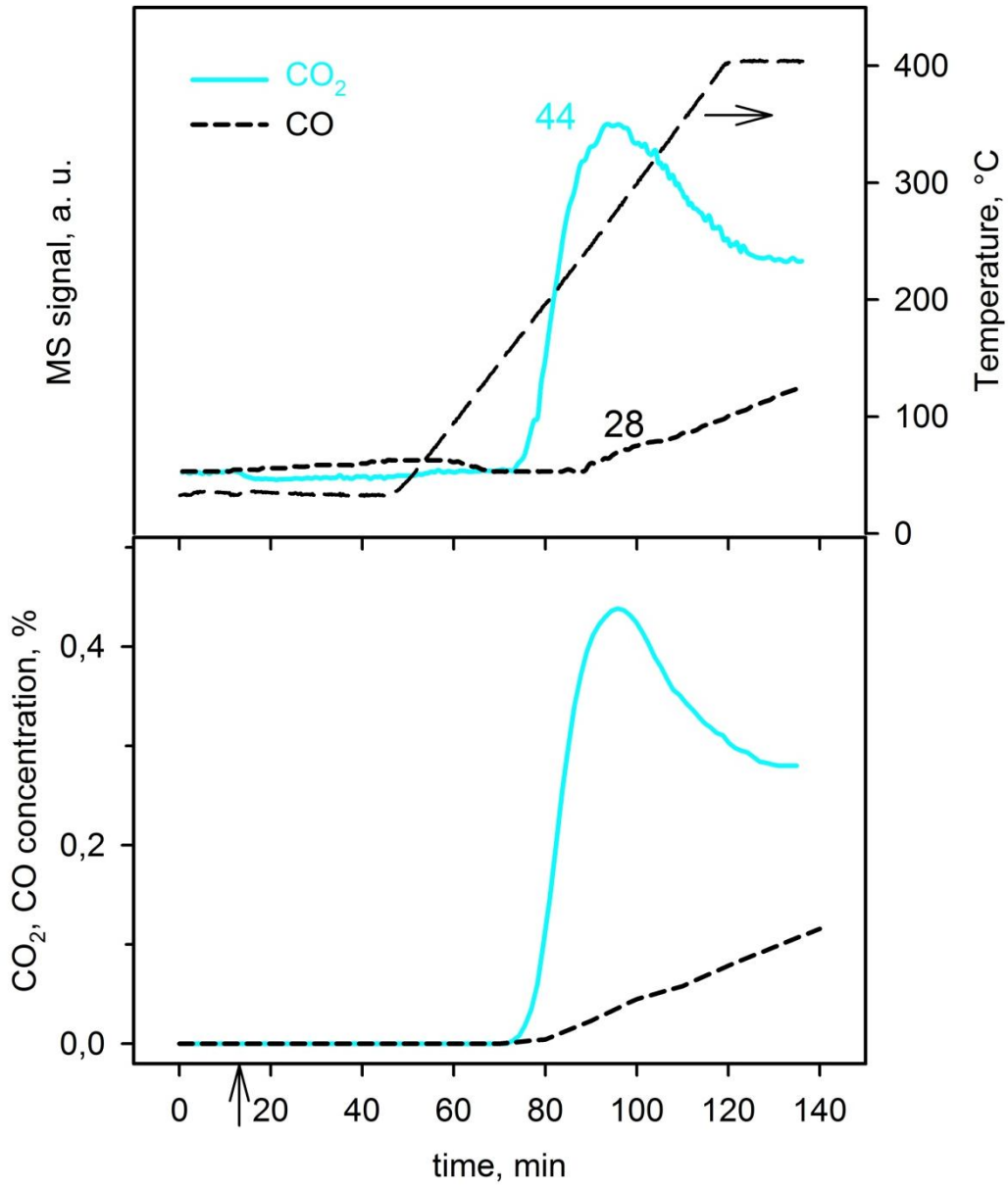

Fig. 5-10. MS signals of masses 44 and 28 (top) and concentration of CO_2 and CO measured with the IR analyzer (bottom) as a function of time in the SRM test on $EMCeCu_8$ pre-reduced in H_2. The arrow on the time axis indicates the introduction of the feed flow into the reactor.

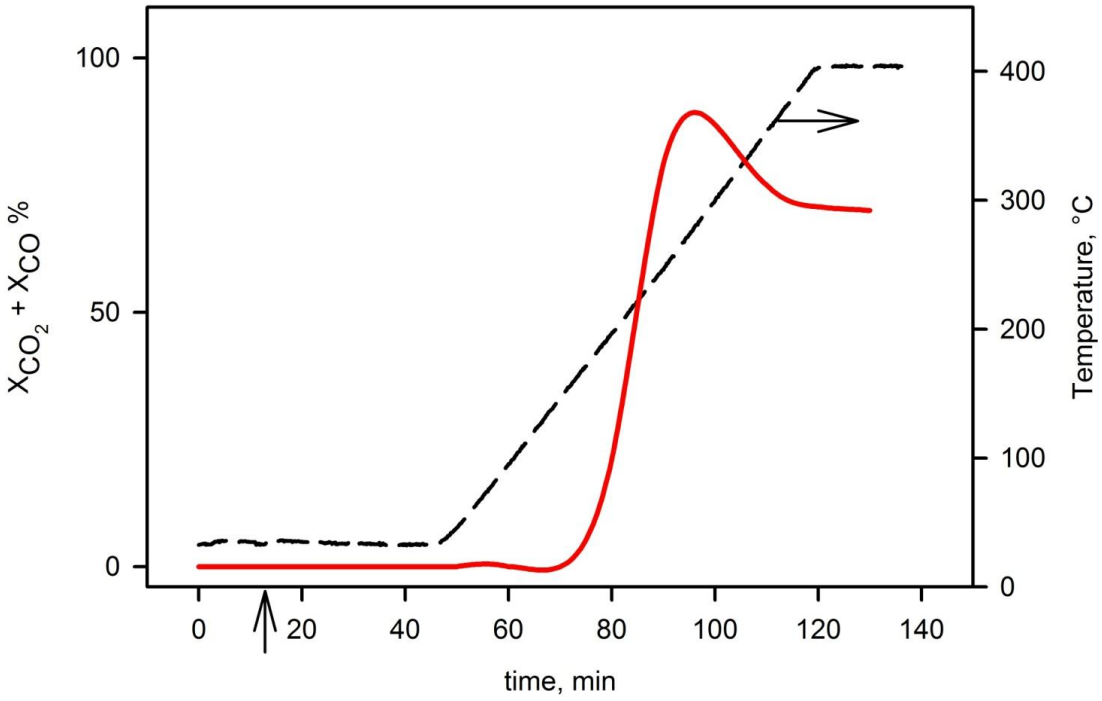

Fig. 5-11. Sum of conversions of methanol to CO_2 and CO as a function of time in the SRM test on pre-reduced EMCeCu$_8$. The arrow on the time axis indicates the introduction of the feed flow into the reactor.

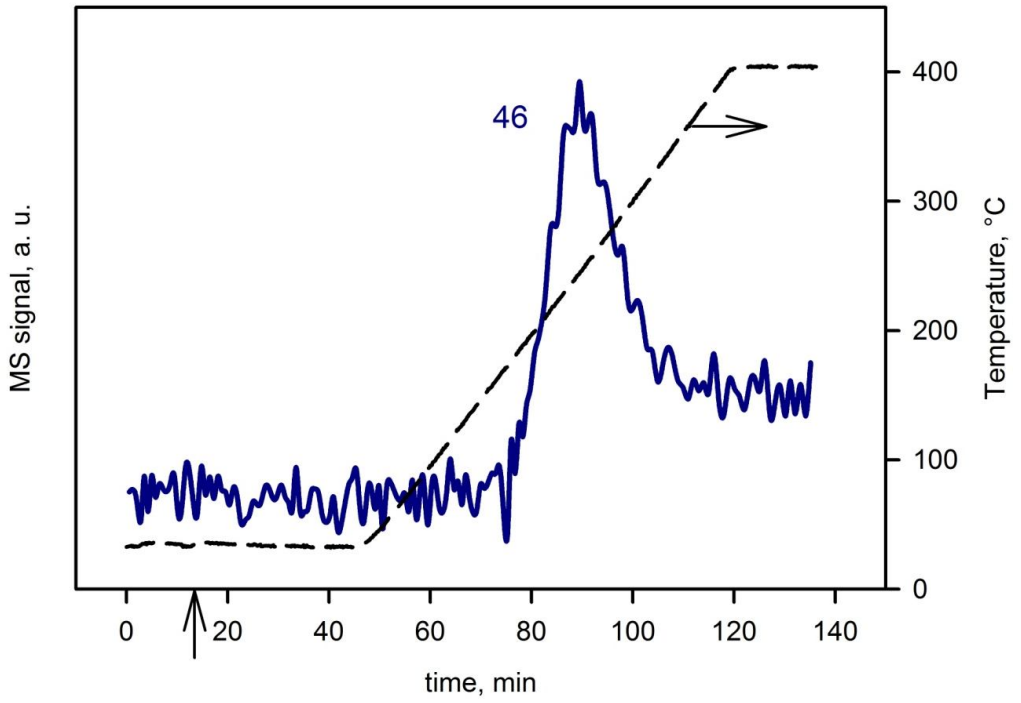

Fig. 5-12. MS signal of mass 46 in the SRM test on pre-reduced EMCeCu$_8$. The arrow on the time axis indicates the introduction of the feed flow into the reactor.

The signal of $(CH_3)_2O$ (mass 46) is reported in Fig. 5-12: the production of this compound begins from 170°C and reaches a maximum at 240°C, showing a rapid decrease at higher temperatures.
These data show that the catalyst studied is active for methanol reforming even when it is not pre-reduced with H_2, but the results are markedly influenced by the previous reduction. The behaviour is different from that observed in previous tests carried out under flow conditions, that showed equivalent results for SRM with samples pre-reduced with H_2 and not pre-reduced (see *Section 4.2.1*). In this case the reduction treatment causes a noticeable decrease of the onset temperature of SRM from 250°C to 180°C and of the temperature of 50% conversion from 300°C to 210°C. Complete CH_3OH conversion is reached at 350°C and at 300°C with the not pre-reduced and the pre-reduced samples respectively. The data obtained with the oxidized catalyst suggest that the catalyst becomes active only when all or most Cu oxide has been reduced to metallic Cu by reaction with methanol. This is evident from Fig. 5-4 showing a clear distinction between the signal of CO_2 deriving from the CuO-CH_3OH reaction and that deriving from SRM.
To explain the different results obtained in the two plants, it has to be considered that they work under different feed conditions (see Chapter 2), so it can be hypothesized that starting from a not pre-reduced catalyst, different active phases can be formed by reaction with methanol, depending on the feed conditions. In particular, the metallic copper obtained using a feed richer in methanol, such as that described in Chapter 3, seems more active than that obtained here using a feed with a lower methanol concentration. So the activity for SRM observed with sample not pre-reduced is equal to that obtained with the pre-reduced catalyst only when copper is reduced under strong reducing conditions, that is high methanol concentration, because under these conditions it reaches the same properties of copper pre-reduced with H_2.
To analyze the state of the copper under reaction conditions and identify possible differences between that present in the pre-reduced and in the not pre-reduced catalyst, the samples used in the catalytic test were characterized by TPR and by measurement of Cu dispersion through the standardized method of N_2O treatment followed by TPR (see *Section 2.2.4*). Such measurements were carried out after cooling the samples to room temperature under pure Ar flow soon after the catalytic tests.
The result of the TPR measurements performed after the catalytic runs are reported in Fig. 5-13 in comparison with the TPR spectrum obtained on the fresh (not pre-reduced not tested) sample. The corresponding values of consumed H_2 are reported in Table 5-1. The TPR profile of the not pre-reduced used catalyst appears very different from that of the fresh one, showing only two peaks of

low intensity at 170 and 224°C. The amount of H_2 consumed (Table 5-1) corresponds to an average Cu oxidation state of 0.22, indicating that a large fraction of Cu is in the metallic state, in agreement with the above described activity for SRM.

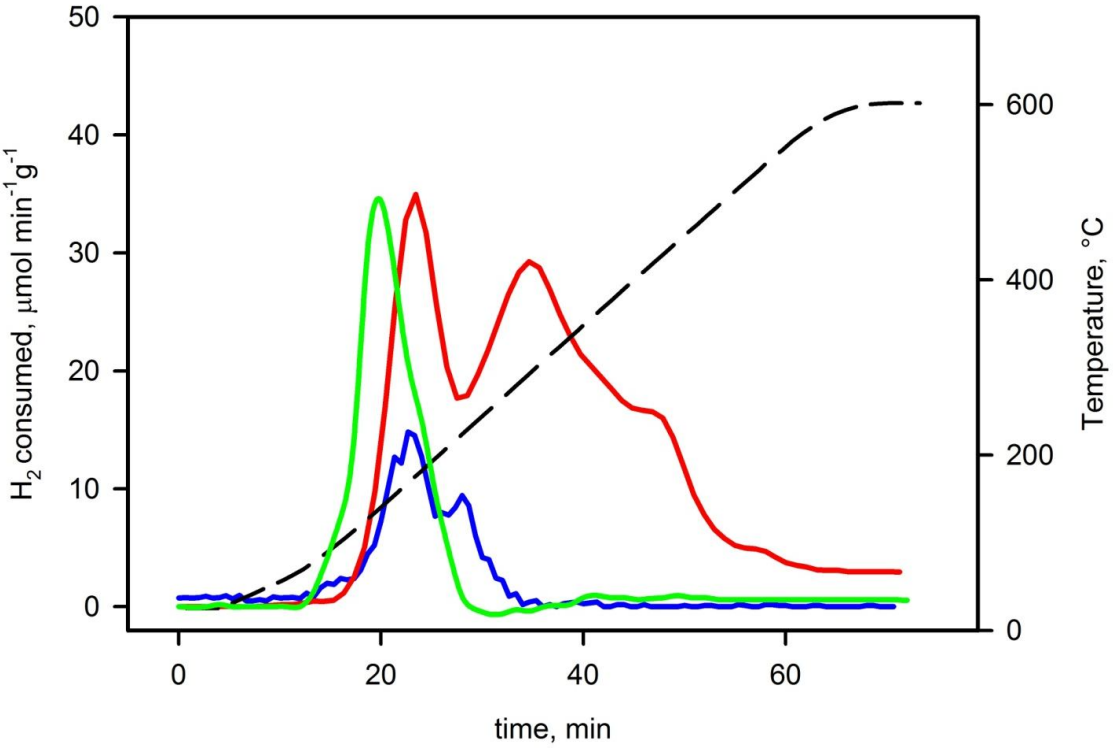

Fig. 5-13. TPR spectra on the catalysts after SRM tests. Blue line: not pre-reduced catalyst; green line: catalyst pre-reduced in H_2; red line: not pre-reduced not tested sample.

Table 5-1

TPR and Cu dispersion data of the catalyst before and after SRM tests.

Sample	Fresh catalyst			Used catalyst		
	H_2 consumed mmol g^{-1}	Cu oxidation state	Cu dispersion %	H_2 consumed mmol g^{-1}	Cu oxidation state	Cu dispersion %
$EMCeCu_8$ oxidized	0.69[a]	1.33[a]	-	0.115	0.22	54[b]
$EMCeCu_8$ pre-reduced	-	0	69[a]	0.235	0.45	69[b]

[a] Data relating to the fresh catalyst are taken from Table 3-6.

[b] Cu dispersion = surface Cu /total Cu x 100.

The TPR spectrum of the sample pre-reduced in H_2 and tested in SRM is reported in the same Fig. 5-13. In this case only one TPR peak is observed at low temperature and the amount of consumed H_2 (Table 5-1) corresponds to an average Cu oxidation state that is about twice the value found for the sample that was not pre-reduced in H_2. These data confirm that the catalyst works in a partially oxidized state under SRM conditions. Such state can be related to the presence of an oxygen layer on the working metallic surface, implying an oxidation of surface Cu to Cu^+, as hypothesized to describe the reaction mechanism under SRM conditions [150]. This agrees with the low temperature of the TPR signals of the used catalysts. After each catalytic test the sample was characterized for Cu dispersion as described above (see *Section 2.2.4*) and the results are reported in the same Table 5-1. A higher value of Cu dispersion is observed for the catalyst previously reduced in H_2, as appears from Table 5-1. This means that the reduction of Cu(II) species with H_2 produces a larger Cu metallic surface compared with the reduction of the same species with methanol. It is expected that the larger metallic surface leads to a higher amount of oxygen that can be bonded to the surface and so to a higher average oxidation state, as observed from TPR measurements (Table 5-1). The higher dispersion of the sample previously reduced in H_2 explains its higher activity, as shown from the lower temperatures of onset of SRM and of 50% conversion. One can also suppose that the lower Cu dispersion measured on the not pre-reduced sample is the result of incomplete reduction of Cu(II) to metallic Cu, due to the milder reduction conditions. It can be noted that the Cu dispersion of the pre-reduced catalyst after the SRM run is the same as before the reaction: this suggests that the active phase is not modified during the reaction.

5.2 Conclusions

SRM tests performed in the experimental plant pointed out that also the unreduced material $EMCeCu_8$ showed a noticeable activity for the SRM process, indicating that the metallic phase can be formed directly under reaction conditions. It was supposed that methanol reacted with CuO present in the oxidized catalyst, according to a reaction of partial or total oxidation, reducing it to metallic copper. These data confirm that the catalyst works in a partially oxidized state under SRM conditions. Such state can be related to the presence of an oxygen layer on the working metallic surface, implying an oxidation of surface Cu to Cu^+, as hypothesized to describe the reaction mechanism under SRM conditions [150]. However, the reduction conditions strongly influenced the properties of metallic copper obtained, as confirmed by TPR and dispersion measurements

performed on the used catalyst. After reduction with H_2, the catalyst showed a higher copper surface than that obtained after reduction with methanol under reaction conditions, and this higher dispersion could explain its higher activity. Comparing the results from the two plants employed for testing catalytic activity, it was inferred that also the concentration of methanol influenced the properties of metallic copper, since copper obtained under strong reducing conditions (high methanol concentration) was more active than that obtained using a low methanol concentration.
Cu dispersion measurements showed that the dispersion of the pre-reduced catalyst after the SRM run is the same as before the reaction: this suggests that the active phase is not modified during the reaction and that it is stable.

6 Overall conclusions

The object of this thesis was the study of Cu/ZrO_2 and $Cu/CeO_2/Al_2O_3$ catalysts prepared by modified sol-gel methods with the aim of investigating on the possibility of employing these systems as selective catalysts for the OSRM process. Two different sol-gel method were employed to reach this purpose: a modified sol-gel method for the preparation of Cu/ZrO_2 systems and a totally new sol-gel method for the preparation of $Cu/CeO_2/Al_2O_3$ systems. Both preparation methods, involving the direct incorporation of the metal salt into the synthesis gel used to prepare the support, allowed to obtain more homogeneously dispersed mixed oxides samples. Copper oxide was in fact present in a highly dispersed form in all materials, and gave, after reduction, a nanometric metallic phase with an exceptionally high surface area. Moreover the preparation method of $Cu/CeO_2/Al_2O_3$ catalysts was a totally new sol-gel approach, in which metal salts (stearates) were used both as Cu and Ce sources and as structural directing agents: this method produced catalysts with an organized mesoporosity and a very narrow pore size distribution.

Two sol-gel procedures based on different Cu precursors were investigated for the preparation of Cu/ZrO_2 catalysts and it was found that the preparation method strongly influenced all the properties studied. Using copper nitrate as Cu precursor, a crystallisation delay of zirconia was observed, that allowed to obtain high surface area samples, even after long reduction treatments, high Cu reducibility and exceptional Cu dispersions. On the other hand, using acetate copper as Cu source, low surface area samples, especially after high temperature treatments, were obtained, due to the high cristallinity of these systems. For all samples the presence of zirconia seemed to stabilize Cu^+ species: this is advantageous since Cu^+ species are probably involved in the mechanism of OSRM.
The catalytic activity of Cu/ZrO_2 systems for the oxidative steam reforming of methanol appeared interesting compared to that of previous Cu based catalysts, taking into account the absence of any promoter. H_2 pre-reduction was not strictly required for catalytic activity and this confirmed the hypothesis that under reaction conditions the CuO species were reduced by methanol to metallic Cu. The catalytic activity was strongly influenced by the preparation method: this was explained by the effect of the preparation method on both surface area and Cu dispersion. A serious drawback of these systems is the noticeable activity of the zirconia support towards the production of undesired compounds, such as dimethylether and formaldehyde. It is expected that the performance of the

catalyst would be greatly improved by using suitable promoters and pre-treatment conditions that depress the adverse activity of the support.

$Cu/CeO_2/Al_2O_3$ catalysts showed a huge surface area and contained very dispersed CeO_2 and CuO phases on a poorly crystalline alumina matrix, confirming the effectiveness of the new single-step sol–gel method to prepare high surface area mesostructured systems. After a reductive treatment with H_2, a highly dispersed Cu metallic phase was obtained and surface area was not affected. The presence of CeO_2 favoured the Cu^+ oxidation state, that is important for the OSRM reaction as observed above. The activity of all pre-reduced catalysts resulted high, in terms of hydrogen production rate, if compared with data on similar Cu/Ce/Al systems, notwithstanding the absence of the well known promoter ZnO. Also for these systems the unreduced materials showed a noticeable activity for the OSRM process, indicating that the metallic phase, although with lower activity, can be formed directly under reaction conditions. The different catalytic performances observed in OSRM and SRM tests indicate a strong influence of the presence of O_2 in the reaction system. The activity for SRM, in the absence of oxygen was, in fact very low. This behaviour was explained either considering the occurrence of H spillover or the CeO_2 assisted oxidation of Cu to Cu^+.
Also in this case, it is expected that the performance of the catalysts would be greatly improved by using suitable promoters, such as ZnO.

The reduction of copper under reaction conditions was further investigated and it was found that the catalytic activity was strongly related to the reducing strength of the atmosphere (reduction with H_2 or methanol at different concentrations). In particular it was found that metallic copper obtained under stronger reducing conditions (reduction with H_2 or high methanol concentration) was more active for SRM than that obtained using a low methanol concentration and that this higher activity was probably correlated to its higher dispersion.
These data confirm that the catalyst works in a partially oxidized state under SRM conditions. Such state can be related to the presence of an oxygen layer on the working metallic surface, implying an oxidation of surface Cu to Cu^+, as hypothesized to describe the reaction mechanism under SRM conditions [150]. Cu dispersion measurements showed that the dispersion of the pre-reduced catalyst after the SRM run is the same as before the reaction, suggesting the stability of the active phase during the reaction.

References

[1] BP Statistical review of world energy, full report 2009.

[2] University of Copenhagen, Synthesis report from climate change Global Risks, Challenges & Decisions Copenhagen 2009, 10-12 March, Available online at: http://climatecongress.ku.dk/pdf/synthesisreport.

[3] Rogner, H.-H., D. Zhou, R. Bradley. P. Crabbé, O. Edenhofer, B.Hare (Australia), L. Kuijpers, M. Yamaguchi, 2007: Introduction. In Climate Change 2007: Mitigation. Contribution of Working Group III to the Fourth Assessment Report of the Intergovernmental Panel on ClimateChange [B. Metz, O.R. Davidson, P.R. Bosch, R. Dave, L.A. Meyer (eds)], Cambridge University Press, Cambridge, United Kingdom and New York, NY, USA.

[4] Tans, P. Trends in Atmospheric Carbon Dioxide - Mauna Loa, NOAA/ESRL, Available online at: http://www.esrl.noaa.gov/gmd/ccgg/trends.

[5] Climate Change 2007:Synthesis Report, Contribution of Working Groups I, II and III to the Fourth Assessment Report of the Intergovernmental Panel on Climate Change Core Writing Team, Pachauri, R.K. and Reisinger, A. (Eds.) IPCC, Geneva, Switzerland. pp 104.

[6] R. F. Service, Science 285 (1999) 682.

[7] Celle a combustibile, Stato di sviluppo e prospettive della tecnologia, M.Ronchetti, ENEA, 2008.

[8] B. Lindström, L.J. Pettersson, Inter. Jour. of Hydrogen Energy 26 923 (2001).

[9] J. Agrell, M. Boutonnet, J.L.G. Fierro, Appl. Catal. A 253 (2003) 213.

[10] D. J. Moon, K. Srekumar, S. D. Lee, B. G. Lee, H. S. Kim, Appl. Catal. A: General 215 (2001) 1.

[11] A. K. Avci, Z. I. Onsan. D. L. Trimm Appl. Catal. A: General 216 (2001) 243.

[12] P. Kluger, Int. J. Hydrogen Energy 26 (2001) 1137.

[13] J. Agrell, H. Birgersson, M. Boutonnet, I. Melian-Cabrera, R.M. Navarro, J.L.G. Fierro, J. Catal. 219 (2003) 389.

[14] J.O.M. Bockris, Int. J. Hydrogen Energy 24 (1999) 1.

[15] R. Shiozaki, T. Hayakawa, Y. Liu, T. Ishii, M. Kumagai, S. Hamakawa, K. Suzuki, T. Itoh, T. Shishido, K. Takehira, Catal. Lett. 58 (1999) 131.

[16] T. Shishido, H. Sameshima, K. Takehira, Top. Catal. 22 (2003) 261.

[17] W. Cheng, C. Shiau, T.H. Liu, H.L. Tung, J. Lu, C.C. Hsu, Appl. Catal. A 170 (1998) 215.

[18] S. Velu, K. Suzuki, T. Osaki, Catal. Lett. 62 (1999) 159.

[19] M.L. Cubeiro, J.L.G. Fierro, Appl. Catal. A 168 (1998) 307.

[20] J.B. Breen, J.R.H. Ross, Catal. Today 511 (1999) 521.

[21] S. Velu, K. Suzuki, T. Osaki, Chem. Commun., (1999) 2341.

[22] G. Shen, S. Fujita, S. Matsumoto, N. Takezawa, J. Mol. Catal. A:Chem. 124 (1997) 123.

[23] C.J. Jiang, D.L. Trimm, M.S. Wainwright, Appl. Catal. A 97 (1993) 145.

[24] B.A. Peppley, J.C. Amphlett, L.M. Kearns, R.F. Mann, Appl. Catal. A 179 (1999) 21.

[25] O. Korotkikh, R. Farrauto, Catal. Today 62 (2000) 249.

[26] S. Murcia Mascaròs, R. M. Navarro, L. Gomez-Sainero, U. Costantino, M. Nocchetti, and J. L. G. Fierro, J. Catal. 198 (2001) 338.

[27] B. Lindstrom, L.J. Pettersson, P.G. Menon, Appl. Catal. A 234 (2002)111.

[28] S. Velu, K. Suzuki, M. Okazaki, M.P. Kapoor, T. Osaki, F. Ohashi, J. Catal. 194 (2000) 373.

[29] J. Agrell, H. Birgersson, M. Boutonnet, J. Power Sources 4654 (2002)1.

[30] J. Papavasiliou, G. Avgouropoulos, T. Ioannides, Catal. Commun. 5 (2004) 231.

[31] J.R.Lattern, M.P.Harold, Appl.Catal. B:Environ.56 (2005) 149.

[32] Y. Uemura, S. Churei, M. Iwama, Y. Hatate, Kagoshima Daigaku Kogakubu Kenkyu Hokoku 32 (1990) 99.

[33] T. B. Su, M. H. Rei, J. Chin. Chem. Soc 38 (6) (1991) 535.

[34] M. M. Gunter, T. Ressler, R. E. Jentoft, B. Bems, J. Catal. 203 (2001) 133.

[35] M. Laniecki, Studies in Surface Science and Catalysis 135 (2001) 3986.

[36] S. Wellach, M. Hartmann, S. Ernst, J. Weitkamp, Proc. Int. Zeolite Conf., 12th (1999) vol. 2 p. 1409, CAN 131:301404.

[37] Y. Liu, T. Hayakawa, K. Suzuki, S. Hamakawa, Catalysis Communications 2 (2001) 195.

[38] Y. Liu, T. Hayakawa, K. Suzuki, S. Hamakawa, T. Tsunoda, T. Ishii, M. Kumagai, Appl. Catal. A: General 223 (2002) 137.

[39] L. Ma, B. Gong, T. Tran, M. S. Wainwright, Catal. Today 63 (2000) 499.

[40] T. Takahashi, M. Inoue, T. Kai, Appl. Catal. A: General 218 (2001) 189.

[41] P. Tsai, M. Yoshimura, Appl. Catal. A: General 214 (2001) 237.

[42] N. Iwasa, T. Mayanagi, S. Masuda, N. Takezawa, Reaction Kinetics and Catalysis Letters 69 (2000) 355.

[43] N. Iwasa, T. Mayanagi, N. Ogawa, K. Sakata, N. Takezawa, Catal. Lett. 54 (1998) 119.

[44] L. Alejo, R. Lago, M. A. Pena, J. L. G. Fierro, Appl. Catal. A: General. 162 (1997) 281.

[45] M. L. Cubeiro, J. L. G. Fierro, J. Catal. 179 (1998) 150.

[46] N. Takezawa, N. Iwasa, Catal. Today, 36 (1997) 45.

[47] H. Y. H. Cahn, C. T. Williams, M. J. Weaver, C. G. Takoudis, J. Catal. 174 (1998) 191.

[48] M. P. Zum Mallen,L.D.Schmidt, J. Catal. 161 (1996) 230.

[49] F. Basile, G. Fornasari, M. Gazzano, A. Vaccari, Applied Clay Science, 16, 185 (2000).

[50] Y. Liu, K. Suzuki, S. Hamakawa, T. Hayakawa, K. Murata, T. Ishii and M. Kumagai, Chem. Letters (2000) 486.

[51] J. Agrell, K. Hasselbo, K. Jansson, S. G. Järås, M. Boutonnet, Appl. Catal. A: General 211 (2001) 239.

[52] S. Velu, K. Suzuki, M. P. Kapoor, F. Ohashi, T. Osaki, Appl. Catal. A: General 213 (2001) 47.

[53] H. H. Kung, T. L. Reitz, E. D. Schrum, M. C. Kung, Preprints of Symposia-American Chemical Society, Division of Fuel Chemistry 46 (2001) 665.

[54] Y. Jiang, Q. Huang, F. Wang, M. S. Lim, D. H. Kim, Ranliao Huaxue Xuebao 29 (2001) 207, CAN 135:124772.

[55] T. L. Reitz, P. L. Lee, K. F. Czaplewski, J. C. Lang, K. E. Popp, H. H. Kung, J. Catal. 199 (2001) 193.

[56] S. Fukahori, T. Kitaoka, A. Tomoda, R. Suzuki, H. Wariishi, Appl. Catal.A: Gen. 300 (2006) 155.

[57] F. Raimondi, B. Schnyder, R. Kotz, R. Schelldorfer, T. Jung, J. Wambach. A. Wokaun, Surface Science (2003), 532, 383.

[58] T.L. Reitz, S. Ahmed, M. Krumpelt, R. Kumar, H.H. Kung, Journal of Molecular Catalysis A: Chemical (2000), 162, (1-2), 275.

[59] F.Raimondi, K.Geissler, J. Wambach, A. Wokaun, Applied Surface Science (2002), 189, (1-2), 59.

[60] J.K. Lee, J.B. Ko, D.H. Kim, Appl. Catal. A:General 278 (2004) 25.

[61] S.Catillon, C. Louis, R. Rouget, Topics in Catalysis (2004), 30/31, (1-4), 463.

[62] I. Ritzkopf, S. Vukojevic, c. Weidenthaler, J.D. Grunwaldt, F.Schuth,Applied Catalysis, A: General (2006), 302, (2), 215.

[63] A. Szizybalski, F. Girgsdies, A. Rabis, Y. Wang, N. Niederberger, T. Ressler, Journal of Catalysis (2005), 233, (2), 297.

[64] H.Purnama, F. Girgsdies, T.Ressler, J.H. Schattka, R.A. Caruso, R. Schomaecker, R. Schloegl, Catalysis Letters (2004), 94, (1-2), 61.

[65] I. Ritzkopf, C. Kiener, S. Vukojevic, R. Brinkmann, H. Boennemann, F. Schueth, DGMK Tagungsbericht (2003), 2003-2 (Proceedings of the DGMK- Conference„Innovation in the Manufacture and Use of Hydrogen",2003, 49.

[66] J.Papavasiliou, G. Avgouropoulos, T. Ioannides Applied Catalysis, B: Environmental (2007), 69, (3-4), 226.

[67] J. Papavasiliou, G. Avgouropoulos, T. Ioannides, Catalysis Communications (2004), 5, (5), 231.

[68] W.Shan, Z. Feng, Z. Li, J. Zhang, W. Shen, C.Li, J. Catal.228 (2004) 206.

[69] J. Papavasiliou, G. Avgouropoulos, T. Ioannides, Catalysis Communications (2005), 6, (7), 497.

[70] B. Lindstrom, J. Agrell, L.J. Petterson Chemical Engineering Journal (Amsterdam, Netherlands) (2003), 93, (1), 91.

[71] B. Lindstrom, L.J. Pettersson, P.G. Menon, Appl. Catal. A: Gen. 234 (2002) 111.

[72] P.H. Matter, D.J. Braden, U.S. Ozkan, Journal of Catalysis (2004), 223, (2), 340.

[73] P.H. Matter, U.S. Ozkan, Journal of Catalysis (2005), 234, (2), 463.

[74] J.B. Wang, C.H. Li, T.J. Huang, Catalysis Letters (2005), 103, (3-4), 239.

[75] A. Mastalir, B. Frank, A. Szizybalski, H. Soerijanto, A. Deshpande, M. Niederberger, R. Schomacker, R. Schlogl, T. Ressler, Journal of Catalysis (2005), 230, (2), 464.

[76] H.Oguchi, T. Nishiguschi, T. Matsumoto, H. Kanai, K. Utani, Y. Matsumura, S. Imamura, Applied Catalysis, A: General (2005), 281, (1-2), 69.

[77] A.A. Khassin, V.V. Pelipenko, T.P. Minyukova, V.I. Zaikovskii, D.I. Kochubey, T.M. Yurieva, Catal. Today 112 (2006) 143.

[78] E.D. Batyrev, J.C. van den Heuvel, J. Beckers, W.P.A. Jansen, H.L.Castricum, J. Catal. 229 (2005) 136.

[79] D. Duprez, Z. Ferhat-Hamida, M.M. Bettahar, J. Catal. 124 (1990) 1.

[80] L.A. Espinosa, R.M. Lago, M.A. Pen˜a, J.L.G. Fierro, Topics Catal. 22(2003) 245.

[81] G. Fierro, M. Lo Jacono, M. Inversi, P. Porta, F. Cioci, R. Lavecchia, Appl. Catal. A: General 137 (1996) 327.

[82] M. Turco, G. Bagnasco, U. Costantino, F. Marmottini, T. Montanari, G.Ramis, G. Busca, J. Catal. 228 (2004) 56.

[83] I. A. Fisher, A. T. Bell, J. Catal. 184 (1999) 357.

[84] L.C. Wang, Q. Liu, M. Chen, Y.M., Liu, Y. Cao, H.Y. He, K.N. Fan, J. Phys. Chem. C 111 (2007) 16549.

[85] Z.Y. Ma, W. Wei, W.H. Li, Y.H. Sun, J. Mol. Catal. A: Chem. 231 (2005) 75.

[86] R. Pérez-Hernández, G. Mondragón Galicia, D. Mendoza Anaya, J. Palacios, C. Angeles-Chavez, J. Arenas-Alatorre, Int. J. Hydrogen Energy 33 (2008) 4569.

[87] V. Ramaswamy, M. Bhagwat, D. Srinivas, A.V. Ramaswamy, Catal. Today 97 (2004) 63.

[88] Y. Zao, K. Tao, H.L. Wan, Catal. Commun. 5 (2004) 249.

[89] G. Águila, S. Guerrero, P. Araya, Catal. Commun. 9 (2008) 2550.

[90] V.R.Chary Komandur, V. Sagar Guggilla, S. Srikanth Chakravarthula, V.R. Vattkonda, J. Phys. Chem. B 111 (3) (2007) 543.

[91] R. A. Köppel, C. Stöcker, A. Baiker, J. Catal. 179 (1998) 515.

[92] M.K. Dongare, V. Ramaswamy, C.S. Gopinath, S. Scheurell, . Bruckner, E. Kemnitz, J. Catal. 199 (2001) 209.

[93] L. Castro, P. Reyes, C. Montes Correa, J. Sol-Gel Sci. Technol. 25 (2002) 159.

[94] T. López, M. Alvarez, R. Gómez, D.H. Aguilar and P. Quintana, J. Sol-Gel Sci. Technol. 33 (2005) 93.

[95] Y. Wang, R.A. Caruso, J. Mater. Chem. 12 (2002) 1442.

[96] J.P. Shen, C. Song, Catal. Today 77 (2002) 89.

[97] R. Perez-Hernandez, A. Gutierrez-Martinez, C.E. Gutierrez–Wing, Int. J. Hydrogen Energy 32 (2007) 2888.

[98] S. Patel, K.K. Pant, J. Power Sources 159 (2006) 139.

[99] Y. Men, H. Gnaser, R. Zapf, V. Hessel, C. Ziegler, G. Kolb, Appl. Catal. A: Gen. 277 (2004) 83.

[100] Y. Liu, T. Hayakawa, T. Tsunoda, K. Suzuki, S. Hamakawa, K. Murata, R. Shiozaki, T.Ishii, M. Kumagai, Top. Catal. 22 (2003) 205.

[101] C.-Y. Shiau, M.W. Ma, C.S. Chuang, Appl. Catal. A: Gen. 301 (2006) 89.

[102] G. Marban, A.B. Fuertes, Appl. Catal. B: Environ. 57 (2005) 43.

[103] S. Patel, K.K. Pant, Fuel Process. Technol. 88 (2007) 825.

[104] L. Li, Y. Zhan, Q. Zheng, Y. Zheng, X. Lin, J. Zhu, Catal. Lett. 118 (2007) 91.

[105] Y. Li, Q. Fu, M. Flytzani-Stephanopoulos, Appl. Catal. B: Environ. 27 (2000) 179.

[106] B. Skarman, D. Grandjean, R.E. Benfield, A. Hinz, A. Andersson, L.R. Wallemberg, J.Catal. 211 (2002) 119.

[107] W. Shen, X. Dong, Y. Zhu, H. Chen, J. Shi, Microporous Mesoporous Mater. 85(2005) 157.

[108] M.-F. Luo, J.-M. Ma, J.-Q. Lu, Y.-P. Song, Y.-J. Wang, J. Catal. 246 (2007) 52.

[109] S. Hocevar, U.O. Krasovec, B. Orel, A.S. Arico, H. Kimd, Appl. Catal. B: Environ. 28 (2000) 113.

[110] Y. Liu, Q. Fu, M.F. Stephanopoulos, Catal. Today 93–95 (2004) 241.

[111] A. Martınez-Arias, M. Fernandez-Garcıa, O. Galvez, J.M. Coronado, J.A. Anderson,J.C. Conesa, J. Soria, G. Munuera, J. Catal. 195 (2000) 207.

[112] D.H. Kim, J.E. Cha, Catal. Lett. 86 (2003) 107.

[113] Z. Liu, R. Zhou, X. Zheng, J. Mol. Catal A: Chem. 267 (2007) 137.

[114] E. Moretti, M. Lenarda, L. Storaro, A. Talon, T. Montanari, G. Busca, E. Rodrıguez-Castellon, A. Jimenez-Lopez, M. Turco, G. Bagnasco, R. Frattini, Appl. Catal. A: Gen.335 (2008) 46.

[115] X. Zhang, P. Shi, J. Mol. Catal. A: Chem. 194 (2003) 99.

[116] Z. Liu, R. Zhou, X. Zheng, J. Mol. Catal A: Chem. 267 (2007) 137.

[117] G. Avgouropoulos, T. Ioannides, H. Matralis, Appl. Catal. B: Environ. 56 (2005) 87.

[118] A.Pintar, J. Batista, S. Hočevar, J. Coll. Inter. Sci. 285 (2005) 218.

[119] D. Trong On, D. Desplantier-Giscard, C. Danumah, S. Kaliaguine, Appl. Catal. A: General 222 (2001) 299.

[120] A. Taguchi, F. Schüth, Microp. Mesop. Mater.77 (2005) 1.

[121] G. Ertl, H. Knözinger, J. Weitkamp, Handbook of heterogeneous catalysis, VCH-Wiley, New York(1997) 264.

[122] H. Huang, S. Wang, Appl. Catal. 24 (1986) 287.

[123] R. O. Idem, N. N. Bakhshi, Chem. Eng. Sci. 51 (1996) 3697.

[124] C.J. Brinker, S.W. Scherer, Sol-Gel science: the physics and chemistry of sol–gel processing. Academic Press, New York, 1990.

[125] C.J. Brinker, B.C. Bunker et al., Structure of Sol-Gel Derived Inorganic Polymers: Silicates and Borates, Am. Chem. Soc., part II 1988.

[126] R.W. Jones, Fundamental Principles of Sol-Gel Technology 1989.

[127] L.C. Klein, G.J. Garvey, Effect of Water on Acid- and Base-Catalyzed Hydrolysis of Tetraethylorthosilicate (TEOS), Mater. Res. Soc. Sym. Proc. 1984, 32.

[128] K.D. Keefer, The Effect of Hydrolysis Conditions on the Structure and Growth of Silicate Polymers, Mater. Res. Soc. Sym. Proc., 1984, 32.

[129] C.B. Hurd, Chem. Rev. 1938, 22, 403.

[130] J.D. Lockwood, Nanostructure Science and Technology, Surface Effects in Magnetic Nanoparticles; Springer: New York, 2005.

[131] L.Q. Nguyen, C. Salim, H. Hinode, Appl. Cat. A: Gen. 2008, 347, 94.

[132] J. Livage, M. Henry, C. Sanchez in: Sol-Gel Science, The Physics and Chemistry of Sol-Gel Processing, Academic press, New York 1990.

[133] Aronne, P. Pernice, A. Marotta, J. Mater. Sci. Letter 10 (1991)1136-1138.

[134] Aronne, P. Pernice, A. Marotta, M. Catauro, Thermochim. Acta 275 (1996) 75-82

[135] F. Rouquerol, J. Rouquerol, K. Sing, Adsorption by Powders and Porous Solids:Principles, Methodology and Application, Academic Press, London, 1999

[136] M. Turco, G. Bagnasco, U. Costantino, F. Marmottini, T. Montanari, G. Ramis, G. Busca, J. Catal. 228 (2004) 43

[137] G.C. Bond, S.N. Namijo, J. Catal. 118 (1989) 507

[138] Y. Kim, P. Kim, C. Kim, J. Yi, J. Mater. Chem. 13 (2003) 2353.

[139] E. Moretti, M. Lenarda, L. Storaro, R. Frattini, P. Patrono, F. Pinzari, J. Colloid Interface Sci. 306 (2007) 89.

[140] J. Cějka, P. Kooyman, L. Veselá, J. Rathouský, A. Zukal, Phys. Chem. Chem. Phys. 4 (2002) 4823

[141] S. Poulston, P.M. Parlett, P. Stone, M. Bowker, Surf. Interf. Analysis 24 (1996) 811.

[142] R. B. Bird, E. N. Lightfoot, W. E. Stewart, Fenomeni di trasporto, Casa Editrice Ambrosiana Milano(1997) 253

[143] D.W. Green, R. H. Perry, Perry's chemical engineers' handbook, McGraw-Hill(1997), table 2-129.

[144] D.W. Green, R. H. Perry, Perry's chemical engineers' handbook, McGraw-Hill(1997), 5-15.

[145] D.W. Green, R. H. Perry, Perry's chemical engineers' handbook, McGraw-Hill(1997), table 2-221.

[146] W.M. Shaheen, A.A. Ali, Mater. Res. Bull. 36 (2001) 1703-1716

[147] M. Labaki, J.F. Lamonier, S. Siffert, A. Aboukaïs, Thermochim. Acta 427 (2005) 193-200

[148] M.C. Muñoz, S. Beltrán, J.I. Cerdá, Surf. Sci. Rep. 61 (2006) 303-344

[149] G. Águila, J. Jiménez, S. Guerrero, F. Gracia, B. Chornik, S. Quinteros, P. Araya, Appl. Catal. A: General 360 (2009) 98-105

[150] M. Turco, G. Bagnasco, C. Cammarano, P. Senese, U. Costantino, M. Sisani, Appl. Cat. B:Environ 77 (2007) 46-57

[151] S. Salasc, V. Perrichon, M. Primet, M. Chevrier, N. Mouaddib-Moral, J. Catal. 188 (2000) 401

[152] S. Piras, A. Colussi, A. Trovarelli, V.Sergo, J. Llorca, R. Psaro, L. Sordelli, J. Phys. Chem. B 109 (2005) 11110.

[153] J.Z. Shyu, W.H. Weber, H.S. Ghandi, J. Phys. Chem. 92 (1988) 4964. and ref. therein.

[154] A.Martinez-Arias, J.C. Cataluña, J.C. Conesa, J. Soria, J. Phys. Chem. B 102 (1998) 809

[155] T. Shishido, M. Yamamoto, D. Li, Y. Tian, H. Morioka, M. Honda, T. Sano, K. Takehira, Appl. Catal. A: General 303 (2006) 62

[156] T.A. Semelsberger, K.C. Ott, R.L. Borup, H.L. Greene, Appl. Catal. A: General 309 (2006) 210.

[157] F. Giordano, A. Trovarelli, C. de Leitemburg, M. Giona, J. Catal. 193 (2000) 273.

[158] E. Aneggi, M. Boaro, C. de Leitemburg, G. Dolcetti, A. Trovarelli, J. Alloys Compd. 408 (2006) 1096

[159] M.C. Cabus-Llaurado, Y. Cesteros, F. Medina, P. Salagre, J.E. Sueiras, Microporous Mesoporous Mater. 100 (2007) 167

[160] L. Qiu, F. Liu, L.Zhao, Y. Ma, J. Yao, Appl.Surf. Sci., 252 (2006) 4931.

[161] G. Avgoropoulos, T. Ioannides, Appl. Catal A:General 244 (2003) 117.

[162] P.A. Dilara, J.M. Vohs, J. Phys. Chem. 97 (1993) 12919-23., R.G. Silver, C.J. Hou, J.G. Ekerdt, J. Catal. 118 (1989) 400-416

[163] J. Zhu, J. G. van Ommen, L. Lefferts, J. Catal. 225 (2004) 388-397

[164] S. Patel, K.K. Pant, Appl. Catal. A: Gen. 356 (2009) 189.

[165] C.N. Satterfield, Heterogeneous Catalysis in Practice, McGraw-Hill, NewYork, 1980, p. 195.

[166] P.B. Malla, P. Ravindranathan, S. Komarneni, E. Breval, R. Roy, J. Mater. Chem. 2 (1992) 559

[167] F. Kooli, V. Rives, W. Jones, Chem. Mater. 9 (1997) 2231.

[168] R. Burch, S.E. Golunski, M.S. Spencer, Catal. Lett. 5 (1990) 55.

[169] W. Lin, A.A. Herzing, C.J. Kiely, I.E. Wachs, J. Phys. Chem. C 112 (2008) 5942.

[170] K.A. Pokrovski, A.T. Bell, J. Catal. 241 (2006) 276.

[171] G.-S. Wu, D.-S. Mao, G.Z. Lu, Y. Cao, K.N. Fan, Catal. Lett. 130 (2009) 177.

[172] S.D. Jones, L.M. Neal, H.E. Hagelin-Weaver, Appl. Catal. B: Environ. 84 (2008) 631.

[173] M. Turco, C. Cammarano, G. Bagnasco, E. Moretti, L. Storaro, A. Talon, M. Lenarda, Appl. Catal. B: Envir. 91 (2009) 101.